

A study of the SA SKA RFI Measurement Systems

by

Sydney Bobby Dunn

A thesis submitted to the Department of Electrical Engineering,
University of Cape Town, in fulfilment of the requirements
for the degree of

Master of Science

at the

UNIVERSITY OF CAPE TOWN



© University of Cape Town
February 2008

Declaration

I declare that this dissertation is my own, unaided work. It is being submitted for the degree of Master of Science in Engineering in the University of Cape Town. It has not been submitted before for any degree or examination in any other university.

Signature of Author

Cape Town

15 February 2008

Abstract

The Square Kilometre Array (SKA) is an ambitious multi-billion rands project to build the worlds's largest and most sensitive radio astronomy telescope. The telescope will have a collection area of 1 million square metres and will be able to look at a larger portion of the sky than current telescopes. The sensitivity of this telescope is of such a nature that isolation of this instrument from the negative effects of man-made noise is paramount. As such a campaign to measure the levels of electromagnetic radiation at the prospective sites had to be conducted. In response to this, the South African (SA) SKA team developed the RFI Measurement System 2 to perform these measurements.

This dissertation documents the findings of a study of the functionality of RFI Measurement System 2 that was conducted by the author. An in depth study of MEMO 37 (RFI Measurement Protocol) was employed first. After which, an exhaustive audit of all the equipment used and a thorough analysis of the method of data collection and processing was conducted. A sample of raw uncalibrated, MODE 1 field measurement data was scrutinized. The data chosen was for RF signals in the 70 - 150 MHz frequency range and following similar data processing procedures as that of the SA SKA team, the plots of Spectral Flux Density versus Frequency were generated in the laboratory using MATLAB.

It was found that for the frequency range 80 MHz to 150 MHz, these graphs closely matched that of the SA SKA team and that for this bandwidth, both the SA SKA graph and that replicated by the author were within their tolerance limits. A relatively strong correlation coefficient of 0.4430 was observed for the maximum values graph. The range 70 MHz to 80 MHz lies outside the operational ability of the antennas as prescribed by the manufacturers and for this reason some differences between the work of the SA SKA team and that of my work was observed for this range.

In memory of my son Jamian Sydney who was tragically taken away on the 4th of
January 2005, at the young and tender age of 4.

Acknowledgements

Firstly, I would like to thank the SKA for their financial support without whom this piece of work would not have been made possible. I would also like to thank my supervisor, Prof. Mike Inggs for his wisdom and invaluable insight into the subject and for steering me in the right direction.

I am greatly indebted to Dr. Richard Lord for his support and assistance and to Simon for his willingness to assist me and for being a constant source of inspiration and encouragement.

I would like to thank my friends Rozanne and Sadhna for their love and support and for believing in me during the many times I found myself groping in a *sea of darkness*.

A big and heartfelt, *thank you!* goes to my dear friend and UCT librarian, Ms. Amina Adam, for proof reading this document.

I am grateful to my friend Dr. Shakila Reddy (*UKZN*) for her positive comments regarding my work and to my ex-wife, Magistrate K. Dunn for looking after our daughter during my period of abscondment.

But mostly, I would like to thank Mr. Paul Manners (SA SKA employee and Rhodes University student) for clarifying most of the questions surrounding the systems, for demystifying the data and for maintaining his composure during the many times I wrote to him for clarification.

Paul, “*you’re a little known star among millions and I hope the SKA will help bring your heavenly goodness to the fore.*”

And last but not least, I would like to thank GOD for giving me the strength and courage to embark on this lonely and tiresome journey and for giving me this wonderful opportunity.

“For by him were all things made, and without him was not anything made that was made.”

John 1:3 (King James Version).

Contents

Declaration	i
Abstract	ii
Acknowledgements	iv
List of Symbols	xiv
List of Symbols	xvi
1 Introduction	1
1.1 Background	1
1.2 Radio frequency allocation in South Africa	2
1.3 Problems of Radio Frequency Interference on Radio Telescopes	4
1.4 The Square Kilometre Array (SKA)	4
1.5 Implementation of the SKA Protocol in South Africa	6
1.6 The SKA RF Measuring Systems	7
1.7 Objectives of Dissertation	8
1.8 Summary of Results	9
1.8.1 Sources of Data	9
1.8.2 Method of Procedure and Performance Criterion	10
1.8.3 Findings	11
1.8.4 Significance of findings	13
1.9 Structure of the Dissertation	14
2 Summary of the SKA Protocol	16
2.1 Scope	16
2.2 Technical Specification	17
2.3 Recommended equipment	17

2.4	Calibration Procedure	18
2.5	Measurement Procedure	18
2.5.1	Mode 1	18
2.5.2	Mode 2	19
2.6	Measurement times	20
2.7	Pulsed Signals	24
2.8	Summary	25
3	Literature Review	26
3.1	Introduction	26
3.2	Frequency Spectrum Management	27
3.3	Electromagnetic Interference	28
3.3.1	Types and sources of EMI	28
3.3.2	Description of some types of EMI	31
3.3.3	Escape Mechanisms	31
3.3.4	EMC testing	32
3.3.5	Preventative Measures for EMC/EMI	32
3.4	Various subsystems of the RFI Measuring System	33
3.5	Receivers	33
3.5.1	Receiver characteristics	33
3.5.2	Selectivity	34
3.5.3	Nonlinearities, TOI, SOI, Linearity and Sensitivity in circuits	35
3.6	Amplifiers	42
3.7	Filters	42
3.8	Mixers	43
3.9	Antenna design	43
3.9.1	Radiation Resistance	43
3.9.2	Radiation Pattern	44
3.9.3	Beamwidth and Gain of an antenna	44
3.9.4	The position and magnitude of its side lobes	45
3.9.5	Bandwidth	45
3.9.6	Antenna Aperture	46
3.9.7	Antenna Correction Factor	46
3.9.8	Polarization	47
3.10	Noise	47

3.11	Spectrum Analyzer theory	50
3.11.1	Spectrum analyzer performance and selection criteria	51
3.11.2	Spectrum analyzer sensitivity and noise	51
3.11.3	Spectrum Analyzer operation and functionality	52
3.12	Summary	53
4	Implementation of the SKA protocol in South Africa	54
4.1	Description of the RFI Measurement system 2	54
4.1.1	Data transfer from the Spectrum Analyzer to the computer	57
4.2	Method and Measurements	59
4.2.1	Description and sources of Data	59
4.2.2	Data Processing Procedure	60
4.2.3	Measurement Schedule	61
4.3	RF Module of RFI System 2	62
4.4	Summary	64
5	Results	65
5.1	Design discrepancies	65
5.2	Analysis of results	67
5.2.1	Degree of Dispersion of Data	68
5.3	Spectral Occupancy	68
5.3.1	Minimum	70
5.3.2	10 Percentile	72
5.3.3	Mean	73
5.3.4	Median	74
5.3.5	90 Percentile	76
5.3.6	Maximum	77
5.4	Considering the tolerances	78
5.5	Summary of Results	80
5.6	Significance of Results	81
6	Conclusion	82
6.1	Summary	82
6.2	Inference	83
A	Flexible Image Transport System	91

B	Components of RFI System 2	92
C	Formula Derivation	93
D	K-Factor Values of Antenna HL033	94
E	Matlab Generated Code	95

List of Figures

1.1	Radio Frequency Interference plot for the 70 - 150 MHz band: OPTION 1- (Top) Reprocessed (Bottom) SA SKA Measurement. It can be seen (<i>through direct observation</i>) that the (Top) plot has more spectral activity than the (Bottom) Plot.	11
1.2	Radio Frequency Interference plot for the 70 - 150 MHz band: OPTION 2-(Top) Reprocessed (Bottom) SA SKA Measurement	12
1.3	Radio Frequency Interference plot for the 70 - 150 MHz band: OPTION 3-(Top) Simulation (Bottom) SA SKA Measurement	13
2.1	Basic Characteristics of a pulsed waveform showing the Marks and Spaces. The space gives the receiver a false sense of pulse inactivity which is not necessary the case.	24
3.1	Structure showing the various types and categories of EMI as taken from <i>Keiser (1987) [12]</i>	31
3.2	Illustration of linear dynamic and spurious free dynamic range (from[18])	40
3.3	Dynamic range versus distortion and noise (from[22])	40
3.4	Representative input-output AGC curves (from [30])	42
3.5	Block diagrams of a classic superheterodyne spectrum analyzer (from[22, 40])	53
4.1	Block diagram showing the complete RFI Measurement System 2	55
4.2	Radiation beam patterns of R&S HL 033 (left)[53] and R&S HL 050 (right) [54] antennas	56
4.3	Block Diagram of RFI System 2 (from[17])	62
5.1	Gain vs Frequency (from[53])	66
5.2	Plot of Coefficient of Variation (%) versus Frequency (MHz)	69

5.3	<i>The above two plots show the spectral occupancy as a function of frequency (RBW). The top plot shows the number of signals which exceed the median spectral flux density by 6 dB in each frequency bin, whilst the bottom plot depicts the number of signals exceeding the median spectral flux density by 6 dB in each frequency bin as a fraction of the total signals available</i>	69
5.4	Plot of Frequency versus Spectral Flux Density. The plots were derived using the <i>minimum spectral flux density values</i> and <i>10 percentile SFD values</i> . Top graph shows the <i>reprocessed plot</i> as performed by the author whilst the bottom shows a plot derived by the <i>SA SKA team</i> . The correlation between the two curves is 0.3218.	71
5.5	Plot of Frequency versus Spectral Flux Density. Top graph shows the <i>reprocessed plot</i> as performed by the author whilst the bottom shows a plot derived by the <i>SA SKA team</i> . The plots were constructed using the <i>ten percentile spectral flux density values</i>	72
5.6	Plot of Frequency versus Spectral Flux Density. Top graph shows the <i>reprocessed plot</i> as performed by the author whilst the bottom shows a plot derived by the <i>SA SKA team</i> . The plots were constructed using the <i>mean spectral flux density values</i> . The two plots show maximum values of -166.4 dBW/m ² /Hz at a frequency of 102.5 MHz and -164.8 dBW/m ² /Hz.	73
5.7	Plot of Frequency versus Spectral Flux Density. Top graph shows the <i>reprocessed plot</i> as performed by the author whilst the bottom shows a plot derived by the <i>SA SKA team</i> . The top plot was constructed using the <i>median spectral flux density values</i> whilst the <i>bottom plot is that of mean values</i>	75
5.8	Plots of Frequency versus Spectral Flux Density. Top graph shows the <i>reprocessed plot</i> as performed by the author whilst the bottom shows a plot derived by the <i>SA SKA team</i> . The plots were constructed using the <i>90 Percentile spectral flux density values</i>	76
5.9	Plot of Frequency versus Spectral Flux Density. Top graph shows the <i>reprocessed plot</i> as performed by the author whilst the bottom shows a plot derived by the <i>SA SKA team</i> . The plots were derived using the <i>maximum spectral flux density values</i>	77

5.10	The above plots shows the spectral flux density as a function of RBW frequency. The <i>top most</i> plot shows the <i>spectral flux density as function of frequency</i> for a <i>worst case scenario</i> . This is when the positive tolerances of the components are taken into account and this reduces the theoretical system gain. The <i>best case scenario</i> is when the system gain is increased by subtracting the tolerances. The second to last plot depicts the plot as generated by SA SKA whereas the second plot from the top is an attempt to replicate the SA SKA plot.	79
D.1	Antenna Factor values of the R&S HL033 Log. Periodic Broadband . . .	94

List of Tables

1.1	Typical frequencies for <i>Distance Measuring Equipment</i> of Aircraft [13].	2
1.2	Radio spectrum allocation in South Africa: 30 - 1427 MHz. This table was taken from <i>Lord (2000)[83]</i> and was verified by the author against that found in <i>Part 3</i> of the <i>South African Telecommunications Act No. 103 of 1996</i>	3
1.3	Summary of technical specification which the SA SKA RFI systems had to adhere to (from [9])	7
2.1	Summary of the technical specifications (from [9])	17
2.3	This table shows the measurement schedule of Mode 2 Measurements. The table shows the <i>Frequency Band in GHz, RBW in kHz, Dwell Time in ms</i> and <i>S_{0h} in dB (Jy)</i> . It also shows the significance of the various bands (from[9]).	20
2.4	Dwell times (from [9])	23
3.1	Sources of conducted <i>Electromagnetic Interference</i> (from [12])	29
3.2	Sources of <i>Radiated Interference</i> (from [12])	30
4.1	Specifications for the H&S Log-Periodic Broadband Antenna (R&S HL 033) and (R&S HL050)	57
4.2	Spectrum analyzer setting for band 70 to 150 MHz. The values in the table were taken from the Fits Header files.	59
4.3	Table showing the resultant frequency bands (from [17, 27])	63
4.4	Table showing the resultant theoretical system gain for path 1. <i>The information contained in the table was obtained form the Data Sheets of the Manufacturers of the various components</i>	63
5.1	Statistics for Minimum Values Curve (<i>Correlation coefficient = 0.3121</i>)	71
5.3	Statistics: 10 Percentile Values (<i>Correlation coefficient = 0.3121</i>)	72
5.5	Statistics: Mean Values (<i>Correlation coefficient = 0.3645</i>)	73
5.7	Statistics: Median Values (<i>Correlation coefficient = 0.2538</i>)	75

5.9	Statistics: 90 Percentile Values (<i>Correlation coefficient 0.4425</i>)	76
5.11	Statistics: Maximum Values (<i>Correlation coefficient is 0.4430</i>)	77
5.13	Statistical Summary	80
A.1	List of data files used in the analysis	91
B.1	Various Amplifiers used in RFI System 2 Construction	92
B.2	Various components making up the RF Assembly (from [53, 54, 55, 56, 27, 17, 57]	92

List of Symbols

Symbol	Definition
A	— Area (in m^2)
A_{eff}	— Effective Area
B_s	— Signal bandwidth
B_t	— Total Radar Bandwidth
c	— Speed of light in m/s
D	— Directivity
ENR	— Excess Noise Ratio
f	— Frequency
f_{prf}	— Pulse repetition frequency
F	— Noise Factor
$f_{3\text{dB}}$	— 3 dB cut-off frequency
G_r	— Gain of the receiver as a function of frequency
$G_{\text{sys}}(f)$	— Gain of the receiving system as function of frequency
$G_{\text{ant}}(f)$	— Gain of the antenna as a function of frequency
G	— Gain
$G_{\mathcal{P}rac}$	— Practical Gain
J_y	— One Jansky equivalent to $10^{-26}\text{W}/\text{m}^2/\text{Hz}$
K	— Kelvin
L_{DAN}	— Displayed Average Noise Level
NF	— Noise Figure
NF_{SA}	— Noise Figure of Spectrum Analyzer
P	— Power Spectral Density
P_n	— Noise Power
P_s	— Power induced at the terminals of the antenna
P_{SA}	— Power of Spectrum Analyser
SFD	— Spectral Flux Density

S_{0h}	—	Spectral Flux at zero elevation in dBm/m ² /Hz
t	—	Time
t_{bin}	—	Time spent in frequency bin
t_d	—	Dwell Time
t_h	—	Burst time
t_r	—	Rise time
t_{syn}	—	Settling time of synthesizer
t_{sw}	—	Sweep Time
t_{pd}	—	Time in pass band
T_e	—	Equivalent noise temperature
T_R	—	Receiver Temperature in Kelvin
T_{sys}	—	System Temperature
Z_0	—	Impedance of free space
Z_n	—	Impedance
Δf_0	—	Change in frequency
ΔP	—	Change in Power Spectral Density
η	—	Efficiency
λ	—	Wavelength
τ	—	Integration time
ε	—	Antenna efficiency

Nomenclature

Acronym	Definition
AGC	— Automatic Gain Control
ATCR	— Air Traffic Control Radar
CW	— Continuous Waveform
DANL	— Displayed Average Noise Level
DME	— Distance Measuring Equipment
EMI	— Electromagnetic Interference
FITS	— Flexible Image Transport System
H	— Hydrogen
HartRAO	— Hartebeesthoek Radio Astronomy Observatory
ICASA	— Independent Communications Authority of South Africa
IF	— Intermediate Frequency
IGM	— Intergalactic Medium
ISSC	— International SKA Steering Committee
ISPO	— International SKA Project Office
ITU	— International Telecommunications Union
ITU-R RA.769-2	— ITU Recommendations on Radio Astronomy Number 769-2
L-band	— Frequency band between 1 - 2 GHz
LNA	— Low Noise Amplifier
LO	— Local Oscillator
LPD	— Low Power Devices
MHz	— Mega Hertz
NRF	— National Research Foundation
PRF	— Pulse Repetition Frequency
RA	— Radio Astronomy
RBW	— Resolution Bandwidth
RF	— Radio Frequency
RFI	— Radio Frequency Interference
RMS	— Root Mean Square

RRSG	—	Radar Remote Sensing Group
RSA	—	Republic of South Africa
SA	—	South Africa
SABRE	—	South African Frequency Band Re-Planning Exercise
SADC	—	Southern African Development Community
SKA	—	Square Kilometer Array
SA SKA	—	South African Square Kilometer Array
SASSC	—	South African SKA Steering Committee
SSESC	—	SKA Site Evaluation and Selection Committee
TDF	—	Trace Data Format
UHF	—	Ultra High Frequency
VBW	—	Video Bandwidth
VHF	—	Very High Frequency

Chapter 1

Introduction

1.1 Background

Radio Astronomy was, traditionally, assigned a band of frequencies at the higher end of the radio frequency spectrum. A band of frequencies at the lower end of the spectrum was designated for commercial applications and usage by other sectors. Industrialization and the accelerated growth in electronic, telecommunication, broadcasting and other related sectors led to an increased usage of frequencies designated for commercial use. This resulted in a greater need for bandwidth in the upper portion of the frequency spectrum [66]. As a result of this, an over-crowding of the Radio Frequency Spectrum designated for commercial use occurred and a need for more frequencies became apparent. This “encroachment” on the Radio Frequency Spectrum designated for Radio Astronomy meant that the band of spectrum which traditionally had been set aside for radio astronomy applications is now shared with other commercial applications. An over-lapping of the frequency bands is now evident and as a consequence, radio frequencies from nearby adjacent channels have become a constant source of interference on the radio astronomy telescopes, thus concealing the scientific benefits which can be derived from observing astronomical sources using radio telescopes.

A good example of signals which overlap or share frequency space is that of signals generated by the Distance Measuring Equipment (which occupies the 960 - 1400 MHz frequency band) used in aircraft for measuring distance and navigation and inter-galactic spectral line of neutral hydrogen (H) emissions which is detected in the frequency band of 1370 - 1427 MHz [9, 13, 14, 16, 76].

A portion of the radio frequency spectrum allocation in South Africa is tabulated in Table 1.2.

CHAPTER 1. INTRODUCTION

Table 1.1: Typical frequencies for *Distance Measuring Equipment* of Aircraft [13].

Service	Ground to Air	Air to Ground
Radar transponder	1030 MHz	1090 MHz
DME	962 -1024 MHz	1025 - 1150 MHz
DME	1151 - 1213 MHz	1025 - 1150 MHz

Further to this, more and more South Africans are becoming technologically savvy. Cellular telephony is no-longer the exclusive “toy” of the rich and famous, but has become a primary mode of communication (for both rich and poor) in urban and rural areas alike. This proliferation of cellular telephony, wi-fi and other bandwidth intensive devices and applications such as Facebook [79] and Mxit [80] has placed an upward pressure on the national telecommunications and broadcasting regulator (ICASA).

Further evidence of increased frequency usage and consequent frequency clash is contained in the Independent Communication Authority of South Africa’s (ICASA) endeavours referred to as SABRE-1 and SABRE-2. This South African Frequency Band Re-Planning Exercise (SABRE) which was aimed primarily at re-allocation, migration of certain services and sharing of certain frequency bands, arose out of the need for more frequency channels and an increased desire for more bandwidth usage [50, 51].

Annexure I of Rec. ITU-R RA.769-2 [43] defines the sensitivity of a single radio astronomy observation as:

$$\frac{\Delta P}{P} = \frac{1}{\sqrt{\Delta f_0 t}} \quad (1.1)$$

where ΔP and P are power spectral density of the noise, and Δf_0 and t are the bandwidth and integration time respectively. From the above formula it can be seen that more sensitive observations are made when the bandwidth is wider.

1.2 Radio frequency allocation in South Africa

The table below is a summary of the spectrum allocation in South Africa for the band 30 MHz to 1427 MHz. Only the frequencies for the major allocations is shown [83].

The table shows how the entire HF / VHF / UHF bands have been proliferated by various commercial or industrial applications. It also confirms the fact that not much spectrum allocation has been set aside for radio astronomy applications within these bands.

CHAPTER 1. INTRODUCTION

Table 1.2: Radio spectrum allocation in South Africa: 30 - 1427 MHz. This table was taken from *Lord (2000)[83]* and was verified by the author against that found in *Part 3 of the South African Telecommunications Act No. 103 of 1996*.

Frequency Band (MHz)	Main Allocations
30.01-74.8	Mobile / Fixed / Amateur
74.5-75.2	Aeronautical Navigation
75.2-87.5	Mobile / Fixed
87.5-108	FM Sound Broadcasting
108-137	Aeronautical Radionavigation / Aeronautical Mobile
137-138	Mobile-Satellite / Meteorological-Satellite / Space Operation
138-144	Mobile / Fixed
144-146	Amateur / Amateur-Satellite
146-148	Mobile / Fixed
148-149.9	Mobile-Satellite (E-to-S) / Mobile / Fixed
149.9-150.05	Radionavigation-Satellite / Land Mobile-Satellite
150.05-174	Mobile / Fixed / Maritime Mobile
174-238	TV Broadcast Channel 4 to 11
238-246	Mobile / Fixed
246-254	TV Broadcast Channel 13
254-328.6	Mobile / Fixed
328.6-335.4	Aeronautical Radionavigation
335.4-399.9	Mobile / Fixed
399.9-400.5	Radionavigation-Satellite / Land Mobile-Satellite
400.5-400.15	Standard frequency and Time Signal
400.15-401	Mobile-Satellite / Meteorological-Satellite / Space Research
401-406	Meteorological Aids / Space Operation (S-to-E)
406-406.1	Mobile-Satellite (E-to-S)
406.1-430	Mobile / Fixed
430-440	Amateur Radio Allocation
440-470	Mobile / Fixed
470-854	TV Broadcasting Channels 21-68
854-862	Fixed
862-960	Mobile / Fixed
960-1215	Aeronautical Radionavigation (DME / Secondary Surveillance)
1215-1240	Radionavigation / Radiolocation / Satellite (LPD)
1240-1260	Radionavigation / Radiolocation / Amateur (ATCR)
1260-1300	Radiolocation / Amateur (ATCR)
1300-1350	Aeronautical Radionavigation (ATCR)
1350-1400	Fixed / Mobile / Radiolocation
1400-1427	Radio Astronomy / Space Research

1.3 Problems of Radio Frequency Interference on Radio Telescopes

Radio Frequency Interference from mobile, terrestrial and airborne (DME of aircraft) sources pose a threat to the future of Radio Astronomy [16]. This is due to the fact that the power levels of RF signals originating from these sources are many decibels higher than the levels of signals arriving from distant cosmic sources and thereby “hide” the desired cosmic signals thus making their detection difficult.

This problem is further compounded by the fact that radio telescope receivers are extremely sensitive as they are designed and built to detect minute signals originating from the furthest reaches of our universe. Typical signal strengths detected by radio telescopes are in magnitudes of 10^{-26} Watts per square metre of receiving area per hertz of frequency (one Jansky (J_y)).

By contrast, however, man-made impulsive noise or RFI is comparatively higher and thus pose a major problem to radio telescopes as they can sometimes drive the low noise amplifier (LNA) of the telescope radiometer into saturation and ultimately cause irreversible and permanent damage to the telescope receivers (*according to ITU-R RA.769-2[43], the tolerable interference power level should be no more than 1% of the receiver noise power*). Saturation of the receiver leads to non-linearity, and operating the receiver in its non-linear region leads to the generation of spurious signals such as intermodulation products and their harmonics. These problematic signals, which are difficult to cure, can be interpreted and confused for good astronomy data by novice astronomers. Even seasoned astronomers for that matter.

According to [14], 10 -20 % and sometimes all of the pulsar data detected by the radio telescopes at Aracebo and GBT are infected by man-made noise.

The problems of RFI on radio telescopes is so huge that for frequencies below 40 MHz the interference effects of a “transmitter situated anyway on earth” can be observed on radio astronomy data [43].

1.4 The Square Kilometre Array (SKA)

In an attempt to further enhance the study of astronomy, the International Astronomy Community embarked on an international project to build a new generation radio telescope with an operating frequency range of 70 MHz to 22 GHz. This telescope which is supposed to be 100 times more sensitive than current radio telescopes should be able to detect extremely small signals with power levels in the range 10^{-26} W/m² and some with incoming signal to noise ratios (SNR) in the region of -30 to -60 dBs[2]. The benefits of this project are wide and varied. Further information on the advantages and scientific ben-

CHAPTER 1. INTRODUCTION

efits of this radio telescope can be found in the CRAF handbook for Radio Astronomy[76] and many other scholarly publications.

The proposed radio telescope will comprise of an array of antennas with a combined effective receiving or collection area of 1000,000 m² or 1 square kilometre. The name Square Kilometre Array is thus derived from this association. It has been suggested that 12 m cylindrical dishes be used for the construction of this instrument. This would entail linking and aggregation of some 8842 antenna tiles in order to achieve the envisaged 1000,000 m² receiving area. By linking so many antennas, it is hoped that the telescope will achieve a larger collection area than currently existing telescopes and this in turn will provide longer baselines within the operating frequency range whilst looking at a greater portion of the sky.

The cost associated with the development, design and construction of this gigantic telescope is “astronomical”. Current cost estimates range between \$ 1 billion to \$ 4 billion dollars depending on the size of telescope dishes. It is envisaged that construction will commence in 2015.

In light of the above discussion, construction of the SKA radio telescope, is governed by the following key factors:

1. the cost of building this radio telescope,
2. identification and location of a RFI free site,

Because of the huge cost associated with this venture, proper identification, location and selection of a suitable site is critical.

Like other radio telescopes, the SKA is not immuned from the negative effects of some RFI. One of the many suggested ways of mitigating the effects of terrestrial and airborne radio frequency interference on radio astronomy observatories, is simply to build radio telescopes in outlying and less densely populated remote areas “where the density and strength of unwanted man-made signals is greatly reduced”[3].

This entails identification of an area “where the interference received by the radio astronomy station concerned does not exceed the thresholds necessary for this station to operate at its maximum sensitivity”[4] i.e where a radio-quiet environment exists. As an example, it has been established at Hat Creek Radio Observatory and at the Green Bank Telescope that terrain suppresses RFI by as much as 100 dB’s. This is in addition to the normal propagation loss [14, 27]. The theoretical propagation studies and digital terrain models conducted by the South African SKA team confirmed the shielding effect of terrain on RFI [27]. From the above, and given the sensitivities that is to be achieved, it follows therefore that “the choice of a radio-quiet site is paramount”[5].

However, choosing an appropriate site is often tedious, challenging, difficult and problematic and requires that RF Measurements be conducted first, in order to rule out the

CHAPTER 1. INTRODUCTION

presence of any unwanted electromagnetic emissions and to gauge the amount and level of possible interference at that particular site. This measurement data could be used to enable ranking of individual sites according to “how good or bad they are” in relation to each other. The problem of choosing an appropriate site is further elevated by the fact that a number of countries have registered their intention of hosting the SKA. The countries bidding to host the SKA are Australia, China, South Africa and Argentina. These countries are not only motivated by the beautiful contribution to astronomy that this project will impart, but by the financial and economic “spin-offs” (in the form of foreign direct investment, tourism and employment) that this project is likely to generate. Because of the huge economic and financial gain to be derived, there is a slight possibility of over-exaggeration of the RFI levels by prospective host countries. As a result, a working group (on RFI measurements) of the International SKA Site Evaluation and Selection Committee was established and immediately compiled a document called the “RFI Measurement Protocol for candidate SKA Sites”. This document is a guideline which seeks to establish an international standard or norm into how the measurements should be conducted, what type of equipment to use, the calibration procedures to adopt, the number and modes of measurements to perform, as well as, the documentation required at the end of the measurement process. This protocol also details the frequency ranges to be scanned (and at what resolution bandwidths), as well as, dictates the dwell times to be achieved.

As of late, only two countries, South Africa and Australia, are still in the running to host the SKA. The other countries’s bid has been rendered unsuccessful.

South Africa’s trump card is due to its geographical advantage rather than the suitability of its site on the basis of lowered RFI emissions. Therefore, the need for this study is still relevant.

1.5 Implementation of the SKA Protocol in South Africa

In order to facilitate and advance the RFI measurements process in South Africa, a South African chapter of the SKA was established and referred to as the South Africa SKA Steering Committee (SASSC)[52]. This organization which is partly funded by both the South African Government as well as the International SKA Steering Committee, was mandated to advance the bid process. Similar to the SKA, the SASSC established a working group to perform RFI measurements. This working group headed by Professor Justin Jonas and Dr G Nicholson (and here-in referred to as SA SKA) designed and constructed three RFI Measuring Systems, RFI System 1, 2 and 3 [17, 27]. These three systems are similar in design and operation with the exception of system 2 which was designed with an additional amplification stage. In my study, I concentrated particularly on RFI System 2. This system was used extensively at the Karoo core site referred to as K3.

Other important functions performed by the SA SKA team includes amongst others:

CHAPTER 1. INTRODUCTION

1. Drafting a guideline into how the measurement campaign was to be conducted[17],
2. Conducting field RFI measurements locally and in neighbouring Southern African Development Community (SADC) countries[27],
3. Compiling the required bid documentation associated with the measurement campaign and tendered the bid document to the International SKA Steering Committee in support of its intention to host the Square Kilometre Array [27].

1.6 The SKA RF Measuring Systems

The SA SKA Radio Frequency Interference Measuring System is a general purpose receiving instrument, designed and developed by the South African SKA team, with the sole purpose of detecting and receiving a wide variety of RF signals which have the propensity to interfere with the normal workings of a radio telescope. This system was designed and constructed in order to adhere to the technical specifications outlined in the table below.

Table 1.3: Summary of technical specification which the SA SKA RFI systems had to adhere to (from [9])

Sensitivity	Defined by ITU-R RA.769-2
Frequency Band	70 MHz to 22 GHz
Polarization	Vertical and Horizontal
Antenna Height	$5\text{m} \pm 1\text{m}$
Receiver Temperature for Mode 1	$T_R \leq 3 \times 10^4\text{K}$
Receiver Temperature for Mode 2	$T_R \leq 300\text{K}$
Coverage	Entire 360° of azimuth

There have been numerous references to the system as being an RFI measuring system, however, during my research, it was found that the system does not measure radio frequency interference but, rather, measures the power levels of RF signals present at its antenna surroundings. The question to be asked is: how do you measure interference? The system designed, does not come close to measuring interference, but rather, it measures the power levels of radio frequency signals which could impact negatively or have the undesired effect of interfering with the normal operation of the Radio Telescope equipment. To say, therefore, that the system measures Radio Frequency Interference is a misnomer and is misleading in the least. However, it is believed that this error emanated from the requirements specification of the ISSC entitled, “RFI Measurement Protocol for Candidate SKA Site”. It was also discovered that the authors of the “RFI Measurement Protocol for

CHAPTER 1. INTRODUCTION

Candidate SKA Site” had previously written numerous other documents with similar misleading titles [63, 64]. Therefore, this error was left unchecked and simply carried over during their drafting of the SKA requirements protocol. It is regrettable therefore, that the South African team has used the same title in their bid documentation. Similar error was also detected in the Chinese submission. Although, I was not privy to the Australian Bid documentation, it was found that the Australians referred to their systems (correctly) as RF measuring systems rather than RFI measuring systems.

For the sake of conformity, we shall use RFI Measuring Systems, however, it should be borne in mind that we are referring to RF measuring systems.

1.7 Objectives of Dissertation

The terms of reference of my research are to demonstrate an understanding of the functionality and performance of scanning receivers such as spectrum analyzers, and to use the knowledge gained to independently assess, verify, validate and to some extent “rubber stamp” the RF measurement work previously performed by SA SKA. By verify and validate, I mean, to go over their work and to see whether the RFI measuring systems and the RF measurements were designed and conducted respectively in accordance with the guidelines and stipulation of the SKA protocol.

My research is guided by the following key performance areas or specific objectives:

1. Perform an independent audit of the equipment used in the RFI Measurement systems that were designed and built by the SA SKA team and discuss how these systems measure up or compare against the requirements of the “Protocol”;
2. Perform an independent analysis of a few samples of the raw RFI field measurements obtained at the core site. This process involves going over the work of SA SKA (with a fine comb) and verifying that they captured and done everything correctly. This includes, but not limited to, taking the uncalibrated raw field measurement data obtained from SASKA and (by working backwards) independently calculating the spectral flux density present in the area where the measurements were conducted and comparing the results with that achieved by the SA SKA team;
3. Find out and discuss how RF measurements are conducted, in line with best practices in RF metrology;
4. Analyse, review, and objectively assess and understand the content of the “RFI Measurement Protocol for Candidate SKA Sites”;
5. Ensure that the guidelines that were followed to conduct measurements comply with the recommendations of the “SKA Protocol” and if it does not explain the reasons for non-compliance.

CHAPTER 1. INTRODUCTION

6. Discuss the implication of increasing the dwell time, RBW, sweep rate and sweep range and “shed more light” on the effects of measuring signals with varying or different duty cycles such as pulsed DME.

In my study, I focussed specifically on analyzing the available SA SKA data for the frequency range of 70 MHz to 150 MHz. This band is important to astronomy for a number of reasons.

First and foremost, it has long been hypothesized through “big bang cosmology”, that shortly after the “big bang”, the extreme heat generated reduced matter to its composite ions and that some 500,000 years later, this plasma cooled sufficiently enough to recombine thus forming hydrogen [23, 77]. This period of recombination is generally referred to as the *Epoch of Re-ionization*. The intergalactic medium (IGM) is believed to largely consist of re-ionised hydrogen and helium gas. There has been increasing scientific evidence which seem to suggest that these discrete spectral H (Hydrogen) emission lines which normally occur in the frequency range 1370 - 1427 MHz (*See Table 2.4 in Chapter 2*) are (as a result of the expansion theory of the universe) and through the Doppler Effect, reshifted to the band of 10 MHz to 240 MHz. *Chippendale(2006)* suggests that the redshift frequency, in fact, lies somewhere in the band between 45-200 MHz. It follows therefore, that, studying these hydrogen and helium spectral emission lines, would help scientists unravel the mysteries surrounding the birth of our universe.

Secondly, observations have revealed that Pulsars are more pronounced and observable somewhere in the frequency range between 50 MHz and 600 MHz. Since the frequency range, 70 MHz - 150 MHz is common to both cases, the signals occupying this frequency range is important and warrants an intense study in order to determine their power levels so as to help classify and characterize the environment at the core site.

1.8 Summary of Results

This section gives a brief explanation of the data that was used, the findings obtained and the method that was used to arrive at these results. Detailed discussion in respect of the above three issues is given in the relevant chapters.

1.8.1 Sources of Data

The measurement data used in this experiment was collected by the SA SKA team during a two day measurement campaign commencing on 24 November 2005 and ending on 25 November 2005. The data was provided to Dr Richard Lord of the *meerKAT* Project in CD format. Dr Richard Lord downloaded this data onto the RRSg database called DATA under directory which the author was able to access, albeit with limited access.

CHAPTER 1. INTRODUCTION

Since the author was not party to the hand-over of the disc nor was he present during the downloading of this data, he cannot conclusively *vouch* for its integrity. However, it is my humble belief that no manipulation or addition to this data was performed.

1.8.2 Method of Procedure and Performance Criterion

It is well accepted in RF metrology that using an uncalibrated system to measure power will introduce flaws and discrepancies to the measured results [71]. This situation is undesirable. If one takes the measurement data obtained from the output of a spectrum analyzer and by working backwards calculate the power received at the input of the system, one is able to determine the theoretical equivalence of the power flux density in which the antenna and system is immersed. The formulas and theory utilised are discussed in subsequent chapters.

Our plan was to use the theoretical values of parameters published by the manufacturers of the components making up the system and by using the indicated tolerances determine both the *worst* case and *best* case scenarios of the spectral flux density and to compare these to the actual values derived by SA SKA. By doing this we hoped to achieve the following:

1. we hoped to obtain values of spectral flux density which was to some extent equivalent to that obtained by SA SKA. In other words we hoped that the plots of spectral flux density versus frequency as generated by the SA SKA team will be strongly correlated with that performed by us using MATLAB,
2. we believe that the spectral flux density values mentioned in 1 above, should lie within the range determined by the *worst* case and *best* case scenarios.

It was our belief that by doing this experiment, we can test the “mettle” and effectiveness of the calibration techniques employed by SA SKA team and this can be used as a good indicator of the performance of the RFI system.

In order to test our hypothesis we conducted a number of experiments and processed the data using different approaches which varied slightly. The reason for the number of methods is due to the fact that, it was not clear from the available documentation how the data was processed. At a meeting with Professor Justin Jonas, it was pointed out that the median values were used. However, Mr Paul Manners (of the SA SKA team) who coded the software used, seems to have had a different view to that of Prof Justin Jonas. The detailed data processing procedures and methods used by Mr Paul Manners and that were used by the author to arrive at our results, is documented in subsequent chapters.

CHAPTER 1. INTRODUCTION

1.8.3 Findings

The various data processing procedures resulted in a number of options being generated with differing results for each option. These options are described below.

In OPTION 1, ten values of each column for all six files were binned together and the statistical analysis was performed on all values prior to the calculation of spectral flux density. There were 5 columns in each file resulting in 300 data values being binned.

OPTION 2, was about finding the median of each column first, and then binning all 30 medians and working out the statistics prior to the determination of spectral flux density.

In OPTION 3, the spectral power flux densities were calculated and binned together. Flux densities were then sorted and the statistics calculated.

A summary of the findings for MODE 1 measurements are recorded below for each option. MODE 1 Measurements are those that were performed to rule out or indicate the presence of strong RF signals which could impact negatively on the operation of the radio telescope. The assumptions used during the derivation of these spectral flux density plots are also indicated.

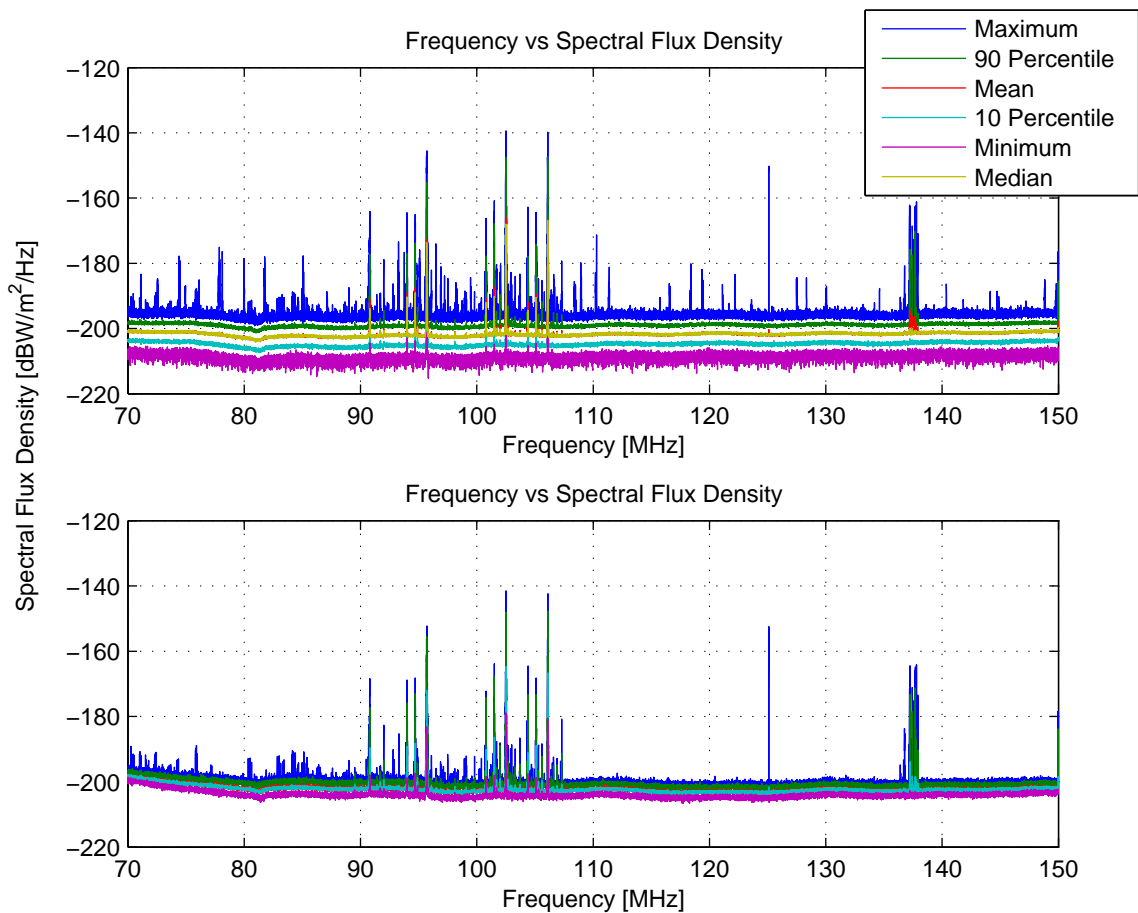


Figure 1.1: Radio Frequency Interference plot for the 70 - 150 MHz band: OPTION 1- (Top) Reprocessed (Bottom) SA SKA Measurement. It can be seen (*through direct observation*) that the (Top) plot has more spectral activity than the (Bottom) Plot.

CHAPTER 1. INTRODUCTION

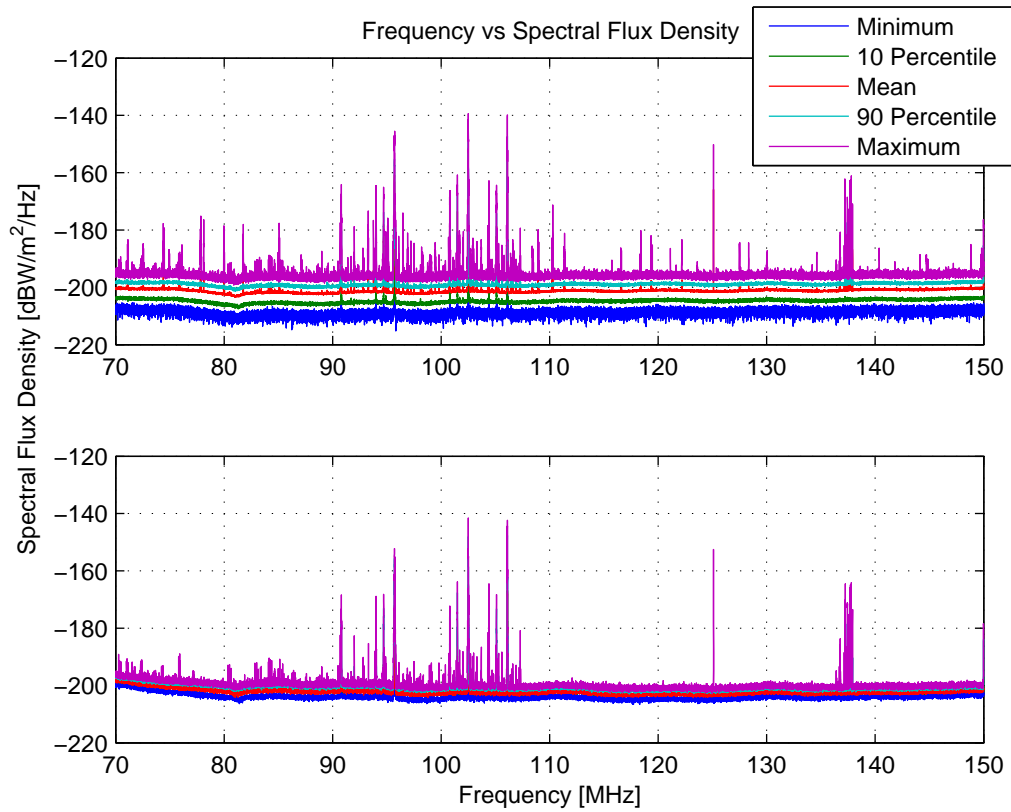


Figure 1.2: Radio Frequency Interference plot for the 70 - 150 MHz band: OPTION 2-(Top) Reprocessed (Bottom) SA SKA Measurement

CHAPTER 1. INTRODUCTION

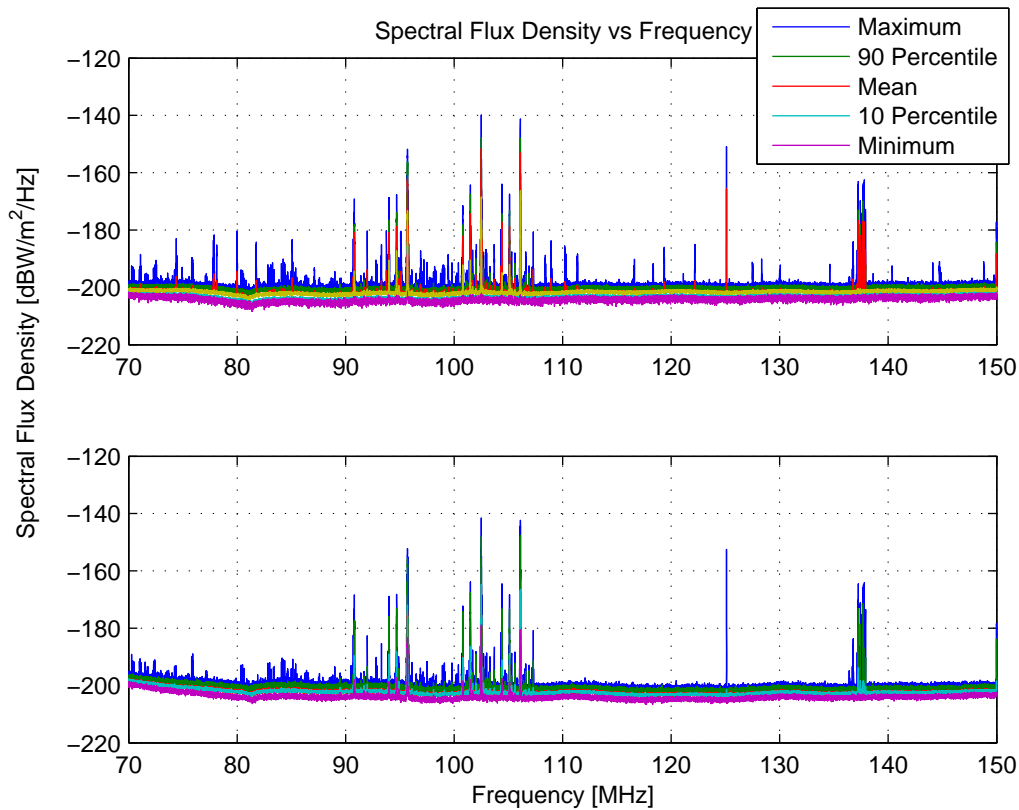


Figure 1.3: Radio Frequency Interference plot for the 70 - 150 MHz band: OPTION 3-(Top) Simulation (Bottom) SA SKA Measurement

In all three options, the top plot was generated by the author, after careful calibration of the data, using MATLAB. The detailed data processing procedures and the formulae used are documented in the respective chapters. An obvious observation is that the Reprocessed (top) plots show far more spectral activity than that which was performed by SA SKA. The reasons for the differences are discussed later. From the plots, it can be seen that the region of strongest activity is that due to the FM Broadcast band (87 - 108 MHz) in which the signals reach a high of $-140 \text{ dBW/m}^2/\text{Hz}$. The signals in the region between 137 and 138 MHz are also more pronounced with a high of $\pm 161 \text{ dBW/m}^2/\text{Hz}$. From the table of frequency allocation (Table 1.2), the latter region is allocated to *Mobile-Satellite / Meteorological-Satellite / Space Operation*.

1.8.4 Significance of findings

1. Our findings revealed that there is a strong correlation between the plots of spectral flux density versus frequency as performed by the SA SKA team and the MATLAB audited results by the author and that these spectral flux density results were within their tolerance levels.
2. The differences between SA SKA graphs and the replicas derived by the author through MATLAB processing revealed that the SA SKA team had in some areas (

CHAPTER 1. INTRODUCTION

particularly concerning the graph of frequency channel versus maximum spectral flux density) massaged the data to such an extent that *smooth* graphs were obtained. However, the averaging effect were not of such a nature that they could disguise strong signals or cause them to be indistinguishable, but merely attempted to eradicate system induced RF disturbances. However, the possibility of smoothing out some of the low level man-made RF signals, thereby sabotaging the purpose of the measurement system, is still present.

3. The processes and procedures followed did not differ much from the international best practices with the exception that in RF metrology, the Electromagnetic Field strength and the RMS (Root Mean Square) power levels are the key determinants [71, 60].

1.9 Structure of the Dissertation

In order to avoid confusion and to facilitate proper understanding of the proposed research topic, an attempt is made to present the material under scrutiny, in a concise, comprehensible and structured manner.

First and fore-most, familiarity with the title of the research topic and the problem statement is of utmost importance. These have already been discussed in the title page and in the introduction respectively.

Chapter 2, introduces Memo 37 (RFI Measurement Protocol for Candidate SKA Sites) and dissects the SKA Protocol into various parts in order to assist in discussing the protocol in an easy, simplistic and comprehensible manner. The contents of the protocol is grouped into the following sub-headings:

1. Scope
2. Technical Specification,
3. Equipment,
4. Calibration procedure,
5. Measurement procedure,

Chapter 3 is a survey of relevant literature and is dedicated to the review of key technical concepts that have been referred to, in the protocol, as well as, detailing the operation of the equipment assented to, in the protocol. The equipment mentioned in the protocol are Low Noise Amplifiers (LNA), antennas, high pass filters, spectrum analysers, signal processors and data storage and acquisition devices. The theory behind these equipment is studied in detail. The type, classes and sources of RFI that is likely to be encountered

CHAPTER 1. INTRODUCTION

during the measurement campaign is documented and the characteristics of the RFI at core sites are presented.

In Chapter 4, a basic block diagram of the radio frequency interference measuring system, as designed, built and deployed by SA SKA, is outlined. Further to this, field measurements as obtained from the SA SKA are thoroughly reviewed, assessed and analysed. An audit of the equipment used in the design is thoroughly conducted. The competence and capability of the three RFI Measurement systems to achieve the desired functionality is assessed. The method used to shield and internally arrest locally generated RFI is discussed in detail.

The interpretation and implementation of the SKA protocol in South Africa is investigated and the *critical* issues encountered during the implementation of the protocol are outlined and further analysed. The performance of the spectrum analyser as a scanning receiver is reviewed in greater depth.

Chapter 5 is an in-depth analysis of a sample of the raw field data obtained during the measurement campaign. A comparative study between the spectral flux density (sfd) results obtained by the SA SKA team using measurement data and the findings obtained by the author is undertaken in this chapter. The measurement data obtained from the SA SKA team was independently reprocessed, by the author, using MATLAB.

We conclude, in Chapter 6, by summarizing our work, discussing the challenges encountered and making recommendations.

Chapter 2

Summary of the SKA Protocol

In September 2004, the International SKA Project Office (ISPO) issued a Request for Proposals (RFP) for the siting of the SKA. As part of this call for proposals, the “RFI Measurement Protocol for Candidate SKA Sites” was disseminated. The document was written in order to inform prospective bidding countries as to what is required by the International SKA Project and served to assist proponents in putting forward adequate, satisfactory and competitive proposals.

The purpose of this chapter is to highlight some of the key technical issues addressed in the document and which should be adequately attended to by the SA SKA team in order to deem their measurement campaign a success. It should be borne in mind that a system is only as successful as its ability to meet or exceed the expectations and requirements of the user(s) or customer(s). If it does not meet customer’s needs, it is considered as being defective[81]. In this case the customer is the International SKA Organization.

Although my research was largely a “study”, part of my objectives were to perform an independent audit of the work of the SA SKA team. Therefore by writing this chapter, I wanted to be able to emphatically state that “*this is what the SA SKA was supposed to do and this is what they did*”. From this assessment, I will be in a better platform to draw a more conclusive argument as to the correctness and appropriateness of the work of the SA SKA team.

2.1 Scope

One of the key functionality required from the proposed system is the ability “to identify RFI emanating from both land-based and airborne sources,” with the exception of RFI originating from satellites as it was “considered equal” at all sites. The question is, “*was the system developed by SA SKA able to identify RFI coming from both the land and from the sky?*”

2.2 Technical Specification

In order to perform the function discussed in Section 1.5 above, the system had to adhere to the technical specifications as tabulated in Table 1.3 of Chapter 1. This table is duplicated below for easy reading.

Table 2.1: Summary of the technical specifications (from [9])

Sensitivity	Defined by ITU-R RA.769-2
Frequency Band	70 MHz to 22 GHz
Polarization	Vertical and Horizontal
Antenna Height	$5\text{m} \pm 1\text{m}$
Receiver Temperature for Mode 1	$T_R \leq 3 \times 10^4 \text{K}$
Receiver Temperature for Mode 2	$T_R \leq 300\text{K}$
Coverage	Entire 360° of azimuth

2.3 Recommended equipment

It was recommended that the following equipment be used in order to develop the RFI Measurement System:

1. Log-periodic antennas for horizontal polarization at low frequencies;
2. Horn antennas for horizontal polarization at high frequencies;
3. Discone antennas for vertical polarization;
4. Scanning receiver such as a spectrum analyser;
5. High pass filters;
6. Signal processors , and
7. Data storage and acquisition devices such as high speed computers.

For antennas, it was not mandatory that all three types of antennas be used. As an example, it was possible to use two log-periodic antennas (one for low frequencies and the other for high frequencies) just as long as they are rotated in such a way as to intercept the horizontally polarized electro-magnetic waves as well as the vertically polarized magnetic waves. However, it was important that the antennas be able to cover the entire 360° field of view in the azimuth plane. Log-periodic antennas are highly directional and thus a number of antenna pointings may have had to be affected in order to comply with the 360° coverage requirement of the protocol. The number of antenna pointings required depends on the beamwidth (taken at the 6 dB point) of the radiation pattern of the antenna.

CHAPTER 2. SUMMARY OF THE SKA PROTOCOL

There is no mystical reason for taking the beamwidth at the -6dB point, except that the power at this point is reduced to one quarter whilst a sufficiently large beamwidth is still achievable. The antennas and equipment used by the SA SKA for the construction of RFI System 2 is detailed in Chapter 4.

2.4 Calibration Procedure

The protocol dictates that calibration of the equipment must be performed once every 24 hours and before the commencement of the measurement. It further states that calibration is to be done in the field using an ambient temperature load with a known temperature. Calibration procedure is to be thoroughly documented. No particular method of calibration was, however, specified.

The SA SKA team was able to meet this specification by ensuring that the system designed was able to perform in-field calibration. The Agilent Noise Source (346C) with known noise temperature was used and implemented as shown in Figure 4.3. The frequency range of operation of this device is as shown in Appendix B.

2.5 Measurement Procedure

Measurements are grouped into two broad classes i.e Mode 1 and Mode 2 measurements.

2.5.1 Mode 1

Mode1 measurements are based on the measurement of strong RFI signals. These strong signals could have a negative impact on the linearity of the receivers and “may rule out certain sites or influence the design of SKA receivers”[9].

The protocol specified that the flux (at the horizon or zero elevation) S_{0h} , of the RFI signals which is necessary to induce a signal of -100dBm at the terminals of the antenna. S_{0h} be accordingly calculated from[9]:

$$S_{0h} = \frac{4\pi k T_{sys} f^2}{c^2 \epsilon} \quad (2.1)$$

and that the power induced at the terminals of the antenna be determined from[9]:

$$P_s = \frac{S_{0h} B_s \epsilon c^2}{4\pi f^2} \quad (2.2)$$

The protocol further, specifies the length of time that a channel is examined (dwell time), the resolution bandwidth (spacing between centre frequencies), as well as, the number of

CHAPTER 2. SUMMARY OF THE SKA PROTOCOL

measurement cycles or repetitions required per band of frequency. The total time taken to perform measurements is calculated from the following equation:

$$t_{total} = \frac{(f_2 - f_1) \times t_d \times Repts}{RBW} \quad (2.3)$$

where f_2 and f_1 are the upper and lower frequencies respectively, D is the dwell time, $Repts$ is the number of measurement cycles and RBW is the resolution bandwidth.

2.5.2 Mode 2

Mode 2 measurements entail measurements of weak RFI. This mode of measurements define the sensitivity levels. Mode 2 measurements could adversely affect the detection of cosmic signals as their power levels could be as low as that of the cosmic signals. Removal of such low level RFI may cause the signals of interest to be eradicated, thus losing valuable information. Consequently, weak RFI have a tendency to “obscure signals of interest”. My analysis did not cover this mode.

CHAPTER 2. SUMMARY OF THE SKA PROTOCOL

Table 2.3: This table shows the measurement schedule of Mode 2 Measurements. The table shows the *Frequency Band* in GHz, *RBW* in kHz, *Dwell Time* in ms and S_{0h} in dB (Jy). It also shows the significance of the various bands (from[9]).

Frequency Band	RBW	Dwell Time	S_{0h}	Subtotal	% of subtotal	Uses
0.150-0.153	1	100	52	300	1.31	Continuum
0.153-0.322	3	10	54	564	2.46	
0.322-0.329	3	1000	51	2334	10.21	DI
0.329-0.406	30	10	56	26	0.11	
0.406-0.410	30	1000	43	1334	5.83	Continuum
0.410-0.608	30	10	57	66	0.29	
0.608-0.614	30	1000	46	2000	8.76	Continuum
0.614-1.000	30	10	61	129	0.56	
1.000-1.370	30	300	58	3700	16.20	Continuum
1.370-1.427	30	1000	58	1900	8.32	HI, SETI
1.427-1.606	30	100	64	597	2.61	SETI
1.606-1.723	30	1000	60	3900	17.08	OH, SETI
1.723-2.655	30	10	70	311	1.36	
2.655-2.700	100	1000	62	450	1.97	Continuum
2.700-3.300	100	10	72	60	0.26	
3.300-3.400	100	1000	63	1000	4.60	CH
3.400-4.800	100	10	74	140	0.61	
4.800-5.000	100	1000	67	2000	8.72	H ₂ CO
5.000-6.600	300	10	75	54	0.23	
6.600-6.700	300	1000	67	334	1.45	CH ₃ OH
6.700-8.600	300	10	77	64	0.28	
8.600-8.700	300	1000	69	334	1.45	³ He ⁺
8.700-12.100	300	10	79	114	0.49	
12.100-12.200	300	1000	72	334	1.45	CH ₃ OH
12.200-14.400	300	10	82	74	0.32	
14.400-14.500	300	1000	74	334	1.45	H ₂ CO
14.500-18.300	300	10	84	127	0.55	
18.300-18.400	300	1000	76	334	1.45	C ₃ H ₂
18.400-22.00	300	10	86	120	0.52	
TOTAL				23 025	100.00	

2.6 Measurement times

One of the critical issues facing the design of any RFI measuring system is that of measurement time. This issue, is important both from a cost point of view, as well as, from a system design point of view. In this section we present a number of factors which affect the measurement time. The measurement time of a spectrum analyzer is affected by such internal components as IF band limiting filters, bandwidth and type of filters, envelope detectors, video bandwidth and video filters, trace averaging and post-readout integration[20]. A basic block diagram of a typical spectrum analyzer is shown in Figure

CHAPTER 2. SUMMARY OF THE SKA PROTOCOL

3.5.

In this section we explore such terms as scan time, dwell time, rise time, sweep time, transient time and settling time.

Sweep time is defined as the time it takes to record the whole frequency spectrum of interest[21, 22]. It is a very important feature of a spectrum analyzer. A spectrum analyzer whose sweep time is indefinite is of no significant use. As already mentioned, the sweep time is controlled by the transient response of the IF filters according to the following expression, $t_{resp} = \frac{1}{RBW}$ [20]. In practice, however, Millenaar (2005)[20], found that the sweep time is affected by a combination of a number of variables such as RBW, span, start and stop frequency, filter type, averaging cycles and number of data points per scan and that the practically obtained sweep times exceed that obtained theoretically by calculation, by a factor ranging from 1 to as high as 20.

The transient response of the filters represent the minimum time allowed for proper amplitude detection. Therefore, the minimum permissible sweep time should equal to the transient time of the filter response. The trade-off between the sweep time and the resolution bandwidth (RBW) is governed by the following equation:

$$t_{sw} = k \frac{(Span)}{RBW^2} \quad (2.4)$$

The equation implies that the greater the resolution bandwidth, the smaller the sweep time. The minimum permissible sweep time that can be attained is limited by the transient time of the IF filters and the video filters [21]. Since both filters have their own response times and for a situation where the VBW is less than the RBW, the sweep time is described as [22, 20]:

$$t_{sw} = k \frac{(Span)}{(RBW)(VBW)} \quad (2.5)$$

The IF and video filters determine the resolution bandwidth (RBW) and video bandwidth (VBW) respectively. The filters require a finite time to charge and discharge. In R-C filter circuits, such charging and discharging or decay times are constrained by the resistors and capacitors employed in the circuits. A rule of thumb usually employed is that the time required for adequate charging of capacitors without a significant loss of signal amplitude should be greater than the time constant t_c , where $t_c = R \times C$ and R,C is the resistor and capacitor value respectively. Passing a signal through the filters too quickly would result in the signal amplitude being reduced. The time at which the signal needs to stay in the pass band of the filter is therefore given by[22]:

$$t_{pb} = \frac{(RBW) t_{sw}}{Span} \quad (2.6)$$

CHAPTER 2. SUMMARY OF THE SKA PROTOCOL

This is the time spent on each frequency bin. The frequency bin is characterized by its size in terms of both frequency and time. The size of the frequency bin is determined by

$$\text{Frequency Bin} = \frac{\text{Span}}{(\text{trace points} - 1)} \quad (2.7)$$

A signal will dwell in this bin for a time of t_{bin} , where

$$t_{bin} = \frac{\text{Sweep time}}{(\text{trace points} - 1)} = \frac{t_{sw}}{(\text{trace points} - 1)} \quad (2.8)$$

Since the time spent in the pass band is the same as the time spent in each frequency bin, from Equations 2.6 and 2.8,

$$t_{pb} = t_{bin} = \frac{(RBW)t_{sw}}{\text{Span}} = \frac{t_{sw}}{(\text{trace points} - 1)}$$

This implies that

$$RBW = \frac{\text{Span}}{(\text{trace points} - 1)} \quad (2.9)$$

Since Equations 2.7 and 2.9 are equal, the implication is that the size of the frequency bin is given by the RBW. This is an important assessment.

The charging time of the filter capacitors is given in terms of the *rise time* of the signal and is defined as the time required for a signal to traverse from 10% to 90% of its final value and is mathematically expressed as [24]:

$$t_r = \tau = \frac{k}{RBW} \quad (2.10)$$

where k is the constant of proportionality and is normally in the range of 2 to 3 for filters used by the Agilent spectrum analyzers [22].

Since capacitors are integrating devices, the rise time is also known as integrating time (τ). The integration time (τ) depends on the settling time of the filters used [10]. A signal will under normal circumstances, overshoot its final value. As a result ringing effects are introduced and a finite time is needed for the signal to settle to within some specified amount of the final transition time. This finite time is known as the *settling time* [24].

According to Horing (1998) [10], the settling time together with the integration time make up what is known as the *dwell time*. The dwell time is defined as the time taken to examine a single channel [5] and is expressed mathematically as:

$$t_d = t_{syn} + \tau \quad (2.11)$$

where t_{syn} consists of the settling time of the synthesizer or filters and the time required for

CHAPTER 2. SUMMARY OF THE SKA PROTOCOL

signal processing. The table below shows the specified Mode 1 dwell times as abstracted from Table 1 of the protocol document. These dwell times must be adhered to when performing measurements, otherwise it may be viewed as operating outside the required specification.

Table 2.4: Dwell times (from [9])

Frequency Band (GHz)	RBW (KHz)	S _{0h} (dB)	Dwell (ms)	Reps	Total (s)
0.070-0.150	3	-166	10	5	1334
0.150-0.300	3	-159	10	1	500
0.300-0.800	30	-163	10	1	167
0.800-0.960	30	-155	10	20	1000
0.960-1.400	1000	-168	0.002	10 ⁶	900
1.400-3.000	30	-150	10	1	534
3.000-22.00	1000	-158	10	1	190
TOTAL					4624

From Equation 2.11, in order for the dwell time to be equal to the integration time, the synthesizer time, t_{syn} , must be equal to zero. However, in practice the synthesizer and filters would have time delays and therefore, t_{syn} , would never be equal to zero. and consequently when the measurements are being conducted, care must be taken to ensure that the dwell time exceed the integration time of the filter components of the measurement system by a factor equal to the synthesizer time.

Since $\tau = t_r$, Equation 2.11 can be written as:

$$t_d = t_{syn} + t_r \quad (2.12)$$

From Equation 2.12, it is clear, therefore, that for precise and accurate measurements to be achieved, the dwell time should not be less than or equal to the rise time or the integrating time. This assertion is consistent with the findings that “the dwell time does not correspond with the effective integration time” as concluded by Millenaar (2005)[20]. Using trace and post-readout averaging, Millenaar (2005) concluded that the integration time is equal to

$$t_\tau = NM \frac{k}{RBW} \quad (2.13)$$

where N, is the number of traces averaged in the spectrum analyzer and M, is the number of averaged scans averaged in the software.

Another important factor which affects the measurement cycle is that due to pulsed waveforms. The next section presents a comprehensive approach to dealing with the issues

CHAPTER 2. SUMMARY OF THE SKA PROTOCOL

encountered as a result of the presence of burst mode, pulsed mode and frequency hopping signals with respect to radar, CDMA and DME applications. Attention is strictly dedicated to the time constraint problem. Concepts such as duty cycle, rise times, sweep times and dwell times, and their contribution to the measurement debate are revisited.

2.7 Pulsed Signals

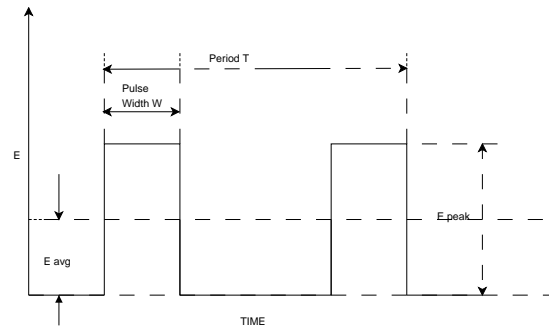


Figure 2.1: Basic Characteristics of a pulsed waveform showing the Marks and Spaces. The space gives the receiver a false sense of pulse inactivity which is not necessary the case.

Pulsed waveform are characterized by the pulse repetition frequency, duty cycle, average amplitude, peak amplitude, period and pulse width. The pulse repetition frequency, which is the frequency at which pulses are repeated or the number of pulses per second is defined as

$$PRF = \frac{1}{T} \quad (2.14)$$

Recall that the duty cycle is that time during which the pulse is on and is given by the ratio of the pulse width to the pulse period, i.e

$$Duty\ Cycle = \frac{Width}{Period} \times 100\%$$

Pulsed signals are measured using a much narrower resolution bandwidth than the bandwidth of the pulse. The power obtained is thus not an exact reflection of the true nature of the signal power and consequently the 1-dB compression point can easily be exceeded[22]. Pulsed signals pose a new dimension to the measurement problem. If a signal of relatively small duty cycle is being measured, it is highly possible for the spectrum analyzer to skip it and proceed with the measurement cycle. The implication is that the signal remains undetected giving the impression that such a signal does not exist. This leads to gross inaccuracies in the measurement results obtained. Another snag which

CHAPTER 2. SUMMARY OF THE SKA PROTOCOL

may be encountered during the measurement campaign is that arising from the presence of frequency hopping and burst signals. Frequency hoppers are signals transmitted at different frequencies according to a certain transmitter algorithm. Devices employing such mode of transmission are generally used in covert and military operations where it is necessary that the transmitted information continue undetected. Burst signals are signals which are transmitted during a certain time and disappear shortly thereafter. They are said to be transmitted in burst mode. Examples of such signals are the CDMA applications used extensively in cellular technology.

One of the suggested ways of dealing with problems associated with pulsed waveform signals is offered by Horing (1998) [10]. Horing (1998) noted that signals with a duration of burst time, $t_h \leq \tau$ remain undetectable, i.e a signal must have a length of at least $t_h > \tau$ to be detectable. Furthermore, the received bursts should have sufficient power for a signal to be detected and that at least one integration time should fall within the burst time and that the hop sequence of the transmitter and sequence of the scanning receiver must co-incide. The hop frequency and the receiver frequency must be equal[10].

2.8 Summary

This chapter highlighted some of the key technical issues that needed clarification and which had to be attended to by the SA SKA team. The technical specifications which the RFI Measurement System had to adhere to and the system functionality which had to be incorporated into the design of the RFI measurement system are also documented.

Chapter 3

Literature Review

3.1 Introduction

The work of the SKA Site Selection and Evaluation Committee requires a thorough grounding and knowledge of the principles of frequency spectrum management. A good and solid understanding of spectral analysis is essential, so is the ability to decipher and make more sense of the gigabyte of measurement data provided. More-over, an adequate understanding of electro-magnetic interference, compatibility and shielding is recommended.

In Chapter 1, an attempt was made to demonstrate the adverse impact of EMI, and more particularly RFI, at radio telescope observatories. In Section 3.3 of this chapter, a more detailed analysis of EMI as encountered by radio telescope receivers is presented.

It is worth-while to note that by presenting the various types, classes, categories, sources and characteristics of EMI which have a down-side effect on the proper functioning and performance of a radio astronomy telescope, we hope to categorically present a case for the types of EM radiation which the measurement campaign should be focused on, and which may possibly be encountered during the measurement campaign. The success of a wideband RFI measuring system, such as that constructed by the SA SKA for detection, identification, locating and excision of RFI, lies to a large extent on knowing certain electrical, physical and spectral characteristics of the interfering signals. The waveform of signals intercepted by the RFI measuring systems can either be narrowband or broadband with regular or irregular (incoherent) characteristics. The spectral characteristics are of fundamental importance.

It is worthy to note at this juncture, that “any fixed frequency device is a potential source of continuous interference and that any electronic device or circuit will generate excess noise and can be a source of interference”[22, 12]. Furthermore, all realistic components comprise of either insulators, semiconductors or conductors[29, 59]. These three substances differ according to the amount of charge they possess.

CHAPTER 3. LITERATURE REVIEW

In good conductors such as copper, the charge carriers or electrons wander about freely. This is due to the fact that the atoms are arranged in close proximity to each other such that the electrons are not bound to any particular nuclei but are free to wander through the crystal lattice structure. At absolute zero temperatures, the atomic ions are deficient of kinetic energy and thus do not vibrate about their neutral positions. This enables the electrons to move freely, thus delivering the greatest amount of charge. As the temperature is increased, however, the ions gain kinetic energy and vibrate, thus colliding with the electrons. This continuous collision of *+ve* ions with electrons poses resistance to the motion of electrons thereby causing the electrons to lose energy. The electrons drift about randomly losing energy at each collision. This energy is dissipated into the surrounding. This results in *random thermal noise* [33, 26]. Random noise can either be *impulsive* (with sharp, widely spaced and relatively infrequent pulses) or *thermal* (temperature dependent with closely spaced, overlapping and frequent pulses). Thermal noise is also called Johnson or Nyquist noise [18, 33]. Other main types of noise include shot noise and low-frequency ($\frac{1}{f}$) flicker noise (due to random motion of charges in solid state devices and electron tubes), plasma noise occurring as result of random motion of charge particles in an ionized gas or sparking electrical contacts and quantum noise resulting from the quantized nature of charge carriers and photons [33, 18].

From the above, it follows therefore, that the electronic devices and circuitry which make up the RFI Measuring System can, itself, be a source of interference and subsequently should be investigated for electromagnetic (EM) emissions and if detected proper excision mechanisms should be put in place to curtail the emissions thus safeguarding against contamination of data by self induced EM emissions.

This chapter documents the relevant theory used throughout this study.

In Section 3.2 we begin by looking at radio frequency spectrum and its management.

Section 3.3 defines EMI and lists the various parameters which aid in the proper characterization of EMI. Subsection 3.3.1 discusses the type and sources of EMI and distinguishes between conducted and radiated EMI. The effects of circuit or device non-linearities is discussed in Section 3.5.3 and the EMI contribution of devices such as amplifiers, mixers, oscillators, filters, antennas and receivers is discussed in succeeding sections.

Section 3.11 exposes the theory behind spectrum analyzers.

3.2 Frequency Spectrum Management

The frequency spectrum is an expensive natural resource. Like most natural resources of a country, ownership in the form of regulatory control resides with the government and private usage requires a permit or licence. In South Africa, the frequency spectrum is managed by the Independent Communications Authority of South Africa (I.CASA). This

CHAPTER 3. LITERATURE REVIEW

is a Chapter 13 organization appointed by the SA government to oversee the planning, allocation and management of the radio spectrum. ICASA has developed a database (called Spektrum) of all frequencies in use in the Republic both allocated and unallocated. The table of frequency allocations depicted in Chapter 1, Table 1.2, is a summary of the type of services allowed in the Republic together with corresponding frequency assignment. A more complete table of frequency allocations can be found in *Part 3 of the Soth African Telecommunications Act 103 of 1996* [50].

3.3 Electromagnetic Interference

Electromagnetic Interference is a phenomenon which occurs as a result of the presence of undesirable voltages and currents in amounts or levels which affect the operation of an electronic device, system or equipment in such a manner as to degrade the performance of the electronic device, system or equipment [12, 15]. This phenomenon is usually an electromagnetic disturbance which can be in the form of electromagnetic noise or the reception of an unwanted signal [15]. When the phenomenon occurs as a result of the reception of unwanted signals in the radio frequency band, Radio Frequency Interference is assumed. The unwanted noise signal can either be conducted from the source to the susceptible device or radiated to the receptor [12, 15]. Conduction occurs when a signal propagates from the source, through a metallic medium such as wiring or any metallic structure to the receptor [12].

Section 3.3.1, explores the sources of EMI (with special emphasis on identifying the system, equipment or devices which are responsible for the generation of electromagnetic interference in an EMI Measuring System). Once the EMI generating components have been correctly identified, they are then isolated, classified and their characteristics determined. Electromagnetic interference can be characterised and sufficiently modelled according to the following significant parameters: frequency, time and duration, position, amplitude, polarization, distance, coding and modulation scheme, positivity, power level and multipath [12].

Section 3.3.3 deals with the various ways in which the electromagnetic energy is released into the environment from the point of origin. Combating this electromagnetic leakage is extremely difficult and requires proper screening of the radiating sources. Shielding and screening methods are dealt with in Section 3.3.5.

3.3.1 Types and sources of EMI

The second paragraph in Section 3.1 illustrates an important principle i.e conductivity decreases with increasing temperature and that noise becomes prevalent.

CHAPTER 3. LITERATURE REVIEW

Conducted EMI

Table 3.1, below lists, the various sources of conducted interference and the frequencies or range of frequencies at which their noise spectrum dominates. It has been established that electronic equipment have a conducted spectrum which stretches from the “lowest observable fluctuation rates” to above 1 GHz [12]. At highest frequencies, however, conducted interfering signals tend to be radiated. This is due to conductor losses, wiring inductance and shunt capacitance and also due to the fact that the wavelengths, λ of signals at this rate is minute by comparison with the wires in the circuits and thus these short wires, which are greater than $\frac{\lambda}{2}$, tend to act as antennas. In fact, at high frequencies, “any wire that carries currents can act as a radiator and any conductor in the vicinity of an electromagnetic field can act as a receiving antenna or transmitting antenna”[12].

Other sources of conducted interference which have not been tabulated, for reason of the fact that their range of frequencies have not been established, are pulse generators, computer clocks, saw-toothed deflection generators, multivibrators, choppers, steppers, stepped motors, ac reference generators, excitors for magnetic amplifiers, gyros, printing devices, solenoids, relays, flip-flop circuits, gates, commutators, diodes, thermostats, various types of switches, and transducers [12].

Table 3.1: Sources of conducted *Electromagnetic Interference* (from [12])

Conducted	Spectrum
Heater Circuits	50 KHz to 25 MHz
Fluorescent Lamps	0.1 to 3 MHz
Computer Logic Box	50 KHz to 20 MHz
Command Programmer signal lines power lines	0.1 to 25 MHz 1 to 25 MHz
Power Supply Switching Circuit	0.5 to 25 MHz
Power Controller	2 to 15 KHz
Mercury Arc Lamps	0.1 to 1MHz
Power Transfer Controller constant noise transients	10 to 25 MHz 50 KHz to 25 MHz
Command Programmer	0.1 to 25 MHz
Multiplexer	1 to 10 MHz
Latching Contactor Coil Pulses Contact Cycling	1 to 25 MHz 50 KHz to 25 MHz
Transfer Switch	0.1 to 25 MHz
Circuit Breaker Cam Contacts	10 to 20 MHz
Corona	0.1 to 10 MHz
Vacuum Cleaner	0.1 to 1 MHz
Magnet Armatures	2 to 4 MHz

CHAPTER 3. LITERATURE REVIEW

Radiated interference

Radiation occurs when electromagnetic energy is released from a source and propagates in space. This can either be intentional such as in X-Ray applications or unintentional such as microwave ovens, incidental such as automotive ignition systems and accidental such as nuclear disasters. When radiated energy causes the receiving devices, systems or equipment to malfunction or interferes with the normal functioning of the receiving devices, systems or equipment then this is termed radiated interference [12, 15].

Radiated interference can occur from a number of sources, some of which are listed in Table 3.2 below.

Table 3.2: Sources of *Radiated Interference* (from [12])

Source	Spectrum
Bistable Circuits	15 kHz - 400 MHz
Harmonic Generator	30 MHz - 1000 MHz
Heater Thermoswitch contact arc	30 kHz - 300 kHz 20 MHz - 200 MHz
Actuator motor switch arcs cams	10 kHz - 400 kHz 30 MHz - 200 MHz 10 MHz - 20 MHz
Teleprinter magnet armatures print magnets	1.8 MHz - 3.6 MHz 1.0 MHz - 3.0 MHz
Transfer switch coil delay contact arc	15 kHz - 150 kHz 20 MHz - 400 MHz
DC Power Supply switching circuit	100 kHz - 30 MHz
Equipment Case untreated access covers	0.1 to 25 MHz 10 kHz - 10 MHz
Fluorescent Lamp arc	100 kHz - 3.0 MHz
Multiplexer solid-state switching	300 kHz- 500 kHz
Power Console circuit-breaker cam contacts power switching devices	10 MHz - 20 MHz 100 kHz - 300 MHz
Power controller power wires chopper, relay, bistable circuits	50 kHz - 4.0 MHz 10 kHz - 200 MHz

CHAPTER 3. LITERATURE REVIEW

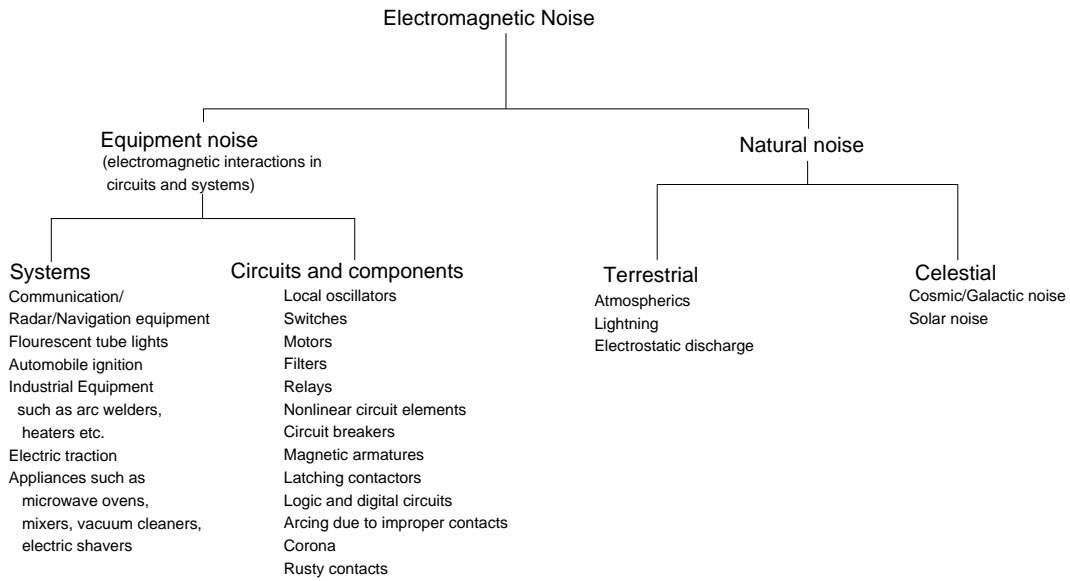


Figure 3.1: Structure showing the various types and categories of EMI as taken from *Keiser (1987)* [12]

3.3.2 Description of some types of EMI

“Interference produced by fluorescent and neon lights has a sinusoidal waveshape with sharp irregular spikes”[12]. Leakage currents from heater transformers to nearby inductive elements also can result in 60 Hz interference.

Automotive sources of interference are the ignition system, generator, voltage regulator, and directional lights switch, windshield wiper motor, fan and hooter [12]. These sources are responsible for both conducted and radiated interference. The ignition system is one of the strongest sources of broadband interference. The spectrum of this noise has a fundamental low frequency component with a multiple number of harmonics and transients that stretch from 10 MHz to well over 100 MHz [12]. Automotive noise tend to be vertically polarised especially below 100 MHz [12]. A possibility of a motor vehicle coming into the area where measurements are being conducted exists. Therefore, knowing the different types of EMI generated by motor vehicles is important.

3.3.3 Escape Mechanisms

Electromagnetic energy is released into the environment as result of case discontinuities, coupling, radiation, and conduction [12]. In the case of RFI Measurement System 2, it was found that a vast majority of the EMI were self-induced and escaped from the primary equipment (such as the spectrum analyzer, UPS, control PC and the electronics control box) to its immediate surrounding via coupling, radiation and due to the discontinuities and or openings in the casing of these equipments.

CHAPTER 3. LITERATURE REVIEW

3.3.4 EMC testing

EMC testing involves performing pertinent tests at components, subsystem, and system level. The entire methodology of EMC testing has been discussed at length by Bernard Keiser [12]. This methodology proposes that an EMC test plan be written. The test plan itself is based on the EMC control plan which is written early on during system development. Contents of the EMC test plan and test plan procedures is dealt with by Bernard Keiser [12].

In my audit of the SA SKA documentation, I found no documentary evidence to suggest that a testing plan existed and I was clearly convinced that EMC testing was performed on an ad hoc basis, if and when EMI was encountered. This lack of a proper testing plan was in itself a manifestation of a much greater wide problem arising from the fact that the system itself was not developed in accordance with any of the well known system development approaches but was done in an ad hoc manner. Obviously this was no fault of the SA SKA team but was due to the tight time deadlines imposed on the team by the International SKA body. Having said this, however, it is very important that I make it clear that the SA SKA team spent a great deal of time and money on EMC testing and preventative measures. Evidence of this, was by the employment of MESA Solutions (Pty) Ltd, a company specializing in RFI measurements in order to perform EMI/EMC tests and to offer advice on how to keep self-induced RFI at bay. MESA conducted EMI tests on the RFI Measurement System 2 at the Houwteq anechoic chamber. As a result of these tests and advice, various strategies were adopted to deal with this issue. These are discussed in the next section. The EMI / EMC test results can be found in the bid documentation [27].

3.3.5 Preventative Measures for EMC/EMI

Protection of sensitive devices involves both shielding of the device from exposure to unwanted electromagnetic emissions and containment of emissions to ensure that the device does not release emissions into its surroundings. To perform this function various mechanisms are employed. These include grounding and shielding.

A rule of thumb used often is to employ conductive shielding (aluminium and copper) for frequencies above 1000 Hz or impedance levels over 1000Ω . For lower frequencies and impedances, magnetic shielding and twisted wire pairs (inter-8 weave wire) are employed. Magnetic shielding is achieved by using super-malloy and mu-metal materials [33].

As already pointed out in preceding Sections 3.3.3 and 3.3.4, EMI manifestations were observed during system testing and preventative steps to deal with this crucial issue were taken. These measures included defeating the self induced RFI by placing the UPS and the other primary equipments in Faraday cages made of copper sheeting and brass wire mesh for physical access to power buttons and other control knobs. Seams were sealed

CHAPTER 3. LITERATURE REVIEW

with aluminium tape to prevent radiation from small openings between joints and feed cables were re-routed and bound with ferrite chokes to prevent coupling.

Routes of common mode currents were identified and a low impedance busbar was installed to offer a much improved grounding and an alternative low impedance path so as to constrain stray currents. Detailed explanations can be found in the bid document.

3.4 Various subsystems of the RFI Measuring System

On page 349-351, Bernard Keiser[12] documents the basic blocks of an EMI Measuring system . These blocks lay the foundation for any EMI Measuring system (both automated and non-automated). We enumerate these as:

1. Antenna,
2. Attenuators,
3. Mixers,
4. Filters,
5. Oscillators,
6. Receivers,
7. Detectors,
8. Display devices, and
9. Amplifiers.

In this section, we attempt to unpack and show the basic blocks of a typical RFI measurement system. By doing this we hope to allow the reader to come to some sort of conclusion as to whether the SA SKA RFI System was designed in accordance with established norms.

3.5 Receivers

3.5.1 Receiver characteristics

The main performance characteristics of a receiver are its sensitivity, dynamic range, linearity, spurious response, selectivity and frequency settling time[21, 30]. These characteristics are largely influenced by the noise induced and by the intermodulation products generated in the system. Other good characteristics are the ability of the receiver to offer

CHAPTER 3. LITERATURE REVIEW

interference-free signal detection, especially in the presence of a large number of very strong and undesirable signals.

The performance of a receiving device, circuit or equipment (such as a spectrum analyzer or RFI measuring system) and its contribution to the performance of a system depends, in large, on characteristics such as sensitivity, dynamic range, linearity, selectivity, spurious response, immunisation from strong signals at the input and the ability to withstand and operate with very little or no adverse effects from internal and external interference. These characteristics are major determinants of receiver performance and subsequently any variation in their values affects the performance of the receiver. These characteristics in-turn are measured by such parameters as signal-to-noise ratio (S/N), noise factor (K), noise figure (NF), temperature, second and third order intermodulation products, third-order intercepts (TOI), second-order intercepts (SOI), 1-dB gain compression point, Displayed Average Noise Level (DANL) and Adjacent Channel Power Ratio (ACPR), gain, Automatic Gain Control and spurious free range [15, 21, 22, 30].

These parameters are excellent measures of the receiver characteristics. They allow for inferences to be made as to the minimum and maximum levels required for the input signal to be detectable[21, 22] and constitute the electrical specifications of the receiver.

By adjusting and manipulating these parameters, the receiver characteristics can be altered, the performance controlled and a criterion for the assessment of the technical competence of the RFI Measuring Systems can be derived.

On page 45, Rohde & Bucher[30] state the following:

“The capabilities of a receiver are best appreciated from its electrical specifications”.

This statement is a direct indictment of what is required in order to arrive at a prudent conclusion regarding the competence of the RFI systems.

By studying the electrical specifications and the EMC nature of the receiver, the capabilities of the receiver can be established and the competence of the system determined.

The evaluation of the technical competence of the RFI Measuring systems will, therefore, be conducted in accordance with the following check-list:

1. Adherence of the system to the technical requirements of the protocol,
2. The presence of self-generated EMI, and
3. Proper system design considerations.

3.5.2 Selectivity

Selectivity is defined as the ability of the receiver to select and tune into a particular desired frequency whilst rejecting adjacent channels, image frequency and interference[18].

CHAPTER 3. LITERATURE REVIEW

Ideally selectivity should be performed using a narrow bandpass filter at the RF stage. However, it has been noted that such filters are impossible to attain at RF frequencies and thus a method of down converting to IF stage and then using a sharp cut off bandpass filter to select the desired frequency band is employed.

There are various receiver circuits such as TRF receiver, homodyne and superheterodyne receivers. The latter receiver is the most popular receiver and thus will be discussed here. The block diagram below depicts the basic diagram of the superheterodyne receiver. This receiver uses a bandpass filter to select the desired RF frequency and then down converting this to a fixed intermediate frequency IF using a local oscillator. The baseband signal is recovered by filtering the IF signal. The Low Noise Amplifier (LNA) is used at the front-end to amplify the relatively weak signal whilst preventing the insertion of additional noise. This amplifier should have a low noise factor and enough gain to boost the weak desired signal to acceptable levels above the noise floor so that the desired signal becomes pronounced and dominant. The amount of gain required is limited to the handling power of the mixer and the S/N ratios desired at the output.

3.5.3 Nonlinearities, TOI, SOI, Linearity and Sensitivity in circuits

Nonlinearity is the effect introduced by the presence of non-linear voltage-current characteristic in either passive or active devices. In passive components such as ferrite isolators, filters, connectors and cables, nonlinearity is due to the non-linear input/output characteristics of the material from which these components are manufactured. Nonlinearity also occurs in non-similar metallic contacts and broken or corroded junctions where the metal surfaces are exposed to the atmosphere and are thus oxidised.

Networks containing semiconductor devices such as amplifiers, rectifiers, mixers, oscillators, transistors, and diodes, exhibit nonlinearity and rely on nonlinearity effects for their proper functioning, as their output does not always follow their input [21]. However, in other devices this effect can be cumbersome. In mixers, nonlinearity causes distortion. Distortion reduces and limits the operation range of the device or system.

In receiver circuits, the distorted signal may combine with the input signal to form a signal with frequencies close to the useful tuned frequency of the receiver or device. This combination effect is known as intermodulation.

Nonlinear effects in mixers, amplifiers create intermodulation products (difference-frequency distortion or sum and difference). The frequency of intermodulation products are given by

$$f_i = pf_1 \pm qf_2 \pm rf_3 \pm \dots \pm zf_n \quad (3.1)$$

CHAPTER 3. LITERATURE REVIEW

or

$$f = |mf_{RF} - nf_{LO}| \quad (3.2)$$

where f_i is the intermodulation frequency and p, q, r, z, m and n are integers the sum of which defines the intermodulation order. The third order product and the third harmonic are the strongest signals generated [12]. The intermodulation products of both even-numbered and odd-numbered order may be a source of interference [21].

It has also been pointed out in the preceding sections that all real devices have at least a small loss and thus exhibit nonlinear behaviour at one point or another. Furthermore, a receiver is exposed to a large number of signals. Some of these signals are so strong that they exceed the rejection of the selective circuits and can cause immediate damage to an unprotected receiver or generally cause distortion, whilst others are so weak that they are masked by the inherent noise of the receiver. It is thus crucial that devices be operated within their useful range of competence. Such a range is called the dynamic range of the device and is defined as the ratio of the maximum allowable power to the minimum allowable power level [18, 30]. The maximum power must be of such a nature that it causes ‘maximum tolerable distortion’ or that it is not so strong that it causes ‘the weak signal to become unacceptable’ and the minimum allowable power must be such that it has the ‘minimum allowable S/N ratio’ [30]. The above definition is more appropriate when referring to the entire receiving system.

When discussing individual components such as an amplifier or mixer, it is better to define dynamic range in terms of the 1-dB compression point (the first point at which the input-output curve deviates from its linear characteristic by 1-dB, where gain compression exists and where the mixer becomes saturated) and also in terms of the third-order intermodulation distortion or harmonic suppression. The linear dynamic range is restricted at the low end by the average noise floor or phase noise and at the high end by the 1-dB compression point [18, 21, 38, 22]. When the input signal exceeds the linear dynamic range of the individual components, harmonics and intermodulation distortions are generated [38]. The diagram below shows the linear dynamic range as well as the spurious-free dynamic range. The dynamic range is dependant on the signal level at the mixer [22].

Mixers, amplifiers and effects such as desensitization, distortion performance, broadband noise floor, cross-modulation, LO phase noise, blocking, spurious signals (signals produced by the receiver in the absence of an input) limit the system dynamic range and contribute significantly to the generation of spurious responses [38, 30, 22]. Spurious responses occur when spurious signals or other strong signals at frequencies, other than that to which the receiver is tuned, leak into the circuit via unsuspected paths and produce an output [30]. Sources of spurious signals are power supply harmonics, parasitic oscillations in amplifiers and IF subharmonics due to feedback and non-linearities [30].

CHAPTER 3. LITERATURE REVIEW

On the other hand, the spurious-free or intermodulation-free dynamic range or maximum harmonic suppression point is bounded by the noise floor at one end and by the maximum level at which the third-order intermodulation products or higher order harmonics becomes equal to the noise level [18, 21]. For a mixer, the noise power levels at which this occurs is given by the following formula:

$$L_{N,rel} = L_R - L_{mix} = -174dBm + 10.Log(B_{N,IF}) + NF - L_{mix} \quad (3.3)$$

where

$L_{N,rel}$ = relative noise level referred to mixer level, in dB

L_{mix} = mixer level, in dBm

L_N = noise level, in dBm

$B_{N,IF}$ = noise bandwidth of resolution filter, in Hz

NF = noise figure of spectrum analyzer, in dB

It can be seen that the power level is dependent on both the mixer level as well as the bandwidth and that reduction in bandwidth leads to an improvement in dynamic range [22].

The relative level of the nth-order intermodulation products is given by

$$L_{IMn,rel} = -(n-1)(IPn_{in} - L_{mix}) \quad (3.4)$$

where

$L_{IM3,rel}$ = relative level of nth order intermodulation products referred to mixer level, in dB

IPn_{in} = input intercept point of nth order of spectrum analyzer (RF attenuation 0 dB)

L_{mix} = mixer level, in dBm

For third order intermodulation products, n=3.

The relative level of 2nd order distortion products (2nd order harmonics) is

$$L_{k2,rel} = -(SHI_{in} - L_{mix}) \quad (3.5)$$

where

CHAPTER 3. LITERATURE REVIEW

$L_{k2,rel}$ = relative level of 2nd order distortion products referred to mixer level, in dB

SHI_{in} = input second harmonic intercept of spectrum analyser, in dBm

The point where the third-order distortion equals the mixer level is known as the third-order intercept point or it is the point where the second harmonic of the input signal at the output of the network is equal to the level of the fundamental [21]. It is also a measure of the dynamic range. This theoretical point is derived from the graph and is not an actual measured point. At this point, the mixer would be driven into saturation [22].

The third-order intercept is given by

$$TOI = A_{fund} - \frac{d}{2} \quad (3.6)$$

$$IP3_{in} = \frac{a_{IM3}}{2} + L_{in} \quad (3.7)$$

where

$TOI/IP3_{in}$ = Third-order intercept point,

A_{fund}/L_{in} = level of the fundamental or of one of the inputs in dBm

d/a_{IM3} = level difference in dBc between the fundamental of the input signal and the intermodulation distortion products (intermodulation-free dynamic range)[21, 22].

The nth-order intercepts are given by

$$IPn_{in} = \frac{a_{IMn}}{n-1} + L_{in} \quad (3.8)$$

For a cascaded two stage network, the nth order intercept point are given from the following equation:

$$IP3_{in,total} = IP3_{in,1} + IP3_{in,2} - 10 \cdot \log \left(10^{\left(\frac{IP3_{in,1} + g_1}{10}\right)} + 10^{\left(\frac{IP3_{in,2}}{10}\right)} \right) \quad (3.9)$$

where,

$IP3_{in,total}$ = 3rd order input intercept of cascaded stages, in dBm

$IP3_{in,1}$ = 3rd order input intercept points of individual stage 1, in dBm

$IP3_{in,2}$ = 3rd order input intercept points of individual stage 2, in dBm

g_1 = gain factor of first stage, in dB [21]

CHAPTER 3. LITERATURE REVIEW

Since the upper limit of the spurious-free dynamic range is the point where the odd-order intermodulation products are equal to the noise level, it follows therefore that this occurs where Equation 3.3 equals Equation 3.4.

Therefore, the maximum dynamic range occurs where the noise level equals the intermodulation distortion level and is given by the following equation

$$DR_{max} = \frac{(n-1)}{n} (IPn_{in} - L_N) = \frac{n-1}{n} (IPn_{in} + 174dBm - 10.log(B_{N,IF}) - NF) \quad (3.10)$$

or in terms of the harmonic suppression, it is given by the following equation

$$DR_{max} = \frac{n-1}{n} (SHI_{in} - L_N) = \frac{n-1}{n} (SHI_{in} + 174dBm - 10.log(B_{N,IF}) - NF) \quad (3.11)$$

Since the dynamic range depends on the input at the mixer, the optimum mixer level at which the maximum dynamic range occurs is given by[21, 22]

$$L_{mix,opt} = \frac{(n-1)IPn_{in} - 174dBm + 10.log(B_{N,IF}) + NF}{n} \quad (3.12)$$

The maximum harmonic suppression is given by

$$L_{mix,opt} = \frac{SHI_{in} - 174dBm + 10.log(B_{N,IF}) + NF}{2} \quad (3.13)$$

The optimum mixer level is achieved by varying the attenuation at the input. A variation of the attenuation at the input by ΔdB causes the harmonic level to vary by the $n = \Delta dB$. The precise attenuation value at which this optimum occurs is given by

$$a_{RF} = L_{in} - L_{mix} \quad (3.14)$$

a_{RF} = RF attenuation, in dB

L_{in} = signal level at spectrum analyzer input, in dBm

L_{mix} = mixer level to be set, in dBm[21]

When electronic devices are fed with too little power for their proper functioning, the charged carriers within the device move about randomly thus generating thermal noise. However, when devices are fed with too much power, material breakdown occurs within the device leading to energy being dissipated into the immediate surroundings. This once, again introduces electromagnetic interference. The minimum allowable power level is

CHAPTER 3. LITERATURE REVIEW

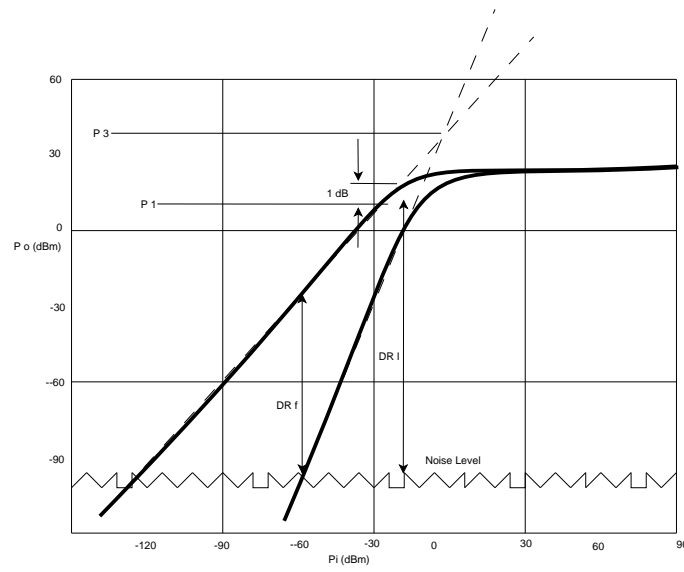


Figure 3.2: Illustration of linear dynamic and spurious free dynamic range (from[18])

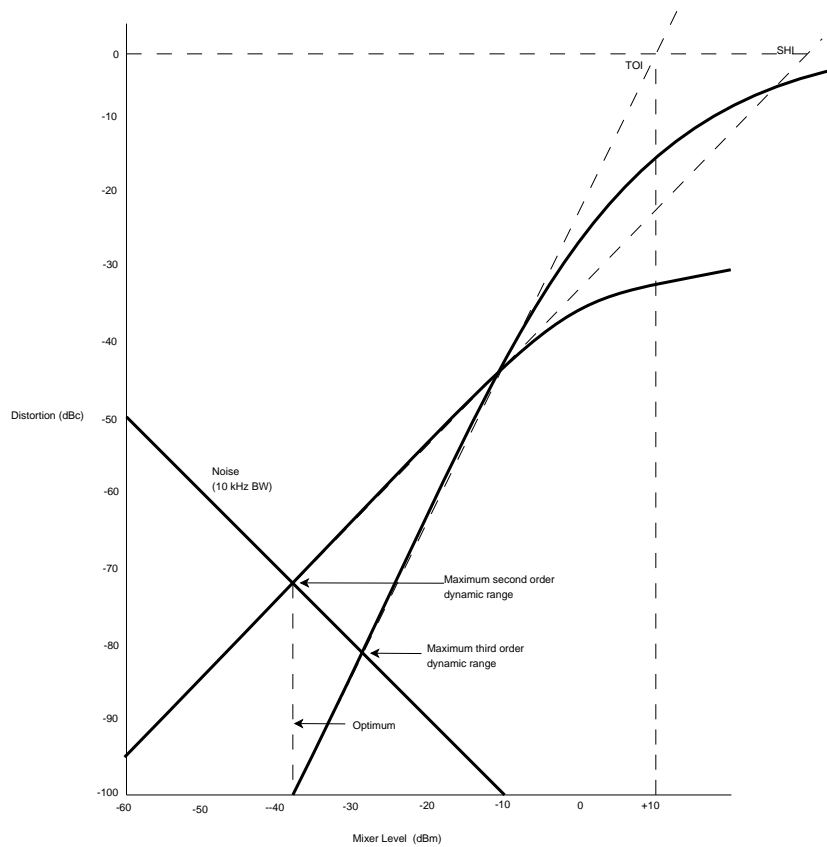


Figure 3.3: Dynamic range versus distortion and noise (from[22])

CHAPTER 3. LITERATURE REVIEW

sometimes referred to as the minimum detectable signal level (MDS) and is defined as the minimum power level that a receiver requires in order to be able to convert the signal to meaningful information [18]. The MDS level forms the sensitivity of the receiver, and the point at which this minimum level is taken is established by a predefined and desired signal-to-noise ratio of the receiver. The sensitivity of the receiver can also be expressed in terms of voltage according to the following expression:

$$V_{i_{min}} = \sqrt{2Z_o S_{i_{min}}} \quad (3.15)$$

$$S_{i_{min}} = KB(T_A + (F - 1)T_0) \left(\frac{S_0}{N_0} \right)_{min} \quad (3.16)$$

where Z_o is the antenna input impedance which is generally taken as 50Ω ; K is the Boltzmann Constant; B is the bandwidth and F and T_A are the noise factor and antenna temperature respectively [18].

In radio astronomy, sensitivity is referenced to the antenna and is given in units of Jansky. The fact that radio receivers have to detect extremely low levels of signals of the order of -110 dBm implies that they have to be capable of boosting these low lying signals to acceptable limits for proper translation into meaningful information [18]. This means that they have to have high gain as high as 100 to 120 dB which must be spread over the RF, IF and baseband stages in order to avoid oscillation and instability. Good design practices require that no more than 50 - 60 dB be concentrated at one stage.

In contrast, however, other signals are intercepted at extremely high power levels which are dangerous to the receiver as they can cause component damage. These signals could be greater than the noise power level by 100 dB or more for communications receivers [30]. It follows therefore, that some form of gain control is needed. This gain varying function is achieved using an automated gain control attenuator which is normally inserted at the IF stage. In some receiver, however, it is placed at the RF stage. Placing the AGC at the RF stage runs the risk of amplifying the noise as well, and corrupting the S/N ratio. The steady-state, control range, input-output curve, attack and delay times are some of the key or capital characteristics of an AGC [30]. Attack and decay times are crucial as they determine the response time of the AGC. An AGC which responds too fast or too slow may introduce ringing effects, and may cause instability in the output baseband or IF voltages. Care should, therefore, be exercised and adherence to the input-output curves of the AGC is a necessity. The curve show a small linear region, followed by a steady-state region and a region where the output starts to decrease [30].

The difference between the point where the output starts to decrease and the region where the linear relationship ends is known as the control range.

CHAPTER 3. LITERATURE REVIEW

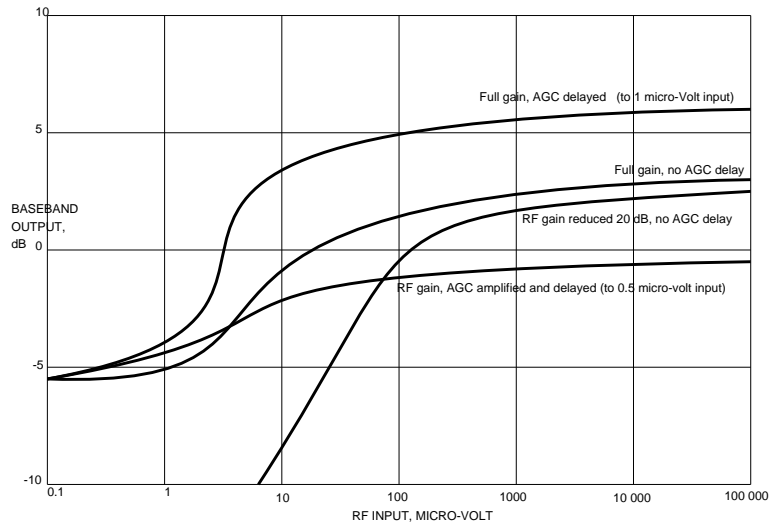


Figure 3.4: Representative input-output AGC curves (from [30])

On the other hand, the allowable maximum power level or threshold of a receiver can also be determined by analysing the third order intercept point of the input of the receiver. The third-order point is defined as the point at which the extrapolation of the linear region of the first order harmonic of signal intercepts that of the third order harmonic. Operating the receiver beyond this point invariably lead to intermodulation distortion. See Figure 3.3 above.

3.6 Amplifiers

There are three categories of amplifiers i.e low noise, power amplifiers and IF amplifiers. The latter being used in the IF stage. Important design consideration include the power gain, intercepts and noise figure (which is the noise factor expressed in decibels).

3.7 Filters

Filters are used to pass frequency components of signals below the frequency cut-off (low noise) whilst rejecting high frequency components, to pass frequency components of signals above a certain cut-off frequency as well as to pass the frequency components at the pass band of the filter.

An ideal filter should have zero insertion loss (at the pass band), infinite attenuation at stop band and a linear response at pass band to avoid distortion. The important filter parameters to be considered are the cut-off frequency, insertion loss, filter ripple and out of band attenuation measured in dB's per decade of frequency. The power loss ratio of a filter is defined as the ratio of the power available from the source to the power delivered to the load. Insertion loss is defined as the amount of attenuation seen by the signal through

CHAPTER 3. LITERATURE REVIEW

the pass band of the filter.

3.8 Mixers

Mixers are non-linear devices [22]. As already pointed out previously, non-linearity results in distortion. Therefore, the mixer generates distortion of its own.

3.9 Antenna design

The antenna is by far the most crucial component of any receiving system. Therefore, design of this component and/or its proper selection is paramount.

An antenna can be characterized according to the following parameters:

1. Its radiation resistance;
2. Its radiation pattern;
3. The beamwidth and gain of its main lobe;
4. The position and magnitude of its side lobes;
5. The magnitude of its back lobe;
6. Its bandwidth;
7. Its aperture;
8. Its antenna correction factor;
9. The polarization of its electric fields that it transmits or receives;
10. The power that it can handle in the case of a transmitting antenna[41]

This section “unpacks” the above-mentioned characteristics in greater detail.

3.9.1 Radiation Resistance

If an antenna is considered as a load that terminates the feeder transmission line, it would have both a self impedance and mutual impedance. The self impedance is the impedance that would be measured at the terminals of the antenna when it is in free space, whereas the mutual impedance is due to coupling between the antenna and the source.

The self impedance is given by the equation: $Z_a = R_a + jX_a$, where R_a is the real antenna resistance accounting for the power absorbed and re-radiated by the antenna and X_a is

CHAPTER 3. LITERATURE REVIEW

the self-reactance. The real antenna resistance $R_a = R_r + R_l$, where R_r is the radiation resistance and R_l is the loss ohmic resistance which contributes to the loss of efficiency of the antenna[41].

3.9.2 Radiation Pattern

It has already been mentioned that the antenna absorbs or radiates power. The power radiated is given by

$$P_r = I^2 R_r \quad (3.17)$$

where I is the current induced in the antenna[41]. This power is radiated in space in a pattern which is known as the radiation pattern of the antenna.

Since the antenna is a reciprocal device (radiates or receives electro-magnetic energy in the same way), the radiation pattern of an antenna is the same, irrespective of whether the antenna is transmitting or receiving power. The received or radiated power is at its maximum along its boresight which is usually plotted at 0 dB. At this position, most of the power is concentrated in the main lobe. When the power is radiated uniformly in all direction, an *omni-directional* pattern is achieved and if this power is uniform, *isotropic* radiation is obtained. From the above, and in order to achieve uniform radiation in all direction, the isotropic radiator would have to be a point source.

The radiation pattern is significant in that it displays, graphically, the power level of the main beam as well as the side lobes. It provides such useful information as the *beamwidth*, *directivity*, *gain*, position of nulls and front to back ratio.

3.9.3 Beamwidth and Gain of an antenna

The *beamwidth* of an antenna, is the width in degrees or radians of the main beam of radiation taken at *boresight*. The 3dB or *half-power* beamwidth is most commonly used and is defined as “the width in degrees or radians at the points on either side of the main beam where the radiated power is half the maximum value[41].”

The SKA Protocol refers to the 6dB beamwidth, which similarly, would be defined as “the width in degrees or radians at the points on either side of the main beam where the radiated power is one quarter of the maximum value.”

The gain of the antenna is defined as “ 4π times the ratio of the radiation intensity in a given direction to the total power radiated by the antenna. The gain of an antenna is calculated from the following formula:

$$G = \eta D \quad (3.18)$$

CHAPTER 3. LITERATURE REVIEW

where η is the efficiency of the antenna (which normally vary between 50% and 90% and is less than unity) and D is the directivity which is the ratio of the maximum radiation from a lossless antenna and the average radiation antenna from an isotropic antenna. The gain can be considered as “a measure of the ability of the antenna to concentrate the energy into a smaller number of angles”[41].

3.9.4 The position and magnitude of its side lobes

An antenna radiation pattern has a main beam of radiation together with a back lobe and numerous side lobes. The “near-in” lobes are often referred to as side lobes[41]. A side lobe is defined as “the peak, where the difference between the peak and an adjacent trough is at least 3dB”[41]. A symmetrical antenna will have positive and negative sets of side lobes with respect to the main lobe. The position and magnitude of the side lobes can be accurately calculated using spectral analysis theory.

The position and magnitude of the antenna side lobes is a critical and important characteristic in Radio Frequency system design. Most RF designs aim to reduce or totally suppress such side lobes. This is due to a desire, by the frequency planning authorities, to conserve natural resources such as bandwidth and to enable the radio frequency spectrum to be shared amongst many users. The frequency planning authorities sometimes dictate what the threshold level of side lobes should be and impose hefty fines on defaulters. For this reason, side lobes are an unwanted “nightmare” to RF system designers. The magnitude of the back lobe with respect to the main beam defines the front-to-back ratio which is a “measure of the ability of the antenna to concentrate the beam in the required forward direction”.

3.9.5 Bandwidth

Bandwidth can be defined as “the range of usable frequencies” which a signal occupies. Frequency usability is defined by the power or voltage levels of the detected signal and is often taken at 50% or 70% respectively. Although, a range of frequencies is often quoted, bandwidth itself is an “absolute” value which is measured in Hz.

The relation below defines bandwidth in percentage form:

$$B = \frac{\Delta f}{f} \times 100\% \quad (3.19)$$

Antennas operate efficiently and exhibit optimum performance at frequency ranges for which they are designed. Outside of these frequency ranges, the signal may be degraded or completely undetectable.

Bandwidth is an expensive natural resource which is protected by international conventions and is assigned and allocated by the national telecommunications and broadcasting

CHAPTER 3. LITERATURE REVIEW

regulatory authority of individual countries.

3.9.6 Antenna Aperture

The aperture size of the antenna is related to its beamwidth and gain. The larger the aperture, the narrower the beamwidth and the higher the gain for any given frequency[41]. The magnitude of the effective aperture is sometimes expressed in terms of wavelengths. For narrowband or single frequency signals, the size of the aperture can be expressed in wavelengths and its physical size can be deduced. However, for broadband applications, the physical dimensions may not resemble the wavelengths of operation. The effective aperture, A_{eff} , wavelength, λ and gain, G , of the antenna are related by the following mathematical expression:

$$G = \frac{4\pi A_{\text{eff}}}{\lambda^2} \quad (3.20)$$

This equation illustrates an important point, that is, the larger the effective area of an antenna, the bigger the gain. By substituting $\lambda = \frac{c}{f}$, the above equation can be recast to

$$G = \frac{4\pi A_{\text{eff}} f^2}{c^2} \quad (3.21)$$

This equation clearly defines the gain of an antenna as a function of frequency. If the gain of the antenna is held constant, the equation shows that the effective area, A_{eff} , decreases with increasing frequency and vice-versa. This point was consistent with the design of RFI systems 1,2,3 which comprised two antennas. A physically larger antenna (R&S HL 033) covering the frequency range from 80 MHz to 2 GHz and a much smaller antenna (R&S HL 050) covering the frequency range from 800 MHz to 26 GHz.

3.9.7 Antenna Correction Factor

When electric field strength measurements are required, the reading at the receiver (which is usually in Volts or μV) is converted to the electric field strength by use of the antenna correction factor, k (units of m^{-1}). The antenna correction factor is defined “as a term or factor that is applied to the reading of the receiver so that the reading can be converted to the field strength in either volts per metre (electric field strength) or amperes per metre (magnetic field strength)”.

This antenna correction factor or k -factor as it is generally known, compensates for the following:

1. The effective height or length of the antenna;
2. The loss in the balun matching network between the antenna and the balun;

CHAPTER 3. LITERATURE REVIEW

3. The loss due to mismatch between the balun matching network and the transmission line that connects the balun to the receiver;
4. The loss due to the total length of the transmission line cables between the antenna and the receiver[41];

In linear terms correction factor is the ratio of electric field strength to the receiver voltage i.e $k = \frac{E}{V}$.

From the practical gain, the antenna factor becomes:

$$k = q \times \sqrt{\frac{4\pi Z_0}{\lambda^2 G_{\text{prac}} Z_n}} \quad (3.22)$$

where $q=2$ for asymmetric antennas in which the conducting surfaces are not actually physically part of the antenna and $q=1$ in other cases; $Z_0 =$ Impedance of free space $Z_0 \approx 120\pi$. By substitution,

$$k = \frac{9.73}{\lambda \cdot \sqrt{G}} \quad (3.23)$$

In logarithmic (dB) units the antenna factor, k equals to:

$$k = 20 \text{Log}(f_{\text{MHz}}) - G_{\text{dBi}} - 29.79 \quad (3.24)$$

3.9.8 Polarization

This term describes the shape and orientation of the electric or magnetic field vector as it varies with time in space. The shape and orientation can be linear and circular or elliptical. Linear polarization give rise to vertical and horizontal polarization. What is important is that the polarization of the receiving antenna must match that of the incident wave in order to extract the most power.

3.10 Noise

Noise is a random signal defined as “any unwanted disturbance that obscures or interferes with a desired signal”[12, 15, 24, 33]. It consists of frequency components whose amplitudes and phase cannot be predicted at any instance in time and sets the limit for the dynamic range and the minimum signal that can be adequately detected and translated into meaningful information[33, 40]. This noise floor defines the sensitivity of a device.

Noise affects just about every receiver characteristic and is omnipresent in most RF and microwave devices. It is a major downside for communications and test receiver performance and is the most important parameter to consider when opting to evaluate the

CHAPTER 3. LITERATURE REVIEW

performance of a radio frequency receiver[18]. Noise plays a significant role in RF and microwave performance and metrics such as the noise figure and equivalent noise temperature are important performance determinants.

In the introduction of this chapter, much has been said about the various types of noise. In Chapter 5, we are interested in the frequency spectrum at which noise dominates. We hope to use this information in order to differentiate between the desired signals, RFI and the self-induced noise.

RF and microwave systems can be characterized by both the equivalent noise temperature and noise figure. In this section, we expound on the types of noise and thoroughly review the characteristics of noise and the affects it has on communications and test receivers.

It has previously been stated that noise originates from a number of sources and that these sources can lead to the generation of different types of noise which include shot noise, flicker noise, plasma noise, quantum noise and thermal noise. These types of noise have already been well described in the introduction. The most prevalent noise in RF and microwave systems is thermal noise sometimes also referred to as Nyquist or Johnson noise. This is white noise which follow a random Gaussian distribution. Another important type of noise is phase noise. This type of noise is, however, not explored in this section.

A vast amount of literature available seems to suggest that the thermal noise power delivered to a match load from a conductor or resistor or any thermal source is given by[18, 24, 26]:

$$P_n = kT_0B \quad (3.25)$$

where k = Boltzman's constant = $1.38 \times 10^{-23} W.sec/^\circ K$; T_0 = temperature of the conductor, in degrees Kelvin; B = noise bandwidth of the measuring system in hertz (Hz)[21, 33, 22]

Fourier analysis suggests that a signal at each particular frequency has a certain amount of energy associated with it and that this energy can be measured[22]. At room temperature ($K = 290$) and at a bandwidth of 1 Hz, this energy or power is -204 dB or -174 dBm/Hz. The above equation implies that the noise power is actually the heating value of the signal and that a decrease in temperature leads to corresponding decrease in noise power[40]. Another implication is that a decrease in bandwidth leads to a decrease in noise power. The above equation is an important derivation.

All devices such as oscillators and mixers contribute a certain amount of losses. These insertion losses are due to the presence of resistive components in these devices. As a signal travels through these devices, they add a finite amount of noise to the signal, degradation of the signal, thus, occurs[44]. This reduction in signal is measured using the noise figure, which is mathematically defined as

CHAPTER 3. LITERATURE REVIEW

$$F = \frac{\frac{S_1}{N_1}}{\frac{S_2}{N_2}} \quad (3.26)$$

$$NF = 10 \log_{10} F \quad (3.27)$$

where F =the noise factor, NF =the noise figure, $\frac{S_1}{N_1}$ = the signal-to-noise ratio at the input and $\frac{S_2}{N_2}$ =the signal-to-noise ratio at the output[42]. The noise factor, F , is a key indicator of the performance of a RF system. The noise figure is defined as the amount of noise added to the output signal by the amplifier circuitry[18]. A low noise figure implies that very little noise is added by the signal hosting device and therefore, an RF system with smaller antennas and lower transmit power can be built for the same system performance[42, 44].

For a passive lossy networks such as cables or attenuators, $F = 10^{\frac{a}{10}}$ and $NF = a$, where a =attenuation of network, in dB. It can be seen, therefore, that the noise figure is directly proportional to the attenuation and that if the attenuation is increased, the noise figure is likewise increased. This implies that noise is increased.

The noise factor and equivalent noise temperature are related by

$$T_e = (F - 1) T_0 \quad (3.28)$$

The total noise factor for a system of cascaded networks is given by

$$F_{Total} = F_1 + \frac{F_2 - 1}{G_1} + \frac{F_3 - 1}{G_1 \cdot G_2} + \dots + \frac{F_n - 1}{\prod_{i=1}^{n-1} G_i} \quad (3.29)$$

where F_i and G_i are the noise and gain factors respectively for an individual stage.

The equivalent noise temperature of a cascaded network is given by[18, 42]

$$T_e = T_{e1} + \frac{T_{e2}}{G_1} + \frac{T_{e3}}{G_1 \cdot G_2} + \dots + \frac{T_{en}}{\prod_{i=1}^{n-1} G_i} \quad (3.30)$$

Consequently, the noise power generated by these devices is, according to Equation 2.18:

$$P_n = k T_e B \quad (3.31)$$

where T_0 is replaced by the equivalent noise temperature (T_e). This noise power is normally referenced to the input of a device. The noise power and equivalent noise temperature due to a passive device, such as a resistor, is minute by comparison with that from an active device such as a noise source. For this reason, active noise diode sources are usually employed. These wide-band noise sources enable and assist in the practical realization of the equivalent noise temperature by employing the Y-factor method[18]. The

CHAPTER 3. LITERATURE REVIEW

Y-factor method which is commonly used in radio astronomy to determine the receiver noise temperatures is defined as

$$Y = \frac{P_{hot}}{P_{cold}} \quad (3.32)$$

where P_{hot} and P_{cold} are the noise powers obtained when the loads are connected to the device under test (DUT) and placed in a hot and cold environment respectively or basically switched ON and OFF in which case the subscripts *hot* and *cold* are simply replaced with *on* and *off* as is the case in the “*Proposal to site the Square Kilometre Array*[27].” The Y-factor method yields the equivalent noise temperature to be[18]

$$T_e = \frac{T_{hot} - Y T_{cold}}{Y - 1} \quad (3.33)$$

The difference between the noise power or temperature of the noise generator and the ambient temperature, T_0 , is the excess noise. The excess noise ratio (ENR) is defined as:

$$ENR(dB) = 10 \log \frac{P_g - P_0}{P_0} = 10 \log \frac{T_g - T_0}{T_0} \quad (3.34)$$

where P_0 and P_g are the respective noise power and equivalent noise temperature of the noise generator.

Other practical methods discharged to determine the equivalent noise temperatures are the continuous wave (CW) generator (or direct gain measurement) approach. With this technique, a frequency synthesizer or generator of known specifications is connected directly to the antenna input terminals of the *front-end* of the device under test (DUT). A spectrum analyzer is used to measure the output power for each particular frequency. From this information, the system gain, noise temperature and spectral flux densities are calculated.

3.11 Spectrum Analyzer theory

A spectrum analyzer resolves a signal into its discrete frequency components and measures the power associated with each and every particular unit of frequency of the signal. The resolving power of the spectrum analyzer is governed by the resolution bandwidth (RBW) IF filters.

It has already been pointed out in previous sections that all real devices exhibit power loss effects and generate internal noise. This equipment specific noise is inherently as result of the presence of passive and active devices such as mixers and filters from which the equipment is composed. Such noise or disturbance is largely due to the combination of harmonics and intermodulation products with the signal from a DUT and also due to the presence of spurious frequency response from the analyzer components itself. When a

CHAPTER 3. LITERATURE REVIEW

spectrum analyzer is switched on and its input terminals terminated with a 50Ω terminator, noise fluctuations is observed on the graticule of the display of the analyzer. The level of this noise is dependent on the sensitivity of the device. However, since the purpose of a spectrum analyzer is to display a signal injected at its input terminals. This observed phenomenon is as if noise is applied at the input terminals from an external source. Hence, the observations constitute the Display Average Noise level[21, 25].

The displayed average noise level (DANL) of the analyzer is given by

$$L_{DAN} = 10.\log \left(\frac{k.T.B_{N,IF}}{1.10^{-3}W} \right) + NF_{SA} - 2.5dB \quad (3.35)$$

$$L_{DAN} = -174dBm(1Hz) + \left(10.\log \frac{B_{N,IF}}{Hz} \right) dB + NF_{SA} - 2.5dB \quad (3.36)$$

where NF_{SA} represents the noise figure of the spectrum analyzer and k, T, B have the same meaning as previously denoted [20].

3.11.1 Spectrum analyzer performance and selection criteria

The performance of a spectrum analyser can be measured by studying the TOI, SHI, 1-dB gain compression and DANL, noise figure, video bandwidth (VBW), resolution bandwidth (RBW) and Adjacent Channel Power Ratio (ACPR)[22]. Spectrum analyzers should provide a display of the signal which is distortion-free. Another essential criterion for the assessment of a spectrum analyser is linearity[21]. The input intercept point (with 0dB RF attenuation) is always stated in the analyzer specifications. The higher the specified intercept point the more linear the spectrum analyzer and the larger the dynamic range.

3.11.2 Spectrum analyzer sensitivity and noise

The sensitivity limit of the spectrum analyzer is by definition, the minimum level of an input signal which causes a 3-dB change in the noise level as viewed on the display of the analyzer[21]. This is also called the minimum detectable signal. Since the analyzer is calibrated to reflect the noise at its input, the noise presented at the display represents an effective noise referenced to the input of the analyzer, it follows therefore, that $10.\log(s+n) = 3dB$ which implies that $s+n = 2$ [22].

The maximum sensitivity is attained by setting the attenuation to 0 dB, minimizing the RBW, using log power averaging and connecting a high gain, low noise pre-amplifier to

CHAPTER 3. LITERATURE REVIEW

the spectrum analyzer[46]. It is for this reason that the SA SKA team included two pre-amplifiers, for each frequency band, in the design of RFI Measurement System 2. High sensitivity of the analyzer is especially important for applications in which the resolution bandwidth is prescribed by standards such as the SKA protocol. In these cases reduction of the resolution bandwidth is not permitted and hence the displayed noise cannot be reduced further than that which is prescribed. Trade-off between low displayed noise and high measurement speed must be maintained.

For the display of signals with very low S/N ratio, it is important to reduce the video bandwidth, as well as, the resolution bandwidth by use of narrowband filters with low sensitivities or to increase sweep time when using RMS detectors. The trace is thus smoothed and the signal is clearly displayed. To reduce the displayed noise, the resolution bandwidth is reduced further. Spectrum analyzers featuring a low noise figure allow the use of greater resolution bandwidths and hence shorter sweep times. If the sensitivity of the spectrum analyzer is not satisfactory, a pre-amplifier can be used. This however, can degrade the noise figure by increasing the noise as both the signal of interest and the undesirable noise is amplified [21]. The Agilent 8563EC spectrum analyser circumvents this problem by employing a logarithmic amplifier, which amplifies lower amplitude signals more than higher amplitude signals [22]. This means that the higher noise values are not amplified as much as the lower values. This results in an output at the envelope detector which resembles a skewed Rayleigh distribution with a mean value of 1.253σ . Averaging over number of traces results in a mean value which is 1.45 dB lower. Since the analyser is a peak responding voltmeter calibrated to indicate the RMS value, it is necessary to convert from peak to RMS. The analyser does this conversion by multiplying the readout by 0.707. Scaling the mean value of the Rayleigh distributed noise results in 0.886σ or 1.05 dB below σ . In total therefore, the DANL is $1.05 + 1.45 = 2.5$ dB too low. This is the reason for the correction factor of -2.5 dB mentioned in Equations 3.34 and 3.35 [22].

3.11.3 Spectrum Analyzer operation and functionality

The sweep time of the analyzer is set automatically to account for the RBW, span and VBW[22]. In the AUTO mode, the relationship between VBW and RBW is that the VBW is equal to 3 times the RBW for SINE[20]. For sinusoidal signals with high S/N ratio the video bandwidth is usually set equal to or larger than the RBW. For pulsed signals VBW is taken to be greater than or equal to 10 times the RBW and the spectrum analyzer has to be set to MANUAL. For low S/N the VBW is made substantially less[20]. The recommended settings of VBW in relation to RBW depends on the application.

CHAPTER 3. LITERATURE REVIEW

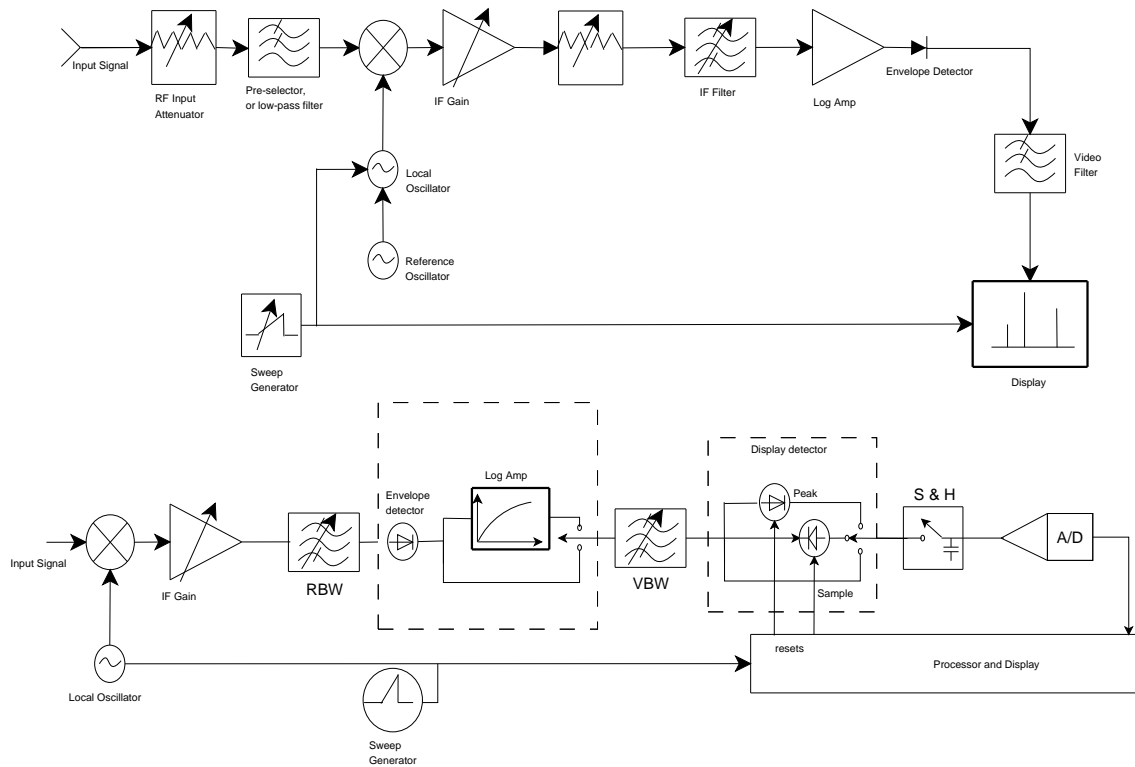


Figure 3.5: Block diagrams of a classic superheterodyne spectrum analyzer (from[22, 40])

3.12 Summary

This chapter discussed the various types of EMI and RFI which was likely to be encountered during the design, development and implementation of RF measurement systems, as well as, presented some of the mechanisms that can be used to combat internally generated EMI. A discussion surrounding the EMI problems encountered by the SA SKA team during the development of RFI Measurement System 2 is also facilitated. The various components used in the development of RFI Measurement System 2 and their operation and parameters of importance are outlined. The key properties of antennas are referred to and concepts such as the k-factor are explained. The concept of noise as encountered in electronic communication systems is discussed in detail. The chapter ends by looking at the theory and operation of the spectrum analyser. Key concepts such as RBW, sweep time, frequency bin, integration time, VBW, DANL are defined. The reason for adding the -2.5 dB correction factor to the results is discussed in depth.

Chapter 4

Implementation of the SKA protocol in South Africa

In this chapter a review of the interpretation and implementation of the SKA protocol in South Africa is presented. A block diagram of the system (RFI Measurement System 2) that was mostly utilized by the SA SKA team at the core site named K3 is revealed and a good description and theoretical interpretation and analysis of the systems is further outlined.

The calibration procedures (as used by the SA SKA team) are uncovered and the differences in calibration results between the various methods (i.e method of direct measurement versus noise diode calibration method) are recorded and the reason for these differences is studied and explained in greater detail. The performance of the spectrum analyser as a scanning receiver is reviewed in greater depth.

This chapter is a detailed dossier outlining “*what the SA SKA team did and how they went about doing it*”. By comparing “*what the SA SKA team was supposed to do*”, Chapter 2, with “*what the SA SKA team did and how they did it*”, Chapter 4, I am in a better position to argue as to the correctness and appropriateness of the work of the SA SKA team.

4.1 Description of the RFI Measurement system 2

RFI Measurement System 2 is a fully automated system designed to scan from 70 MHz to 26.5 GHz. The block diagram of the entire system is depicted by Figure 4.1 below. The diagram shows two vertically polarized antennas, R&S HL 033 and R&S HL 050, atop an adjustable Clark Rotating Mast capable of achieving the required height of 5 metres. The antennas are connected to a G-5500 YAESU Rotator. The G-5500 YAESU Rotator rotates in such a manner as to change the polarization of the antennas from vertical to horizontal and vice-versa. The system was designed to offer both horizontal and vertical polarization in keeping with the stipulation and recommendations of the SKA Protocol

[9].

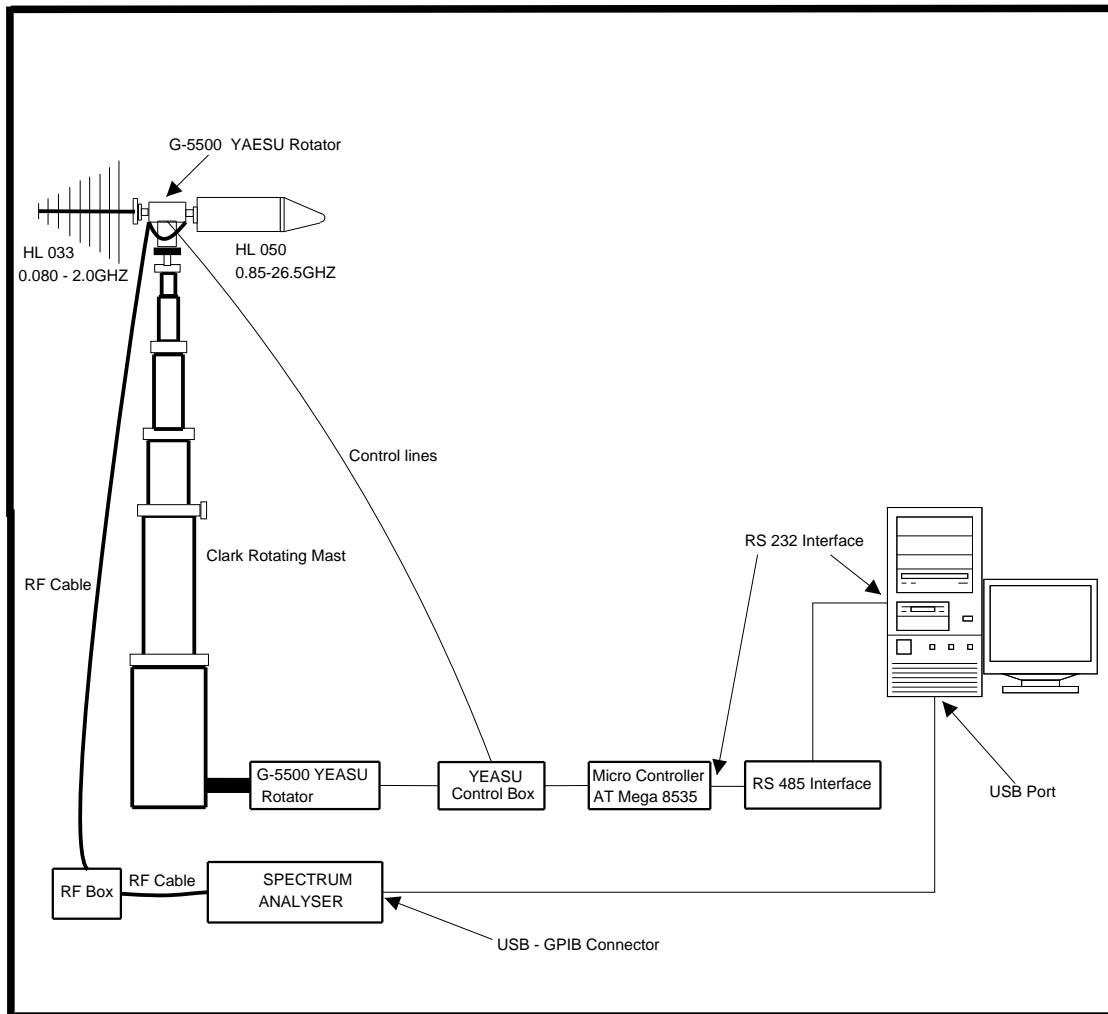


Figure 4.1: Block diagram showing the complete RFI Measurement System 2

The rotating mast is used to change the pointing direction of the antennas in order to achieve the full 360^0 coverage in the azimuth plane. Since the chosen antennas were directional and therefore possessing limited azimuthal coverage, a number of pointing directions were to be affected in order to achieve the full 360^0 coverage as required by the “protocol”[9]. In the case of the R&S HL 033 log-periodic antenna, three pointing directions were conducted for each polarization. For the R&S HL 050 log-periodic antenna, five pointing directions were implemented to achieve the same azimuthal coverage. The reason for the differences in the number of pointing directions is contained in the radiation beam pattern of the antennas. The graphical image, Figure 4.2, below, is an illustration of the beam pattern of the two antennas.

The following equation was used to ascertain the number of pointings, N , to be achieved,

$$N = \frac{360^0}{BW} \quad (4.1)$$

where BW is the beamwidth taken at the $-6dB$ point [9, 17, 27]. At this point the power

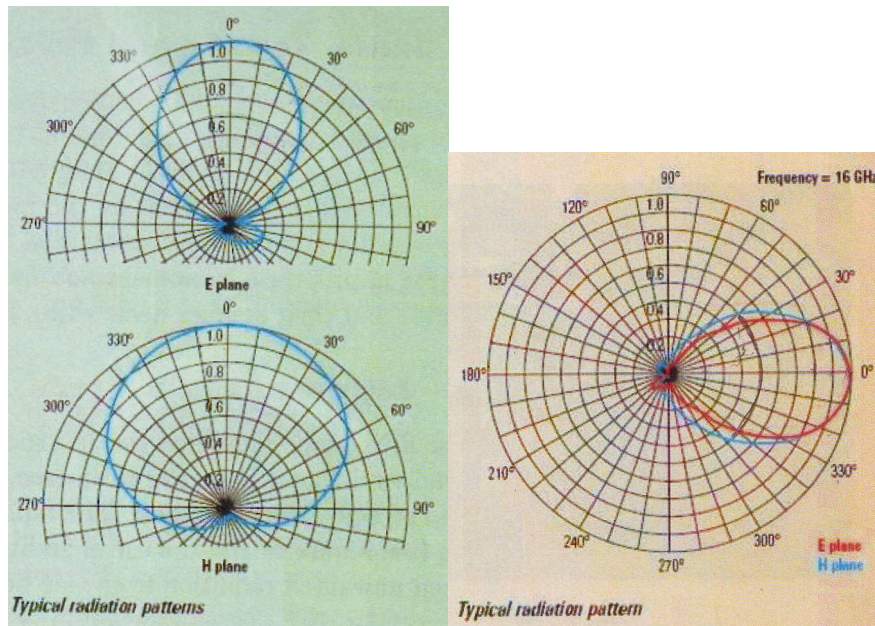


Figure 4.2: Radiation beam patterns of R&S HL 033 (left)[53] and R&S HL 050 (right) [54] antennas

is reduced to one quarter from its maximum. Evaluation of the beam pattern for the R&S HL 033 antenna at the $-6dB$ point revealed a beamwidth angle of 120^0 in the E- plane implying that 3 pointing directions are required in order to achieve 360^0 coverage. The H- plane required even less number of pointings of 2.4. The SA SKA team documented pointing values of 3 for both polarizations for the R&S HL 033 antenna. Although performing measurements in three pointing directions for both polarizations may not affect the results, it does, however, increase the measurement time.

From the radiation plot, the half-power beamwidth of this antenna is 100^0 . Since at $-6dB$ the beamwidth is 120^0 and at $-3dB$ it is 100^0 , this means that when the antenna look angle is increased, its directivity is decreased. The implication is that when the antenna is pointing directly towards the source of radiation, maximum power is received and if the radiating source is situated at an angle of 60^0 or more from the beam centre, the power will be reduced by as much as 0.25 of its maximum. This is not an ideal situation. Especially if you want to survey the environment for strong signals, because some strong signals arriving from angles which are 60^0 or more from the beam centre will be strongly attenuated to almost a quarter of its maximum. These strong signals could then be detected and indicated as weak signals. This is not good. To counter act this problem, a directional antenna with a good response should be employed.

For the R&S HL 050 antenna, the beamwidth angle in the E- plane was found to be 90^0 giving 4 pointing directions according to the above equation. In the H- plane, BW yielded a value of 100^0 . This implied 3.6 pointing directions. Using this antenna, the SA SKA team chose to conduct measurements in five pointing directions [27]. Although this was slightly more than the calculated value of approximately 4 pointing directions. The SA

CHAPTER 4. IMPLEMENTATION OF THE SKA PROTOCOL IN SA

Table 4.1: Specifications for the H&S Log-Periodic Broadband Antenna (R&S HL 033) and (R&S HL050)

Parameter	R&S HL 033	R&S HL050
Frequency Range	80 MHz to 2 GHz	850 MHz to 26.5 GHz
Polarization	Linear	Linear
Input Impedance	50 Ω	50 Ω
Beamwidth angles at $-6dB$ point	$E - 120^0, H - 100^0$	$E - 90^0, H - 100^0$
VSWR	≤ 2	≤ 2.5
Antenna Gain	typ. 6.5 dBi	typ. 8.5 dBi

SKA team provided no documentary evidence or reasons for the use of the antenna with a greater number of pointing directions. However, it is assumed that the lack of documentation of the uncertainty value of the gain of the antennas by the antenna manufacturer may have played a reason for this choice. Conducting measurements in five pointing directions may be a safe option (as it more than covers the 360^0 azimuthal plane) but it does once again increase the measurement times.

The diagram also depicts the interconnection of the various subsystems and clearly points out the type of interfaces used together with their points of interconnect. Of importance is the interconnection of the Agilent 8563EC spectrum analyzer to the rest of the system. From the sketch it can be clearly seen that the output of the RF module is connected directly to the input of the spectrum analyzer via a 10 m Huber+Suhner Sucoflex_104 RF Coaxial Cable and that the USB port of the computer is fed from the GPIB output of the spectrum analyzer. This distinct arrangement allowed for the scanned field measurement data obtained from the spectrum analyzer to be simultaneously and remotely transferred to a computer for processing and storage purposes. This data is sent from the analyzer to the computer as traces composed of 601 data points or trace elements. These traces are, under normal circumstances, stored in the spectrum analyzer as *integers* ranging in value from 0 to 600. The reason for this, is because the spectrum analyzer has a display that has 601 pixels on the horizontal frequency axis and 601 on the vertical amplitude axis with a slight over-range of 10 pixels on the latter axis. Furthermore, the analyzer display has 10 fixed graticule divisions, implying that there are 60 data points per graticule and a 100 dB display range. Although zero represents the bottom-left of the fixed graticule and 600 represents the top graticule line of the spectrum analyzer display, measurements are nevertheless, performed with reference to the top graticule line (600th graticule line).

4.1.1 Data transfer from the Spectrum Analyzer to the computer

One of the major complexities in designing a system of this nature, is that resulting from the transfer of data from the spectrum analyzer to the computer. Data from the 8563EC Spectrum Analyzer is transferred to an external device such as a computer in five different format modes. These modes are extensively described in the Spectrum Analyzer

CHAPTER 4. IMPLEMENTATION OF THE SKA PROTOCOL IN SA

Operations Manual. Choice of the type of mode to employ is ultimately dependent on the measurement speed required and on the availability of adequate computer memory. In my investigation, I could find no documentary evidence to inform me on the type of format mode used by the SA SKA team. A brief description on how the data was to be used was, however, provided in the FITS header files. From this description, I was able to conclude that the TDF-M functionality of the spectrum analyzer was invoked. In this *trace data format*, the data is transferred as measurement units rather than parameter units and the data is in ASCII format which allows for the data to be easily viewed as text files. Since the data is normally processed in the spectrum analyzer as measurement units, transferring the data in this way saves on time and computer memory. This format also allows for each trace element or pixel (*remember*: there are 601 trace elements) to be stored as two 8 bit bytes. Representing pixels in images as byte data is a common practice. Although this format allows for quick aggregation, fast measurement and memory savings, it is nevertheless cumbersome, in that some sort of conversion technique will need to be applied to the output integer data values in order to enable the data to be viewed. This is due to the fact that, the data is stored and transferred to the PC in measurement units rather than parameter units. By this we mean, the conditions under which the data was stored are generally not transferred with the data and therefore some further processing of the data is required in order to reconstruct the conditions so as to view it precisely and accurately on a computer display.

The formula that is generally applied to the data in order to convert the trace data elements (which are linear integer values) to a logarithmic scale is:

$$n = RL + \logScale \times \left(\frac{x}{\frac{600}{10 \text{ divisions}}} - 10 \text{ divisions} \right)$$

where x = integer representation of the binary data, n = real, log data and RL = reference level

Since the SA SKA team performed their measurements with reference to the -10 dBm level [17]. The above equation then reduces to:

$$n = \frac{x}{6} - 100 - 10 \quad (4.2)$$

In my study, it was found that SA SKA had indeed used the above formula to convert the measurements from linear integer values to dBm values.

4.2 Method and Measurements

Section 4.2.1 below describes the way that was used to process the measurement data. This section is more of a statement of the method that was used rather than an assessment of the correctness of the methodology used by SA SKA. The discussion on whether this method was correct or not is a subject of the next section.

4.2.1 Description and sources of Data

The measurement data used in this experiment was collected by SA SKA during a two day measurement campaign commencing on 24 November 2005 and ending on 25 November 2005. For the frequency scan starting from 70 MHz to 150 MHz, fifteen vertical polarization (3 pointing directions \times 5 repetitions) and fifteen horizontal polarization (3 pointing directions \times 5 repetitions) measurements were performed. This totalled 30 full scan measurements contained in 6 different files. Each file contained 5 columns of TAB Delimited data obtained by performing a full scan measurement in one pointing direction five times in line with the stipulation of the “protocol” for the band 70 MHz to 150 MHz as documented in Table 2.3 above. The reason for the different set of pointing directions has already been discussed in Section 4.1 above. This raw measurement data was then stored onto the computer, copied onto DVD’s and delivered to the SA SKA office for further analysis and processing. It was later converted to the binary FITS (Flexible Image Transport System) format for easy transportation and handling. In my analysis, I used the FITS formatted files (as listed Appendix A) as this was the only data format available to me. The important characteristic of the FITS format is that the header portion of the file is separate from the data table portion. The header section is used to describe the conditions, assumptions and constraints under which the data was recorded. The data table portion contains the actual data. In this experiment, the table portion of all the FITS files that were used were exported as tab delimited text files. This enabled the files to be worked on. The measurements were obtained with the spectrum analyzer set to sample detector mode. The spectrum analyzer settings were as tabulated:

Table 4.2: Spectrum analyzer setting for band 70 to 150 MHz. The values in the table were taken from the Fits Header files.

Parameter	Value
Frequency span	0.18 MHz
RBW	3 kHz
VBW	300 Hz
Sweep Time	0.6 sec
No. of repetitions (successive sweeps on the analyser)	5

4.2.2 Data Processing Procedure

In this experiment, all 30 measurement data sets were combined. This was done as follows:

STEP ONE: from the first file, the first row of data for each column was read and assigned to an array. The array was then incremented by 1. There were five columns in each file. This procedure was done ten times until all ten rows of data in each column in each file was binned into the array and then the first ten rows of data from the next file was read into the same array in a different cell. This operation was repeated until data from the first ten rows of each column for all six files was read into the array. This operation resulted in 300 (10 rows \times 5 columns \times 6 files) data values being assigned into the array. This binned data was then sorted in ascending order and the minimum, maximum, average, 90 percentile, 10 percentile and median values were extracted. The above statistical values were then stored in six different arrays each representing for example minimum values, and another array containing maximum values and yet another containing average values and so on and so forth.

The above procedure was repeated until all rows of data from all six files was read. There were in total 267,445 rows of data in each columns of each file. Since each file had five column, this equated to $(267,445 \times 5 \times 6)$ 8,023350 data values and 26744.5 (267 445 data values $\div 10 = 26744$) iterations. This means that the resultant six arrays had 26744 rows of data representing each of the statistical values above.

As already mentioned, each column in each file represents an entire scan from 70 MHz to 150 MHz. This is an equivalent bandwidth of 80 000 000 Hz. Dividing 80 000 000 by a RBW of 300 yields 266 666.666 data values for one scan. If the value 266,666.666 is divided by 600, this equates to 444.444 subscans.

STEP TWO: The data values in each resultant statistical array as defined in step one above, were read back.

STEP THREE: The value read back in step two above was then converted to a dBm power value using Equation 4.2 and the RBW frequency corresponding to this value was determined.

STEP FOUR: Once the frequency was deduced, the receiver gain corresponding to this frequency was intrapolated. It is worthy to note that the receiver gain values were practically measured in 10 MHz frequency steps. Thus the need for intrapolation.

STEP FIVE: Using the value read back in step two, and the frequency and corresponding gain of the receiver, as well as the antenna gain at that frequency, the spectral flux density was calculated from Equation 4.3 below.

STEP SIX: Steps two to five were repeated 26667 times until all the binned values in the array were utilised.

STEP SEVEN: The graph of spectral flux density versus frequency was then plotted. These

graphs are shown in Chapter 5.

STEP EIGHT: Steps two to seven were repeated for all the statistical values i.e for the mean, median, maximum, minimum, 90 percentile and 10 percentiles.

4.2.3 Measurement Schedule

In order to perform the RFI measurements within the required SKA specifications of time, budget, and technical adherence as depicted in SKA Protocol, a measurement strategy and schedule was devised. Table 2.4 in Section 2.6 lists the dwell times, number of repetitions and total measurement times for each of the frequency bands to which the RFI measurement systems had to conform.

If we calculate the frequency span ($Span$) using Equation 2.9 and a RBW of 3 KHz as suggested in the “protocol” and depicted in Table 2.4 we get,

$$Span = (trace\ points - 1) \times RBW = (601 - 1) \times 3000 = 1.8MHz$$

However, if the span is reduced to 0.18 MHz, Equation 2.7 yields a frequency bin value which is equal to 300 Hz ($FrequencyBin = \frac{Span}{(trace\ points - 1)} = \frac{180000}{600}$). This is much narrower than the RBW. Therefore, erroneous results are not expected. In a resolution bandwidth of 3 kHz as specified in the Protocol, this would imply that 10 samples would have to be taken. However, since there was a total of 30 scans, this implied a sample size of 300 power values for each designated frequency. This large number of power values would ensure that a better approximation of the Root Mean Square (RMS) power is achieved. Using 300 samples for each frequency interval was, therefore, in agreement with the Lee Criteria [65]. Lee (1985) [65] found that in order to accurately estimate the local average power of a mobile radio signal, the sufficient number of samples had to be approximately 36. In other words the greater the number of samples taken, the greater the chance of accurately estimating the power level of the transmitted signal.

The sweep time was calculated using Equation 2.6 as ($t_{sw} = \frac{t_{pd} \times Span}{RBW} = \frac{10}{1000} \times \frac{180000}{3000}$) and was found to be equal to 0.6 seconds. This implies that the time taken for each sample is 1 ms ($\frac{0.6}{601-1} \times 1000$).

This value is well within the rise time value of 0.66 ms as calculated using Equation 2.10, ($t_r = \frac{k}{RBW}$), where k is assumed to be equal to 2. The above equation denotes the time required for the charging of filter capacitors. If this value was greater than 1ms, than filter capacitors may not have been fully charged leading to loss of signal amplitude. A value of k = 3, would yield a rise time of 1ms, which would be equal to the sample time of 1ms.

4.3 RF Module of RFI System 2

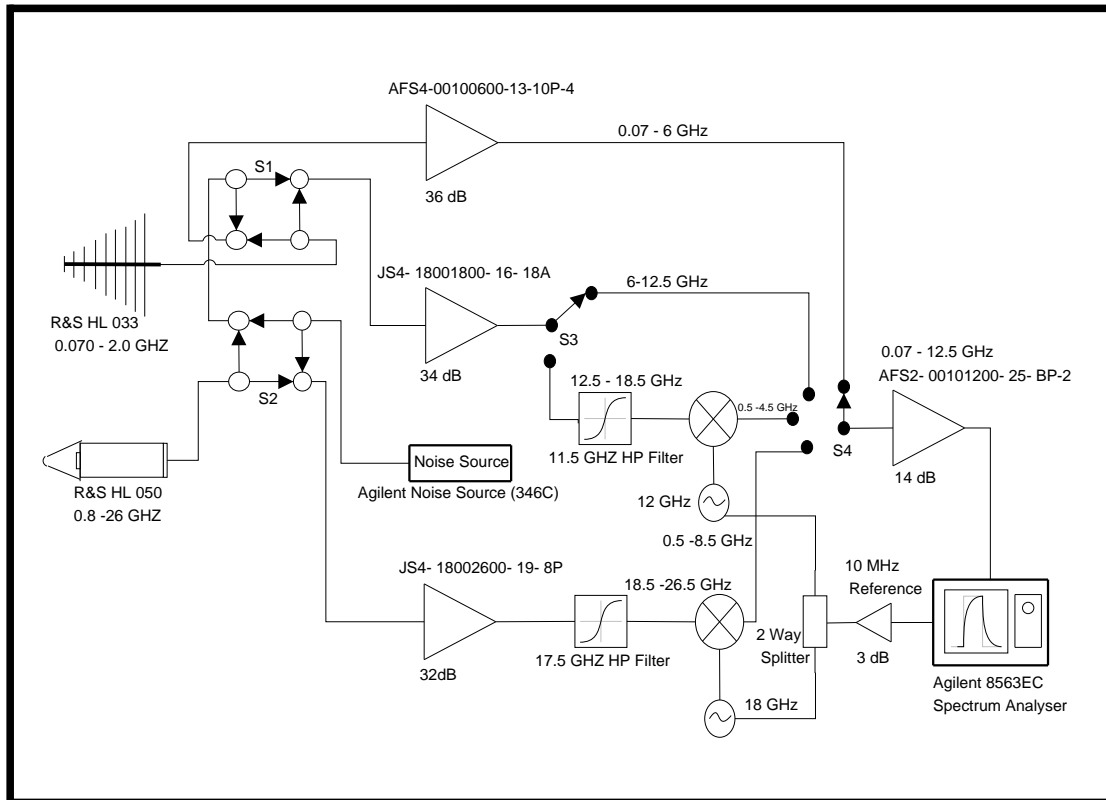


Figure 4.3: Block Diagram of RFI System 2 (from[17])

The above block diagram depicts the RF module of the RFI measurement system 2 as was built by the SA SKA team in compliance with the recommendations of the SKA protocol [9]. This module comprised of two broadband log-periodic directional antennas for the detection of signals, varying in frequency from 70 MHz to 26.5 GHz. Selection of the appropriate antenna was dependent on the desired signal frequency and was done by using one of two switches, S1 and S2. The detected signal was further amplified by the relevant amplifiers as depicted in the sketch and presented to the spectrum analyzer for measurement purposes. Two filters were used for image and spurious frequency rejection. Down conversion of the higher frequency signals was achieved by mixing the selected signal with a signal from a source locked to the 10 MHz reference signal derived from the spectrum analyzer.

The frequency dependency of amplifiers and the fact that “a one size fits all” amplifier could not be found in time (due to project time constraints), resulted in the existence of five different signal paths representing five different frequency bands. These bands are as tabulated in Table 4.4 below. All signals were, however, connected to a common, 14 dB wideband amplifier using a 1-pole 4-throw switch, S4 and delivered to the single input of the spectrum analyzer by means of a 10 metre low impedance sucoflex cable. The types and models of components used in the RF assembly are shown in Appendix B.

CHAPTER 4. IMPLEMENTATION OF THE SKA PROTOCOL IN SA

Table 4.3: Table showing the resultant frequency bands (from [17, 27])

Band Number	Frequency Range
1.	70 MHz - 2 GHz
2.	2 GHz - 6 GHz
3.	6 GHz - 12.5 GHz
4.	12.5 GHz - 18.5 GHz
5.	18.5 GHz - 26.5 GHz

The table below displays the gain budget of the band 1 path. Not all the tolerances of the respective components were recorded in the manufacturers's data sheets. For this reason, It was therefore decided to employ the antenna gain error estimation as used by the Australian team for their LOFAR experiment[73]. Tolerances for the amplifiers were also not specified. In this case, I used the gain flatness values as specified in the manufacturers's data sheets.

Table 4.4: Table showing the resultant theoretical system gain for path 1. *The information contained in the table was obtained form the Data Sheets of the Manufacturers of the various components.*

Component	Specified Gain (dB)	Tolerances (dB)
Antenna	+6.5	± 1
Antenna feed cable loss	-0.2	± 0.1
Switch S1	-0.2	± 0.1
Amplifier 1	+36	± 3
Switch S4	-0.2	± 0.1
Amplifier 2	+14	± 1.5
Sucoflex cable	-1.7	N/A
Analyzer Correction	+2.5	N/A
Total System Gain	+56.7	± 5.8

From Table 4.5 below, the total system gain (including the antenna gain) for band 1 is found to be 56.7 ± 5.8 dB. This means that, in theory, the total system gain should lie somewhere between 62.5 and 50.9 dB. In practice however, this may not be the case. Imperfections in the manufacturing processes could lead to the electrical, chemical and to some extent physical properties of components deviating from their known specifications. It is therefore, highly probable for the system gain to lie outside these boundries especially if the amplifiers are over-driven as was discovered by SA SKA during their measurement campaign. It is for this reason that we decided to work out the *worst case* and *best case* scenario. The best case scenario is when the total system gain is high and the worst case is when it low. By doing this, we hoped to establish whether the spectral flux density calculated by SA SKA was in agreement with that performed by us through the simulation

CHAPTER 4. IMPLEMENTATION OF THE SKA PROTOCOL IN SA

exercise. If true then we are able to confer that the calibration technique was reasonably sound and therefore the measurement system was adequately developed.

It should be borne in mind that the above system gain calculation includes the gain of the antenna. The total system gain is than mathematically represented as follows:

$$G_{sys}(f) = G_{rec}(f) + G_{ant}(f)$$

where $G_{sys}(f)$ =Total System Gain as a function of frequency, $G_{rec}(f)$ and $G_{ant}(f)$ are equal to the gain of the receiver and the antenna respectively as a function of frequency. From the values in Table 4.5 above, $G_{rec}(f) = 50.2$ dB. It is very important that this distinction be made, as the spectral flux density is calculated using Equation 4.3 below which shows a clear demarcation between receiver gain and antenna gain.

$$S(f)[dBW.m^{-2}.Hz^{-1}] = P_{SA}(f)[dBm] - G_{ant}(f)[dBi] - G_{rec}(f)[dB] - 10\log(RBW[kHz]) + 20\log(f[MHz]) - 95.54 \quad (4.3)$$

The above equation was used extensively by the SA SKA team and formed the cornerstone for most of the spectral flux density calculations [27]. The value of -95.54 arises from conversion of the various units. Derivation of this formula is discussed in the Appendix C.

Another important consideration is that concerning the spectrum analyzer correction factor of -2.5 dB. The reason for this correction factor has already been discussed in Section 3.11.2. I was informed that the SA SKA team did not take this factor into account in their calculations. In my calculation I made sure that this correction factor is considered.

4.4 Summary

This chapter showed how the requirements of the “SKA Protocol” were addressed in South Africa. The design and development of the RFI Measurement System 2 was discussed in greater length and the components used in the development of the system were documented. The method of transferring data from the spectrum analyser to the computer is also detailed, so is the procedure followed in processing the vast amount of measurement data obtained during the measurement campaign. The chapter concludes by tabulating a budget of the gains and losses of individual components making up the system. The tolerances of the various components is also included in this table. A total theoretical system gain of 56.7 ± 5.8 dB was calculated and documented.

Chapter 5

Results

In the first chapter of this document, we looked at the problems posed by RFI on radio telescopes and briefly discussed ways to cushion the radio telescopes against the negative effects of RFI. We introduced the SKA and showed how the SA SKA team fits within the overall structure of the International SKA Project. We further listed, in sufficient detail, the objectives of my research and ended the chapter by looking at the data collection methodology, discussing the significance of my study, as well as, the structure of my dissertation.

Chapter 2 was focussed on laying out the theoretical framework for my reasearch and discussing the key technical concepts and knowledge required in order to fully grasp and appreciate this work.

In succeeding chapters, we did not only look at *what the author was required to do* but also focussed on understanding *what the SA SKA team did* and *how they did it*. Since I have already explained the method used to arrive at my results, I will straight-away state my key findings and show how my results compare with that obtained by the SA SKA team.

5.1 Design discrepancies

After an intense study of the system a number of design anomalies were detected. Some of these anomalies were the result of operating some of the RF components at conditions which deviated from their normal operating conditions as specified on the manufacturer's data sheet. The first most blaring and most obvious, was that resulting from the use of the Log-Periodic Broadband Antenna R&S HL 033. This model of the antenna is designed with an operating frequency range stretching from 80 MHz to 2000 MHz. In this system, it was used to lock onto frequencies ranging from 70 MHz to 2000 MHz rather than from 80 MHz to 2000 MHz.

A very important design aspect of the log-periodic antenna is that at 'frequencies of f , rf ,

CHAPTER 5. RESULTS

r^2f, \dots, r^nf it properties are the same and when these frequencies are plotted on a logarithmic scale, these frequencies are equally spaced' [41]. This means that the performance of the antenna is periodic as a function of the logarithm of the frequency [85]. Furthermore, if the 'frequencies are closely spaced, the antenna can provide uniform performance over a wide range' [41]. We can use this knowledge in order to estimate the antenna gain values for frequencies below 80 MHz.

The following diagram shows the gain versus frequency curve of the antenna under discussion.

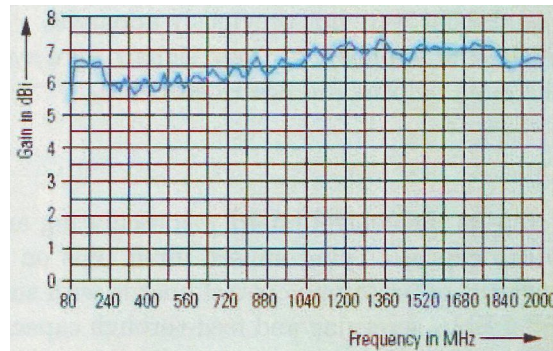


Figure 5.1: Gain vs Frequency (from[53])

The graph of Gain vs Frequency as shown above, confirms the fact that the normal frequency of operation for optimum gain derivation is from 80 MHz to 2000 MHz and not from 70 MHz as indicated by SA SKA documentation. Furthermore, it can be seen that for frequencies between 80 MHz and 800 MHz, the gain flatness is $\pm 1\text{dB}$ and that at 80 MHz the gain is approximately $5.5\text{ dB} \pm 1\text{dB}$. The implication is that it could range between 4.5 dB and 6.5 dB.

Recall that the gain, G , the frequency, f , and the k-factor, k are related by the following mathematical expression:

$$G_{\text{dBi}} = 20\log(f_{\text{MHz}}) - k_{\text{dBi}} - 29.79 \quad (5.1)$$

This equation informs us that if the k-factor and frequency are known, than the gain can be approximated.

Since this antenna is not designed to operate at frequencies below 80 MHz, this implies, therefore, that using Antenna R&S HL 033 to capture signals of frequencies below 80 MHz could lead to inconsistent and erratic results. Another reason is that at frequencies below 80 MHz, it becomes difficult to estimate the antenna gain. Recall that Equation 4.3 (which translates to $P = SAB$) relies on the antenna gain which is a function of frequency. This implies that if the antenna gain cannot be accurately estimated then the spectral flux density cannot be properly established.

In my experiment, however, I used the k-factor values as depicted in Appendix D and predicted through calculation that the antenna k-factor drops to 2.4 dB at 70 MHz from

CHAPTER 5. RESULTS

a high of ± 3 dB at 80 MHz. This value was achieved by plotting 3 dB at 80 MHz, 8 dB at 160 MHz and 12 dB at 240 MHz onto a graph paper and using linear interpolation, the k-factor at 70 MHz was estimated to be 2.4 dB as already mentioned. Once the k-factor was known, Equation 5.1 was utilised in order to calculate the gain at 70 MHz. The gain was found to be 4.71 ± 1 dB. This value is in agreement and within boundary of the values for the 80 MHz range and is therefore acceptable. Using the MATLAB code in Appendix E, the k-factor values, frequencies and corresponding gain values were generated and subsequently the spectral flux densities were established by using Equation 4.3.

From the numerous SA SKA documentation that I perused, I could not find anything to inform me as to the method used by the SA SKA team to determine the gains at this frequency range. I was however, informed that a “rule of thumb” was used. In e-mail correspondance, I was informed that the SA SKA team used the property that the power spectrum of naturally occurring noise, s , can be approximated by $s(f) \propto \frac{1}{f^3}$ [86]. The SA SKA team attempted to get rid of the notch at the 80 MHz, by making the assumption that everything below 70 MHz is noise and thus averaging the noise to look the same as galactic noise. This accounts for the differences in our graphs at this frequency range.

A second important short-coming of the RFI System 2 was the use of the 36dB LNA (AFS4-00100600-13-10P-4). See Appendix B. This LNA has a specified frequency operation values ranging from 100 MHz to 6 GHz. In this system it was used to amplify signals ranging from 70 MHz upwards rather than from 100 MHz.

5.2 Analysis of results

It has already been pointed out that some of the key deliverables required from the SA SKA team were that of graphs showing Spectral Flux Density (SFD) on the vertical axis in units of dBW/m²/Hz versus frequency in Hz. Since the purpose of the measurement campaign was to establish how much EM radiation was present at the prospective SKA sites, it therefore makes sense that the *least* amount (minimum), as well as, the *maximum* amount of EM energy be determined for each unit of frequency in the area. The minimum values determines the minimum detectable signal or the threshold noise and determines the sensitivity of the current system. It could also help with the future RFI mitigation strategies and preventative measures. The maximum is used to rank sites.

It is also wise at this stage to note that although Johnson et al. found that a vast amount of RFI is detectable at very high altitudes [63, 64], the RFI Measurement System 2 was designed to detect signals arriving from the distant horizon and not from the sky. This was done in adherence to the recommendations of the SKA Protocol.

In this section, the minimum, 10 percentile, mean, median, 90 percentile and maximum spectral flux density plots for each unit of frequency are documented. In all cases, the top plot is that determined, reconstructed and generated by the author using MATLAB and

CHAPTER 5. RESULTS

following the procedures and theories as previously discussed in Chapter 2 and 4, whilst the bottom plot is an exact replica of the plots generated by the SA SKA team.

5.2.1 Degree of Dispersion of Data

Before looking at *what was achieved*, we thought it important to examine the actual, raw, uncalibrated data in order to establish first, *what we should be seeing*. We first calculated the standard deviation (for each frequency bin) in order to see how the data varies from the local mean (in that bin) and then by working out the coefficient of variation, we were able to establish the degree of dispersion of the data in each frequency bin. Recall, that too much variation or spread in the data is usually a sign of defect [81]. If the data is too widely dispersed, it could mean that:

1. the data is corrupt, as most spectral flux density values in that frequency bin should lie close to each other,
2. there were some signals which varied immensely from each other. This variation could have been caused by picking up intermittent signal(s) which were not present during the previous measurements such as frequency hopping signals or it could have resulted from non-standardised measurement practice (measurement at different times of the day and in different weather conditions).
3. or it could have been simply as result of locally induced RFI.

The plot above shows the Coefficient of Variation (COV) on the vertical axis in percentage versus Frequency on the horizontal axis. From, the chart above, it can be seen that for frequencies between 90 MHz and 110 MHz, the degree of dispersion is quite high reaching the highest value of 48.04 % at frequency 103 MHz. Also for frequencies of 125 MHz, 138 MHz and 150 MHz high values of dispersion can be seen with a COV value of 40 % occurring at about 138 MHz. The implication of this is that we should observe spikes of extremely high strength at these frequencies.

The above calculation was based on the assumption that the data used follows a Gaussian distribution.

5.3 Spectral Occupancy

In order to determine spectral activity at the Karoo 3 site, the author generated the Spectral Flux Density versus Frequency curves using MATLAB as shown below.

Firstly, we were interested in knowing how many signals exceeded the median value (taken over the entire band) by 6 dB. This is addressed by the top chart in the figure below.

CHAPTER 5. RESULTS

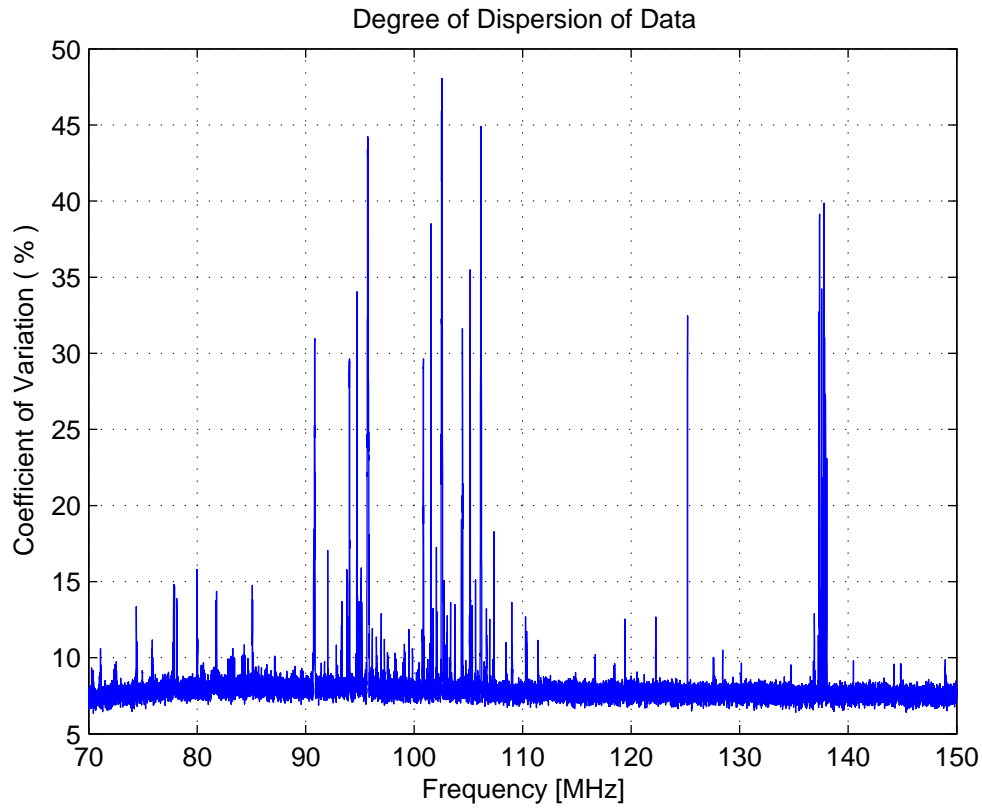


Figure 5.2: Plot of Coefficient of Variation (%) versus Frequency (MHz)

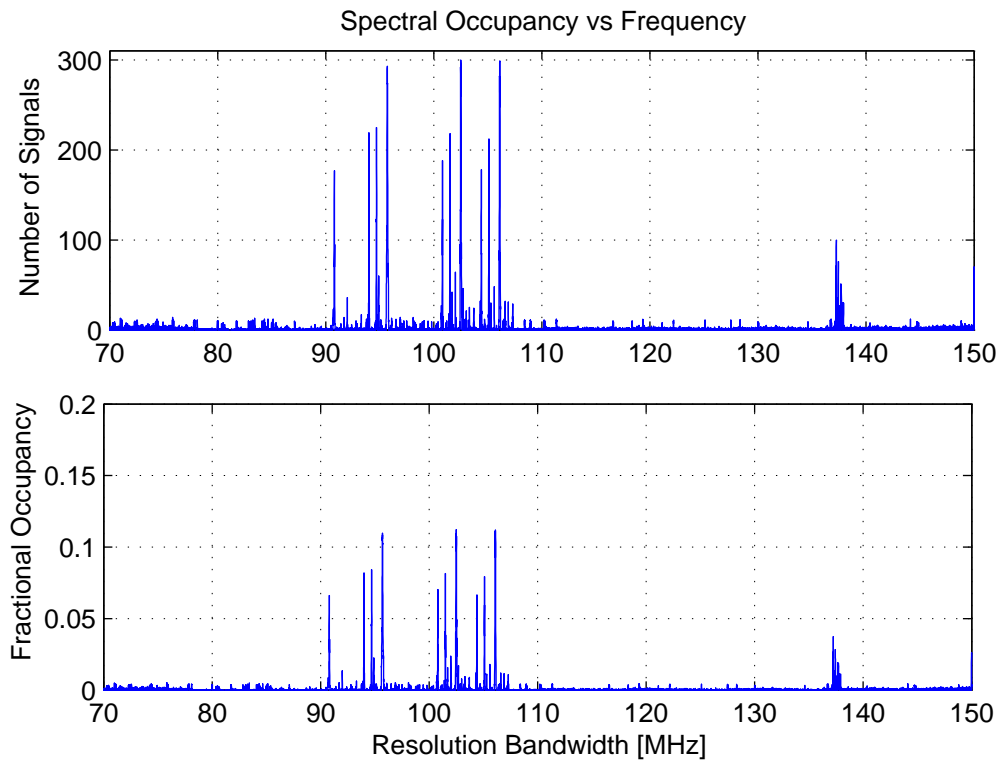


Figure 5.3: The above two plots show the spectral occupancy as a function of frequency (RBW). The top plot shows the number of signals which exceed the median spectral flux density by 6 dB in each frequency bin, whilst the bottom plot depicts the number of signals exceeding the median spectral flux density by 6 dB in each frequency bin as a fraction of the total signals available.

CHAPTER 5. RESULTS

The bottom plot is a ratio of the amount of signals in each frequency bin which exceed the median by 6 dB to the total number of signals in the entire frequency band (70 MHz - 150 MHz). This informs us as to the percentage of signals which exceed the median by 6 dB in each frequency bin and indicates the fractional occupancy. The median was calculated from the SFD values of the entire band.

5.3.1 Minimum

The plots below depict the minimum detectable spectral flux density using RFI Measurement System 2. As already pointed out, this forms the sensitivity of the system. From the graphs it can be seen that the baselines lie somewhere in the region of ± -204 dBW/m²/Hz and that for frequencies below 80 MHz, the plots tend to be uncorrelated with the SA SKA plot over-shooting the -200 dBW/m²/Hz mark at a frequency of 70 MHz and achieving a high of -178.9 dBW/m²/Hz at 102.5 MHz. This is in contrast to my plot which shows a SFD value of -202 dBW/m²/Hz at 70 MHz and a maximum SFD of -177.2 dBW/m²/Hz at 102.5 MHz . The reason for this uncorrelation has already been discussed in length in Section 5.1 above. For most of the graph, however, *similarities* can be observed and there is a tendency for the two graphs to follow each other. The minimum values curve was derived by determining the minimum SFD value found in each frequency bin and plotting this on a system of X-Y co-ordinates. What this implies therefore, is that the curve will not show any value higher than the maximum and consequently the curve will tend to assume a baseline.

CHAPTER 5. RESULTS

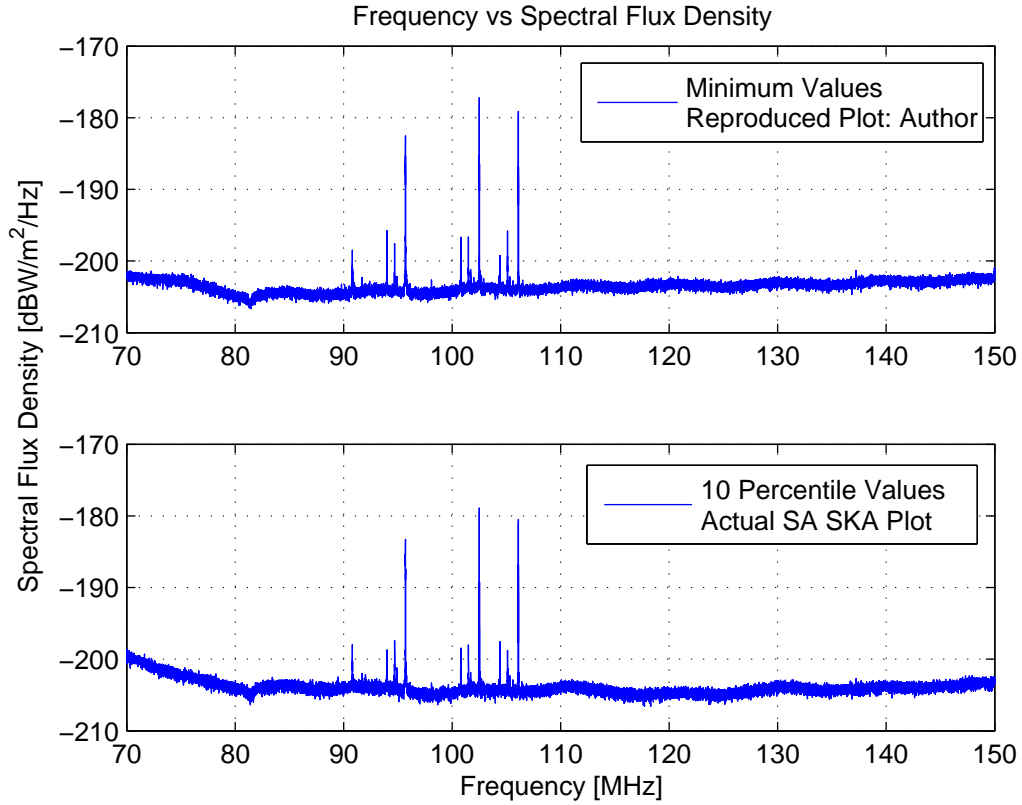


Figure 5.4: Plot of Frequency versus Spectral Flux Density. The plots were derived using the *minimum spectral flux density values* and *10 percentile SFD values*. Top graph shows the *reprocessed plot* as performed by the author whilst the bottom shows a plot derived by the *SA SKA team*. The correlation between the two curves is 0.3218.

Table 5.1: Statistics for Minimum Values Curve (*Correlation coefficient = 0.3121*)

Statistics	Reproduced	Actual SA SKA Plot	Difference
Minimum	-206.7	-206.6	-0.1
Maximum	-177.2	-178.9	-1.7
Median	-203.5	-204.1	-0.6
Mean	-203.5	-204.1	-0.6
Standard Deviation	1.094	1.224	0.13
Range	29.43	27.66	1.77

CHAPTER 5. RESULTS

5.3.2 10 Percentile

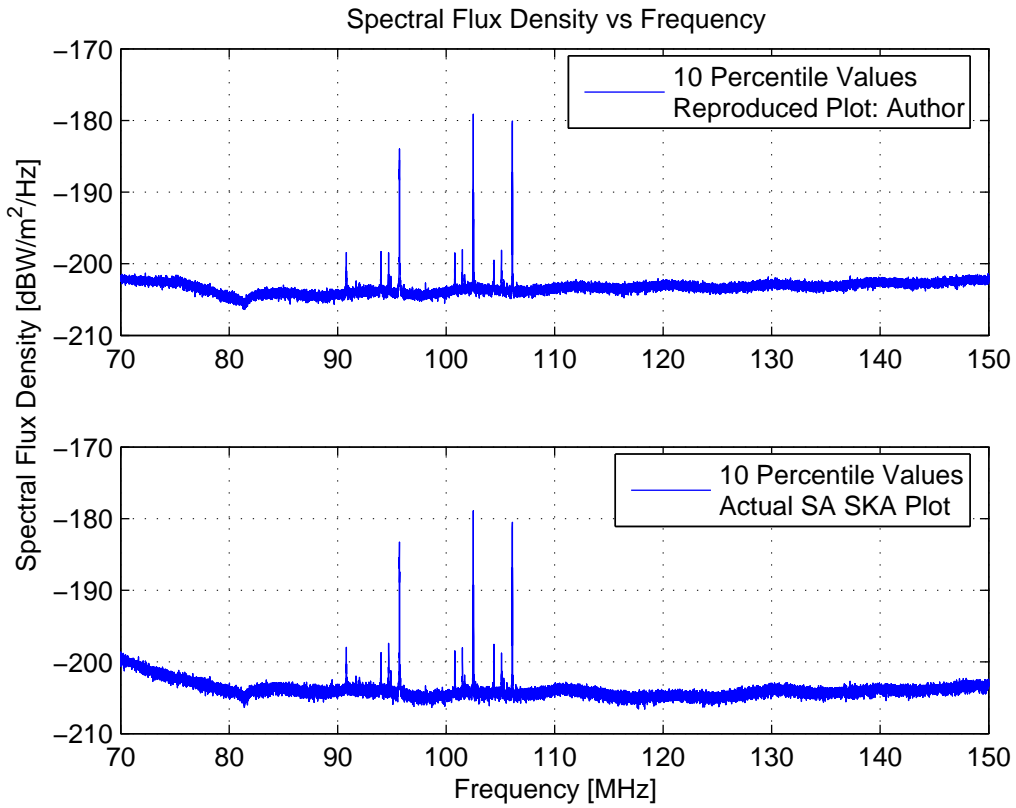


Figure 5.5: Plot of Frequency versus Spectral Flux Density. Top graph shows the *reprocessed plot* as performed by the author whilst the bottom shows a plot derived by the *SA SKA team*. The plots were constructed using the *ten percentile spectral flux density values*.

Table 5.3: Statistics: 10 Percentile Values (*Correlation coefficient = 0.3121*)

Statistics	Reproduced	Actual SA SKA Plot	Difference
Minimum	-206.4	-206.6	-0.2
Maximum	-179.1	-178.9	-0.2
Median	-203.3	-203.9	-0.6
Mean	-203.3	-204.1	-0.8
Standard Deviation	0.9891	1.224	0.2349
Range	27.25	27.66	0.41

The baselines of the above two plots closely match that of the minimum values plots in Section 5.3.1. The reprocessed plots (top) for minimum and 10 percentile are almost similar (correlation coefficient = 0.3121) with both plots peaking at round about -177

CHAPTER 5. RESULTS

dBW/m²/Hz. This similarity is to be expected since the lower SFD values are considered. The important question to ask is *what is the 10 percentile plots suppose to demonstrate?* The ten percentile is supposed to show us 10 % of those values which are closer to the minimum. From this we can therefore infer that the inconsistency is clearly due to the work of the SA SKA team and cannot be attributed to that of the author.

5.3.3 Mean

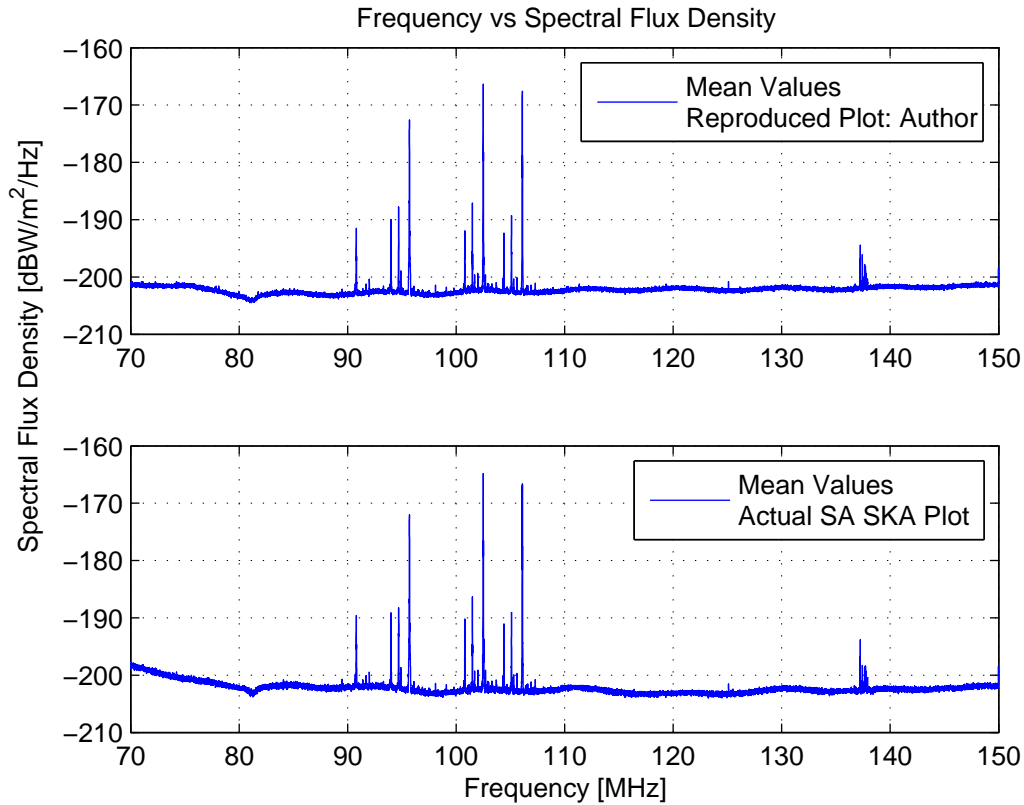


Figure 5.6: Plot of Frequency versus Spectral Flux Density. Top graph shows the *reprocessed plot* as performed by the author whilst the bottom shows a plot derived by the SA SKA team. The plots were constructed using the *mean spectral flux density values*. The two plots show maximum values of -166.4 dBW/m²/Hz at a frequency of 102.5 MHz and -164.8 dBW/m²/Hz.

Table 5.5: Statistics: Mean Values (*Correlation coefficient = 0.3645*)

Statistics	Reproduced	Actual SA SKA Plot	Difference
Minimum	-204.5	-204	-0.1
Maximum	-166.4	-164.8	-1.6
Median	-202.2	-202.2	0.0
Mean	-202.2	-202.4	-0.2
Standard Deviation	1.399	1.643	0.244
Range	38.07	39.15	1.08

CHAPTER 5. RESULTS

The averaging process has a tendency to shift the baseline and is usually biased towards the more dominant values. In other words, in a bin of ten values if there is more higher values than lower values, the tendency is for the average to assume a higher value rather than a low value. This fact is consistent with the top graph which shows a more pronounced signal at 138 MHz. The table above shows us that there is a strong correlation ($\text{corr} = 0.3645$) between the two plots.

5.3.4 Median

In the median values graph below, the signal which was observable at frequency of 138 MHz on the mean values graph is not observable on this plot. This is due to the nature of a median. The median is computed by first sorting the data values from smallest to highest and then considering either one middle value (if there is an odd number of data values) or by taking two middle values and dividing them by two (for even number of data values). The averaging effect gets rid of most of the spectral activity. The end result is a much smoother graph being obtained. This is in strong contrast to the maximum or the minimum plots where the actual values are considered and thus depicting more spectral activity. The plot below is consistent with what has been discussed.

CHAPTER 5. RESULTS

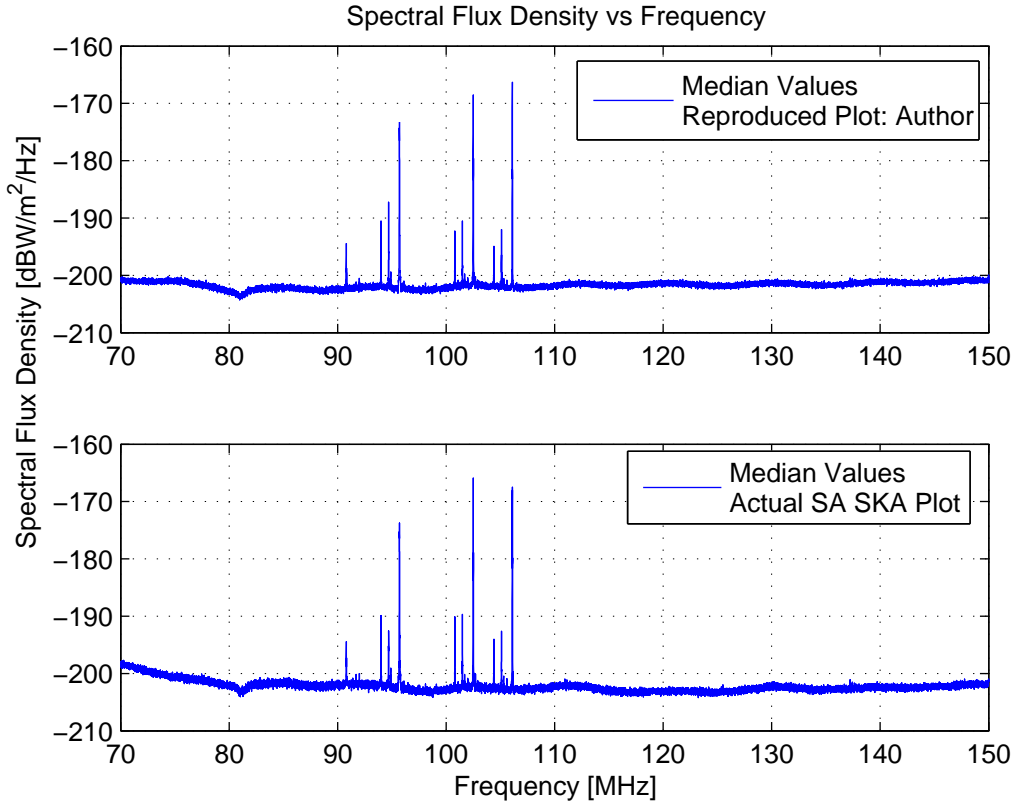


Figure 5.7: Plot of Frequency versus Spectral Flux Density. Top graph shows the *reprocessed plot* as performed by the author whilst the bottom shows a plot derived by the *SA SKA team*. The top plot was constructed using the *median spectral flux density values* whilst the bottom plot is that of *mean values*.

Table 5.7: Statistics: Median Values (*Correlation coefficient = 0.2538*)

Statistics	Reproduced	SA SKA
Minimum	-204.83	-204.2
Maximum	-166.3	-165.9
Median	-201.7	-202.2
Mean	-201.7	-202.2
Standard Deviation	1.215	1.457
Range	37.98	38.26

CHAPTER 5. RESULTS

5.3.5 90 Percentile

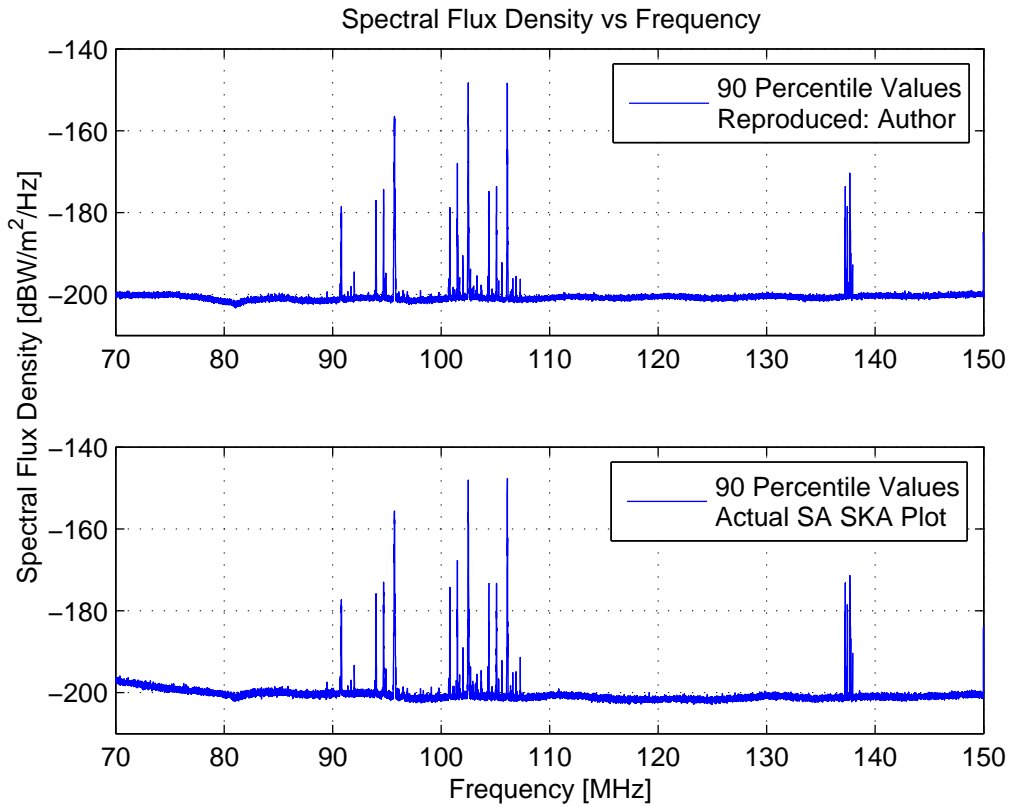


Figure 5.8: Plots of Frequency versus Spectral Flux Density. Top graph shows the *reprocessed plot* as performed by the author whilst the bottom shows a plot derived by the *SA SKA team*. The plots were constructed using the *90 Percentile spectral flux density values*.

Table 5.9: Statistics: 90 Percentile Values (*Correlation coefficient 0.4425*)

Statistics	Reproduced	Actual SA SKA Plot	Difference
Minimum	-203.2	-202.9	-0.3
Maximum	-148.3	-147.7	-0.6
Median	-200.5	-200.4	-0.1
Mean	-200.7	-200.8	-0.1
Standard Deviation	2.538	2.754	0.216
Range	54.88	55.22	0.34

The correlation coefficient for the above two plots is 0.4425. Since, perfect correlation has a coefficient of 1, a value of 0.4425 can be deemed to show strong correlation. The baselines are depicted at -200 dBW/m²/Hz in both graphs. Identical maximum SFD values of ± 148 dBW/m²/Hz are pictured here with the peaks at 138 MHz reaching similar values of ± 171 dBW/m²/Hz for both plots.

5.3.6 Maximum

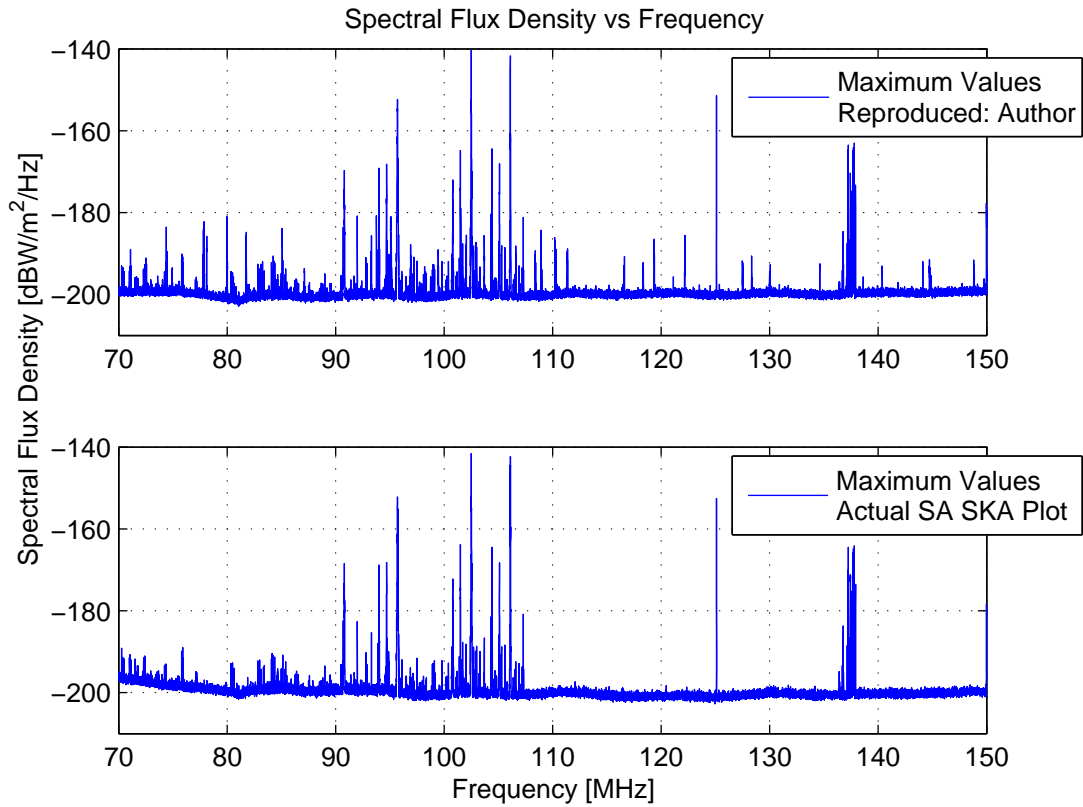


Figure 5.9: Plot of Frequency versus Spectral Flux Density. Top graph shows the *reprocessed plot* as performed by the author whilst the bottom shows a plot derived by the *SA SKA team*. The plots were derived using the *maximum spectral flux density values*.

Table 5.11: Statistics: Maximum Values (*Correlation coefficient is 0.4430*)

Statistics	Reproduced	Actual SA SKA Plot	Difference
Minimum	-202.9	-202.9	0.0
Maximum	-140.4	-140.4	0.0
Median	-199.4	-199.4	0.0
Mean	-200.0	-200.0	0.0
Standard Deviation	3.587	3.587	0.0
Range	62.46	62.46	0.0

The above curves constructed using the maximum SFD values versus frequency also show strong similarities and correlation, with a correlation coefficient of 0.4430 and maximum peaks at ± 140.4 dBW/m²/Hz for both graphs. A signal of strength -152 dBW/m²/Hz which has not been visible in any of the previously discussed graphs is now visible at a frequency of 125 MHz. The peaks at 138 MHz assume similar values of ± 162 dBW/m²/Hz

CHAPTER 5. RESULTS

in both cases. The baselines are once again quite pronounced at $-200 \text{ dBW/m}^2/\text{Hz}$ for both graphs. The top plot that is generated by the author, however, displays far more spectral activity than that provided by the SA SKA team. Important question is *why is there so much more spectral activity in the reprocessed top plot than the actual SA SKA (bottom) plot and why is there a new signal at 125 MHz which is not visible in any of the graphs.*

The maximum values plot is generated by considering and plotting the maximum value (only) found in each bin whereas for example in the mean curve, the average of all the values in the frequency bin are considered and this may shift the peak towards the more dominant values. It is also precisely for this reason that the reprocessed plot above exhibits more activity than the other plots. Based on this assessment it can be concluded therefore that the SA SKA plot was derived after some averaging had been affected.

In the differences column, however, it can be seen that there is no difference between the minimum, maximum, mean and median values, even the range and standard deviation assume identical values. This is proof of the similarity of the two plots. *However, the fact that the maximum plot of the SA SKA differs from that of the author in terms of spectral activity should be frowned upon.*

5.4 Considering the tolerances

The manufacturer of equipment and components usually quote the levels that the components or equipment can tolerate. In RF metrology, it is best practice that components are not operated beyond these tolerances [60, 71]. The tolerances of the equipment and components making up RFI System 2 were considered and using Equation 2.16 the spectral flux densities for each unit of frequency were computed and a plot of Spectral Flux Density versus Frequency for a *best* case and *worst* case scenario was generated . The computation was done by writing a code in MATLAB.

CHAPTER 5. RESULTS

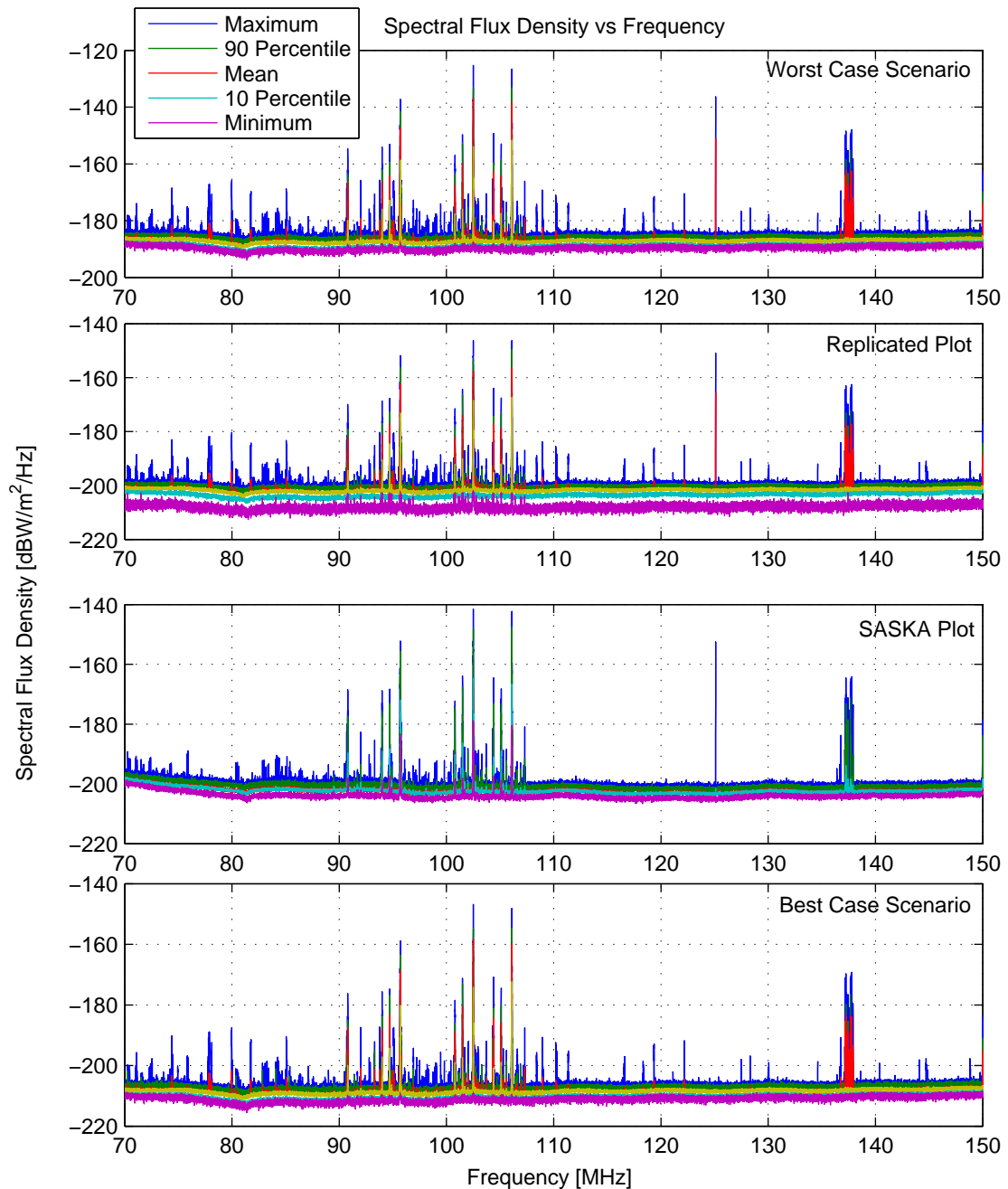


Figure 5.10: The above plots shows the spectral flux density as a function of RBW frequency. The *top most* plot shows the *spectral flux density as function of frequency* for a *worst case scenario*. This is when the positive tolerances of the components are taken into account and this reduces the theoretical system gain. The *best case scenario* is when the system gain is increased by subtracting the tolerances. The second to last plot depicts the plot as generated by SA SKA whereas the second plot from the top is an attempt to replicate the SA SKA plot.

In the Figure 5.5 above, it can be clearly seen that the baselines of the worst case is at approximately -180 dBW/m²/Hz and the baselines of the best case graph lies close to -210 dBW/m²/Hz. The baselines of the SA SKA plots and the replicated plot is at -200

CHAPTER 5. RESULTS

dBW/m²/Hz. which is between the -180 dBW/m²/Hz and -210 dBW/m²/Hz boundaries. Furthermore, the highest point of the SA SKA plot and the replicated plot do not exceed that of the worst case graph which is at approximately -125 dBW/m²/Hz.. *What this confirms, is the fact that the spectral flux densities were calculated to within the acceptable levels and that the technical competence of RFI System 2 was adequate for the purpose under discussion.*

5.5 Summary of Results

Section 5.3 displays the spectral occupancy and fractional occupancy for signals exceeding the median by 6 dB's. In Section 5.2.1, a curve of coefficient of variation (cov) versus frequency is depicted (Figure 5.2). This tells us how the data is distributed about the mean in each frequency bin. Values away from the mean have higher cov than values closer to the mean. The cov values for frequencies of 95 MHz, 103 MHz, 106 MHz, 125 MHz and 138 MHz are 44 %, 48.4 %, 45%, 32.5 % and 40% respectively. This tells us that the data in these frequency bins contain outliers of exceptionally high values and consequently the mean is strongly affected by these outcomes. Therefore, signals of high sfd (in the form of high spikes) should be observed at these frequencies.

Table 5.13: Statistical Summary

Graphs	95 MHz	102.5 MHz	106 MHz	125 MHz	138 MHz
<i>No. of Signals</i>	99	300	299.5	< 20	100
<i>Fractional Occupancy</i>	0.12 %	0.13 %	0.13 %	0.01 %	0.035 %
<i>Coefficient of Variation</i>	44 %	48.4 %	45 %	32.5 %	40 %
<i>Minimum Values (dBW/m²/Hz)</i>	- 182.5	-177.2	-179.5	-203.5	-203.5
<i>10 Percentile (dBW/m²/Hz)</i>	-183.5	-179.1	-180	-203.5	-203.5
<i>Mean Values (dBW/m²/Hz)</i>	-172	-166.4	-168.9	-203	-193.5
<i>Median Values (dBW/m²/Hz)</i>	-172.9	-168	-166.3	-201.7	-201
<i>90 Percentile Values (dBW/m²/Hz)</i>	-155	-148	-148.3	-200	-171
<i>Maximum Values (dBW/m²/Hz)</i>	-152	-140.4	-142	-152	-162

From Table 5.13 above, it can be seen that frequency bin 102.5 MHz has the highest number of signals which exceed the global median (median for the entire frequency band) by 6 dB . In fact all 300 signals exceed the median by 6 decibels. This corresponds to 0.13 % of the total number of signals in the entire band. Furthermore, this frequency bin has the highest dispersion about the mean (48.4 %) meaning that it has the highest number of outliers and therefore it can be expected that the outliers will effect the mean. This fact is confirmed by the fact that the maximum sfd of -140.4 dBW/m²/Hz occurs in this frequency bin.

CHAPTER 5. RESULTS

From the tabulation of sfd values in the table above, it can be seen that the spike at frequency 125 MHz is only distinguishable in the *Maximum Values* graph. This is because the number of signals exceeding the median by 6 dB are low, less than 20 whilst at the same time they assume high sfd values ($\text{cov} = 32.5\%$). This causes the more dominant values to prevail, thus pushing the baseline. Similarly, the signal at 138 MHz, is observable in the *mean values* graph and the *90 percentile* and *maximum values* graphs.

5.6 Significance of Results

Our results showed that:

1. The plots of spectral flux density versus frequency as derived by the SA SKA team are similar (if not identical) to that independently processed by the author using MATLAB and that strong correlation exists between these curves. In areas where differences were observed, reasons for the differences were adequately explained.
2. The SA SKA graphs and the graphs replicated by the author using MATLAB were within their tolerance limits and that RFI System 2 operated as expected for the frequency range 80 MHz to 150 MHz.

Chapter 6

Conclusion

Nothing best summarises the overall goal of my dissertation than the way the title does, “*A study of the South African SKA Radio Frequency Measurement System*”. The emphasis being on the phrase, “*a study*”.

I have thoroughly scrutinized the work of the SA SKA team, beginning first with attempting to gain an advanced level of understanding of the “SKA Protocol”; followed by looking at the deployment of the RFI Measurement Systems in South Africa and looking at the processes and procedures that were used to arrive at their findings and finally analyzing a sample of their data and comparing their results to my own work.

In order for me to have arrived at this advanced level of understanding of this work, I have had to perform a vast amount of literature research, review and study. Proof of this is contained in Chapter 2 (Literature Review) and the vast amount of study material, reading material and scholarly publications that was consulted and is referenced in the bibliography.

I am convinced that the key goal of my research (*that of developing a competence in the way scanning receivers work by studying the South African SKA Radio Frequency Measurement Systems*) has been achieved.

6.1 Summary

In Chapter 2 a detailed discussion surrounding RF theory was discussed. It was found that in RF metrology the Electromagnetic and Power levels (dBm) are usually used as key indicators of signal strength which is in sharp contrast to the SKA measurement campaign where Spectral Flux Density (dBW/m²/Hz) was used. One of the reasons is because the sfd shows the density per unit frequency. This is significant as it shows density of power at each frequency.

In Chapter 2, we also discussed the issue of Electromagnetic Compatibility and Electromagnetic Interference; taking care not forgetting to mention the sources of such EMI.

CHAPTER 6. CONCLUSION

The RFI system was prone to EMI and numerous tests and shielding techniques were employed by the SA SKA team and external consultants. It was observed during this study that although preventative EMI shielding measures were affected, this was done after the system had been built and only when unknown EMI signals were encountered. This proved that the system was not built and designed with the issue of EMC in mind. Evidence of this neglect is in the intensity with which screening techniques were conducted after system construction had been performed. According to Kodali (1996)[15], “overall equipment or system design and construction practices are important in minimizing EMI as postfacto remedial measures by way of EMI fixes are costly, unscientific and non-engineering approaches”.

The “SA SKA Protocol” was critically analysed, reviewed and studied in greater depth and a summary of the key technical areas and major deliverables required were provided in Chapter 3.

Chapter 4, dealt with deployment of the the RFI Measurement Systems in South Africa. A complete audit of the components was conducted. After careful scrutiny of the manufacturers data sheets, it was found that the R&S HL033 Log-Periodic antenna used in the development of the system, had an operational frequency range of 80 MHz - 2 GHz. It was further shown that using this antenna to measure sfd for frequencies below 80 MHz introduced some flaws to the data. According to Rohde & Bucher[30][page 45], “the capabilities of a receiver are best appreciated from its electrical specifications”. Keeping to technical specifications in design, is one of the hallmarks of electrical engineering.

Also in Chapter 4, the RFI System 2 was shown and a detailed discussion surrounding the transfer of data from the spectrum analyzer to the computer was mounted. The method used to process this data was also discussed in detail. The formulae that were utilized to calculate the sfd were defined. Once the data processing method were known, the data was analysed and the results documented in Chapter 5. It was found that the SA SKA (Spectral Flux Density versus Frequency) graphs were closely correlated with that of the author and that the sfd values of the graph of the SA SKA lie within the acceptable tolerance levels as published in the manufacturers data sheets

6.2 Inference

The objectives of this project were documented in Chapter 1. In the summary above I have discussed how I achieved these objectives and what my major findings were. From the above summary, it can be inferred that:

1. The objectives of this dissertation have been met.
2. With the exception of the minor discrepancies and anomalies already discussed, the work of the SA SKA team was in line with and conformed to the major technical

CHAPTER 6. CONCLUSION

requirements of the SKA Protocol.

Bibliography

- [1] P.A. Friedman and W.A. Baan, "RFI Mitigation Methods in Radio Astronomy," *Symposium on Astronomy and Astrophysics*, 8 June 2001.
- [2] R.D. Ekers and J.F. Bell, "Radio Frequency Interference," [Online] Available: <http://www.atnf.csiro.au/SKA/intmit>(June, 2005)
- [3] T.A. Th. Spoelstra, "Regulation of Radio Silence," *17th International Wroclaw Symposium and Exhibition on Electromagnetic Compatibility*, 29 June - 1 July 2004.
- [4] R.J. Cohen, "Radio-Quiet Zones: National and International Perspectives," *17th International Wroclaw Symposium and Exhibition on Electromagnetic Compatibility*, 29 June - 1 July 2004.
- [5] R. Ambrosini, "RFI Selection Criteria for Radio Telescopes," *17th International Wroclaw Symposium and Exhibition on Electromagnetic Compatibility*, 29 June - 1 July 2004.
- [6] M. Goris, "Categories of Radio-Frequency Interference," Doc. No. 415/MG/V2.5, 12 February 1998.
- [7] H. Taub and D.L. Schilling, "Principles of Communication Systems," *McGraw-Hill Book Company*, 2nd Edition, 1986.
- [8] G.W. Milne, E. Jansen, J.J. Roux, J.A. Koekemoer and P.P.A Kotze, "EMC and RFI problems and solutions on the SUNSAT Micro-Satellite," *South African Symposium on Communications and Signal Processing*, vol. 1, no.98EX214, pp.293–298, September 1998.
- [9] R. Ambrosini, R. Beresford, A.J. Boonstra, S. Ellingson and K. Tapping, "RFI Measurement Protocol for Candidate SKA Site," *Working Group on RFI Measurements*, May 23 2003.
- [10] H.C.Horing, "Probability of intercept for frequency hop signals using search receivers," [Online] Available:<http://www.rohde-schwarz.com>(July, 2005)
- [11] A. Shukla, "Feasibility Study into the measurement of man-made noise," UK Ministry of Defense:Radio Communications Agency, March 2001.

BIBLIOGRAPHY

- [12] Bernard Keiser, “Principles of Electromagnetic Compatibility,” Artech House, 3rd Edition, 1987.
- [13] J.R Fisher, “Signal Analysis and Blanking Experiments on DME Interference,” N.R.A.O Internal Report No. 313, April 2004.
- [14] Geoffrey C. Bower, “Radio Frequency Interference Mitigation,” UC Berkeley Radio Astronomy Laboratory, IAU Working Group on Interference Mitigation.
- [15] V. Prasad Kodali, “Engineering Electromagnetic Compatibility: Principles, Measurements, and Technologies,” I.E.E.E Press, 1996.
- [16] Justin L. Jonas, “Threats to Radio Astronomy: Now and the Future,” *South African Symposium on Communications and Signal Processing*, vol. 1, no.98EX214, pp.275–276, September 1998.
- [17] Gerhard Petrick, “Standard Operating Procedure for Joint ICASA and SKA South Africa Radio Frequency Interference Measurements,” *National Research Foundation*, Doc. ID. RFISOP, Doc. No. 018, 2005.
- [18] David M. Pozar, “Microwave and RF Design of Wireless System,” John Wiley & Sons, Incorporation, 2001.
- [19] Donald R.J White, “Electromagnetic Interference and Compatibility,” Volume 3, 3rd Edition, 1981.
- [20] R.P Millenaar, “SSSM System Design Considerations,” Doc. No.ASTRON-RP-013, Rev. 1.0, 31 March 2005.
- [21] Christoph Rauscher, “Fundamentals of Spectrum Analysis,” Rohde and Schwarz, 2001.
- [22] Peterson Blake, “Spectrum Analysis Basics,” Agilent Application Note 150, literature part number 5952-0292, November 1, 1989.
- [23] Jim Cohen, Titus Spoelstra, Roberto Ambrosini, Wim Van Driel, “CRAF Handbook for Radio Astronomy,” European Science Foundation, 3rd Edition, 2005.
- [24] Paul Horowitz, Winfield Hill, “The art of electronics,” Cambridge University Press, 1980.
- [25] “Signal Generator Spectral Purity,” Agilent Application Note 388, literature part number 5952-2019, February 20, 2001.
- [26] Ralph J. Smith, Richard C. Dorf, “Circuits, Devices and Systems,” John Wiley and Sons, 5th Edition, 1992.

BIBLIOGRAPHY

- [27] “Proposal to site the SKA - *Analysis of the Radio Frequency Environment*,” National Research Foundation, 17 March 2006.
- [28] Paul J. Nahin, “The science of radio,” American Institute of Physics, 1996.
- [29] David K. Cheng, “Field and Wave Electromagnetics,” Addison Wesley, 2nd Edition, 1989.
- [30] Ulrich L. Rohde, T.TN. Bucher, “Communications Receivers: Principles and Design,” McGraw-Hill, 1988.h, “Statistical Signal Characterization,” Artech House, 1992.
- [31] Tim Williams, “The circuit Designer’s companion,” Butterworth-Heineman Ltd, 1st Edition, 1991.
- [32] W.H. Hayward, “Introduction to radio frequency design,” Prentic-Hall Inc., 1982.
- [33] C.D. Motchenbacher and F.C. Fitchen, “Low Noise Electronic Design,” John Wiley and Sons, 1973.
- [34] Richard C. Dorf, “The electrical engineering handbook,” CRC Press, 1997.
- [35] Savant, Rodent and Carpenter, “Electronic Design: Circuit and Systems,” Benjamin/Cummings Publishing Company Inc., 2nd Edition, 1991.
- [36] Ferrel G. Stremler, “Introduction to communication systems,” Addison-Wesley Publishing Company, 3rd edition, 1992.
- [37] “Request for proposal for siting the SKA,” International SKA Project Office, 1 September 2004.
- [38] John C. Curlander, Robert N. McDonough, “Synthetic Aperture Radar: Systems and Signal Processing,” John Wiley and Sons, Inc., 1991.
- [39] T.H. Wilmshurst, “Signal Recovery from noise in electronic instrumentation,” IOP Publishers Ltd., 2nd Edition, 1990.
- [40] “Spectrum Analyzer Measurements and Noise,” Application Note 1303, Literature Part Number 5966-4008E, February 11, 2003.
- [41] Thereza Macnamara, “Handbook of Antennas fo EMC,” Artech House Inc., 1995.
- [42] “Fundamentals of RF and Microwave Noise Figure Measurements,” Application Note 57-1, Literature Part Number 5952-8255E, Agilent, 23 March 2004.
- [43] “Protection criteria used for radio astronomical measurements,” International Telecommunications Union, Rec. ITU-R RA.769-2.

BIBLIOGRAPHY

- [44] “Noise Figure Measurement Accuracy- The Y-Factor Method,” Application Note 57-2, Literature Part Number 5952-3706E, 19 March 2004.
- [45] R.P. Millenaar, A.J. Boonstra, “SKA Spectrum Monitoring Plan for Candidate Sites,” Revision 1.1, 9 January 2004.
- [46] “8 hints for better spectrum analysis,” Application Note 1286-1, Literature Part Number 5965-7009E, Agilent, 27 July 2005.
- [47] R.S Hughes, “Logarithmic Amplification,” Artech House Incorporation, 1986.
- [48] “Agilent PSA High-Performance Spectrum Analyzer Series: Amplitude Accuracy,” Literature Part Number 5980-3080EN, Agilent, 31 August 2006.
- [49] “Optimizing Spectrum Analyzer Amplitude Accuracy,” Application Note, Literature Part Number 5968-3659E, Agilent, 1999.
- [50] “The South African Telecommunications Act (Act 103 of 1996),” Government Gazette.
- [51] “South African band Re-planning exercise- 2nd Edition,” *[Online] Available:* <http://www.icasa.org.za> (November, 2006)
- [52] “Representations on the Draft SABRE1 Edition 2 by the South African SKA Steering Committee,” Friday 14 November 2003 *[Online] Available:* <http://www.icasa.org.za>, (December, 2006)
- [53] “Log-Periodic Broadband Antenna R&S HL 033 Data Sheet,” Rohde and Schwarz. *[Online] Available:* <http://www.rohde-schwarz.com> (December, 2006)
- [54] “Log-Periodic Broadband Antenna R&S HL 055 Data Sheet,” Rohde and Schwarz. *[Online] Available:* <http://www.rohde-schwarz.com> (December, 2006)
- [55] “5 to 20 GHz Double Balanced Mixers: Models DM0520LW1 and DM0818LW1 Data Sheet,” Miteq *[Online] Available:* <http://www.miteq.com> (December, 2006)
- [56] “RF Switching Products Data Sheet,” Narda *[Online] Available:* http://www.narda-sts.de/pdf/hochfrequenz/23_micro.pdf (December, 2006)
- [57] “Coaxial Cable Sucoflex_104 Data Sheet,” Huber and Suhner *[Online] Available:* <http://www.hubersuhnerinc.com> (December, 2006)
- [58] “AFS and JS Amplifier Products Data Sheet,” Miteq *[Online] Available:* <http://www.miteq.com> (December, 2006)
- [59] Dan Slater, “Near-Field Antenna Measurements,” Artech House Inc., 1991.

BIBLIOGRAPHY

- [60] John G. Kraemer, “*IEEE Standard for Calibration of Electromagnetic Field Sensors and Probes, Excluding Antennas, from 9 kHz to 40 GHz,*” IEEE Electromagnetic Compatibility Society, 2003.
- [61] B. Peng et al, “*RFI Test Observations at a candidate SKA Site in China,*” *Experimental Astronomy* (17), 2004.
- [62] Rui Fonseca, “*Site evaluation and RFI spectrum measurements in Portugal at the frequency range 0.408-10 GHz for a GEM polarized galactic radio emission experiment,*” *New Astronomy* 11, 2006.
- [63] S.W. Ellingson, J.T. Johnson, “Airborne RFI Measurements over the Mid-Atlantic Coast using LISA,” Project Report, 10 February 2003. [Online] Available: <http://esl.eng.ohio-state.edu/~rsttheory/iip/lisa030102.pdf> (December, 2006)
- [64] J.T. Johnson et al., “Airborne C-band RFI Measurements with PSR/CXI and CISR from the WB-57 Aircraft: Initial Data Examination,” Project Report, 13 March 2006.
- [65] William C.Y. Lee, “*Estimate of Local Average Power of a Mobile Radio Signal,*” IEEE Transactions on Vehicular Technology, Volume VT-34, No. 1, February 1985.
- [66] K. Naicker, S.H. Mneney, “*Propagation measurements and multipath channel modelling for line-of-site links at 19.5 GHz,*” SAIEE Africa Research Journal, Vol 97 No.2, June 2006.
- [67] Willem A. Baan et. al, “Memo 73 Spectrum Protection Criteria for the Square Kilometre Array,” SKA Task Force, November 2005 [Online] Available: <http://www.skatelescope.org/pages/memos> (June, 2006)
- [68] Dina Simunic, Helmut Keller and Zlatko Koren, “Measurement of an Electric Field of a Scanning Radar Antenna,” ([Online] Available: http://www.narda-sts.de/pdf/hochfrequenz/23_micro.pdf (December, 2006)
- [69] Andrew Lam et. al, “Guidelines for the Measurement of Radio Frequency Fields at Frequencies from 3 kHz to 300 GHz,” Canadian Spectrum Management and Telecommunications Guideline, Document No. GL-01, Issue No.2, October 2005.
- [70] John K. Daher, Mark L. Wheeler, “International Space Station Electric Field Measurement Package (EFMP),” Georgia Tech Research Institute, Report No. A-5508F, 20 January 1998.
- [71] Philip Merewood et. al, “A Guide to power flux density and field strength measurement,” UK National Physics Laboratory, Institute of Measurement and Control, 2004.

BIBLIOGRAPHY

- [79] “Common EMC Measurement Terms,” [Online] Available: <http://www.emctest.com>(December, 2006)
- [73] Aaron Chippendale, Michelle Storey and Peter Hall, “Low Frequency Array: RFI Site Report,” CSIRO Australia Telescope National Facility, Sydney, Australia, 10 March 2003.
- [74] E. Marcelo Arnal et. al, “Square Kilometer Array: Argentina Site Report,” Argentina Committee, 26 March 2004.
- [75] Aaron Chippendale, “Mileura RFI Model for All-sky EOR Experiment,” Australia Telescope National Facility, 16 March 2004.
- [76] Jim Cohen, Titus Spoelstra, Roberto Ambrosini and Wim van Driel, “*CRAF Handbook for Radio Astronomy*,” European Science Foundation, 3rd edition, 2005.
- [77] Aaron Chippendale, Ravi Subrahmanyam, “Measuring the metre-wave sky spectrum with milli-kelvin accuracy: Engineering Challenges and Australian Opportunities,” Australia Telescope National Facility, University of Sydney, Australia, 2006.
- [78] A.E.E. Rogers, J.E. Salah, D.L. Smythe, P. Pratap, J.C Carter and M. Derome, “*Interference temperature measurements from 70 MHz to 1500 MHz in suburban and rural environments of the Northeast*,” MIT Haystack Observatory, Westford, MA 01886.
- [79] <http://www.facebook.com>(February, 2008)
- [80] <http://www.mxit.co.za>(February, 2008)
- [81] Mike George, Dave Rowlands, Bill Kastle, “What is lean six sigma?” McGraw-Hill, 2004.
- [82] Joong Geun Rhee, “Statistical Analysis of radio frequency noise spectrum in Korea,” *1999 International Symposium on Electromagnetic Compatibility*, Volume, Issue, May 1999, pp 193 - 196.
- [83] Richard Thomas Lord, “Aspects of Stepped-Frequency Processing for Low-Frequency SAR Systems,” University of Cape Town, February, 2000.
- [84] http://www.sadc.int/member_states/index.php(May, 2008)
- [85] Constantine A. Balanis, “Antenna Theory: Analysis and Design,” John Wiley and Sons, 3rd edition, 2005.
- [86] Xia Mao et. al, “Harmonious graphics generating based on the 1/f function theory,” *Science Direct*, 10 July 2006. [Online] Available: <http://www.sciencedirect.com>(May, 2008)

Appendix A

Flexible Image Transport System

The table below lists all the files that were used in the analysis.

Table A.1: List of data files used in the analysis

File Name
2005-11-24_19-48-46_S2_M1_RFI-K3_70-150_V_P1.fits
2005-11-25_00-00-51_S2_M1_RFI-K3_70-150_V_P2.fits
2005-11-25_04-14-05_S2_M1_RFI-K3_70-150_V_P3.fits
2005-11-25_08-28-01_S2_M1_RFI-K3_70-150_H_P3.fits
2005-11-25_12-39-46_S2_M1_RFI-K3_70-150_H_P2.fits
2005-11-25_16-51-05_S2_M1_RFI-K3_70-150_H_P1.fits

Appendix B

Components of RFI System 2

The tables below lists some of the components used in the development of RFI System 2 as taken from the respective Manufacturers Data Sheets.

Table B.1: Various Amplifiers used in RFI System 2 Construction

Description	Frequency	Gain (dB)	Gain Flatness
LNA (AFS4-00100600-13-10P-4)	0.1 - 6	36	± 3.0 dB
LNA (JS4-06001800-16-10A)	6 - 18	34	± 2.0 dB
LNA (JS-18002600-19-8P)	18 - 26	35	± 1.5 dB
LNA (AFS2-00101200-25-8P-2)	0.1 - 12	14	± 1.5 dB

Table B.2: Various components making up the RF Assembly (from [53, 54, 55, 56, 27, 17, 57])

Description	Frequency	Gain (dB / dBi)
Oscillator	12 GHz	N/A
Local Oscillator	18 GHz	N/A
Mixer (x2) (DM0818LW1)	5 - 20 GHz	9 (max)
High Pass Filter	18 GHz	N/A
High Pass Filter	12 GHz	N/A
Agilent Noise Source (346C)	10 MHz - 26.5 GHz	N/A
DPDT Coaxial Transfer switches (x2)	DC - 26.5 GHz	$\pm(0.2 - 0.7)$
Narda Coaxial 1-pole-2 throw switch	N/A	N/A
Narda SEM143D 1-pole-4 throw switch	DC - 18 GHz	$\pm(0.2 - 0.5)$
Log-Periodic Antenna R&S HL 033	0.080 - 2 GHz	5.5 - 7.5
Log-Periodic Antenna R&S HL 050	0.851 - 26.5 GHz	8 - 9
Huber+Suhner Sucoflex_104 RF Cable	0.01 - 26.5 GHz	$\pm(0.02-1.37)$ dB/m
Agilent 8563EC Spectrum Analyser	9 kHz - 26.5 GHz	N/A

Appendix C

Formula Derivation

We know that $P = \frac{1}{2}SAB$ [27]

Since $\lambda = \frac{c}{f}$ and $A = \frac{G\lambda^2}{4\pi}$ and by re-arranging we have:

$$S = \frac{2P}{AB} = \frac{8\pi P f^2}{G B c^2}$$

Taking the logs of both side:

$$10\log S = 10\log 8\pi + 10\log P + 20\log f - 10\log G - 20\log c - 10\log B$$

$$10\log S = 10\log 8\pi + P[dBW] + 20\log f - G[dB] - 20\log(3 \times 10^8) - 10\log B$$

$$10\log S = 14.002 + P[dBW] + 20\log f - 10\log G - 169.542 - 10\log B$$

$$10\log S = P[dBW] + 20\log f - G[dB] - 10\log B - 155.540$$

$$10\log S = P[dBW] + 20\log\left(\frac{f}{10^6} \times 10^6\right) - G[dB] - 10\log\left(\frac{B}{10^3} \times 10^3\right) - 155.540$$

Recall that $20\log\left(\frac{f}{10^6} \times 10^6\right) = 20\log(f_{MHz}) + 20\log(10^6)$ and $-10\log\left(\frac{B}{10^3} \times 10^3\right) = -10\log(B_{KHz}) - 10\log(10^3)$

$$10\log S = P[dBW] + 20\log(f_{MHz}) + 120 - G[dB] - 10\log(B_{KHz}) - 30 - 155.540 \quad 10\log S = P[dBW] + 20\log(f_{MHz}) - G[dB] - 10\log(B_{KHz}) - 65.54$$

Since $dBW = dBm - 30$, we have:

$$10\log S = P[dBm] - 30 + 20\log(f_{MHz}) - G[dB] - 10\log(B_{KHz}) - 65.54$$

This leaves us with:

$$S[dBW/m^2/Hz] = P[dBm] + 20\log(f_{MHz}) - G[dB] - 10\log(B_{KHz}) - 95.54$$

Appendix D

K-Factor Values of Antenna HL033

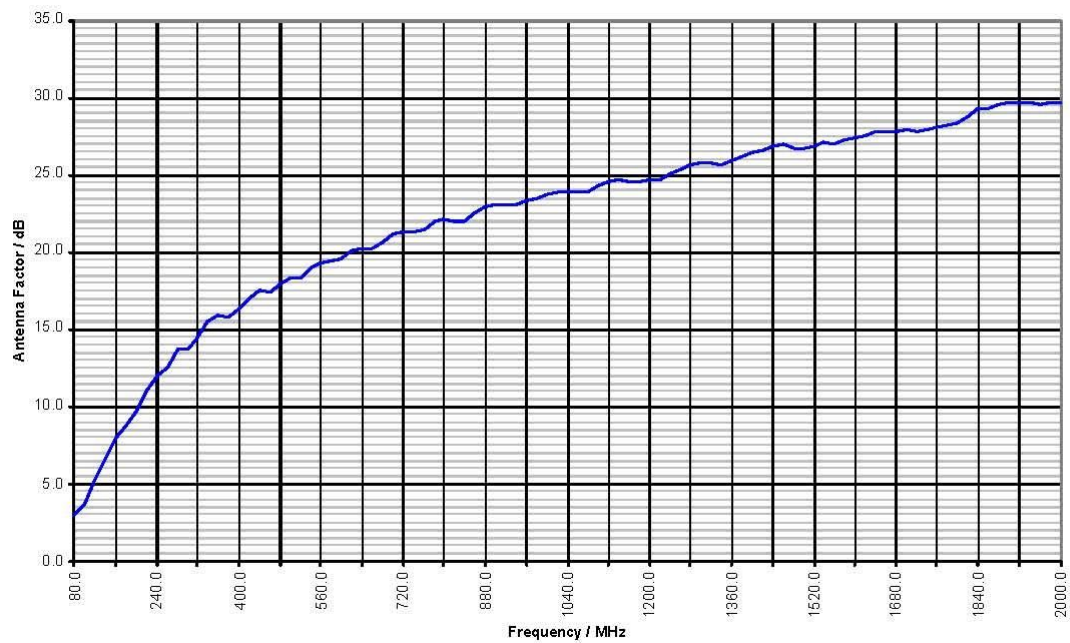


Figure D.1: Antenna Factor values of the R&S HL033 Log. Periodic Broadband

Appendix E

Matlab Generated Code

```
%THIS PROGRAM READS THE RAW RFI DATA AND CALCULATES THE MEDIAN VALUES.
%IT THEN WRITES THESE VALUES TO VARIOUS FILES.
clear all;
close all;
counter=1;
n=1;
int32 i;
i=1;
int32 j;
%%%%%%%%%%%%%%%%%%%%%%%%%%%%%%%%%%%%%%%%%%%%%%%%%%%%%%%%%%%%%%%%%%%%%%%%
%READING FROM FILES
%%%%%%%%%%%%%%%%%%%%%%%%%%%%%%%%%%%%%%%%%%%%%%%%%%%%%%%%%%%%%%%%%%%%%%%%
[scan1_VP1 scan2_VP1 scan3_VP1 scan4_VP1 scan5_VP1]=textread(' 2005-11-24_19-48-
46_S2_M1_RFI-K3_70-150_V_P1.txt', '%f %f %f %f %f');
[scan1_VP2 scan2_VP2 scan3_VP2 scan4_VP2 scan5_VP2]=textread(' 2005-11-25_00-00-
51_S2_M1_RFI-K3_70-150_V_P2.txt', '%f %f %f %f %f');
[scan1_VP3 scan2_VP3 scan3_VP3 scan4_VP3 scan5_VP3]=textread(' 2005-11-25_04-14-
05_S2_M1_RFI-K3_70-150_V_P3.txt', '%f %f %f %f %f');
[scan1_HP3 scan2_HP3 scan3_HP3 scan4_HP3 scan5_HP3]=textread(' 2005-11-25_08-28-
01_S2_M1_RFI-K3_70-150_H_P3.txt', '%f %f %f %f %f');
[scan1_HP2 scan2_HP2 scan3_HP2 scan4_HP2 scan5_HP2]=textread(' 2005-11-25_12-39-
46_S2_M1_RFI-K3_70-150_H_P2.txt', '%f %f %f %f %f');
[scan1_HP1 scan2_HP1 scan3_HP1 scan4_HP1 scan5_HP1]=textread(' 2005-11-25_16-51-
05_S2_M1_RFI-K3_70-150_H_P1.txt', '%f %f %f %f %f');

%%%%%%%%%%%%%%%%%%%%%%%%%%%%%%%%%%%%%%%%%%%%%%%%%%%%%%%%%%%%%%%%%%%%%%%%
for n=1: 26744;
int32 k;
int32 counter;
int32 counter1;
real power101;
real power102;

k=1;
j=1;

%%%%%%%%%%%%%%%%%%%%%%%%%%%%%%%%%%%%%%%%%%%%%%%%%%%%%%%%%%%%%%%%%%%%%%%%
% CREATES AN ARRAY CALLED Z
%%%%%%%%%%%%%%%%%%%%%%%%%%%%%%%%%%%%%%%%%%%%%%%%%%%%%%%%%%%%%%%%%%%%%%%%
while j <=10;
z1(j)= scan1_VP1(i);
z2(j)= scan2_VP1(i);
z3(j)=scan3_VP1(i);
z4(j)=scan4_VP1(i);
z5(j)=scan5_VP1(i);
z6(j)=scan1_VP2(i);
z7(j)=scan2_VP2(i);
z8(j)=scan3_VP2(i);
z9(j)=scan4_VP2(i);
z10(j)=scan5_VP2(i);
z11(j)=scan1_VP3(i);
z12(j)=scan2_VP3(i);
z13(j)=scan3_VP3(i);
z14(j)=scan4_VP3(i);
z15(j)=scan5_VP3(i);
z16(j)=scan1_HP1(i);
z17(j)=scan2_HP1(i);
z18(j)=scan3_HP1(i);
z19(j)=scan4_HP1(i);
z20(j)=scan5_HP1(i);
z21(j)=scan1_HP2(i);
z22(j)=scan2_HP2(i);
z23(j)=scan3_HP2(i);
z24(j)=scan4_HP2(i);
z25(j)=scan5_HP2(i);
z26(j)=scan1_HP3(i);
```

APPENDIX E. MATLAB GENERATED CODE

```
z27(j)=scan2_HP3(i);
z28(j)=scan3_HP3(i);
z29(j)=scan4_HP3(i);
z30(j)=scan5_HP3(i);
j=j+1;
i=i+1;
end
%%%%%%%%%%%%%%%%%%%%%%%%%%%%%%%%%%%%%%%%%%%%%%%%%%%%%%%%%%%%%%%%%%%%%%%%
%STATS
%%%%%%%%%%%%%%%%%%%%%%%%%%%%%%%%%%%%%%%%%%%%%%%%%%%%%%%%%%%%%%%%%%%%%%%%
sort(z1);
sort(z2);
sort(z3);
sort(z4);
sort(z5);
sort(z6);
sort(z7);
sort(z8);
sort(z9);
sort(z10);
sort(z11);
sort(z12);
sort(z13);
sort(z14);
sort(z15);
sort(z16);
sort(z17);
sort(z18);
sort(z19);
sort(z20);
sort(z21);
sort(z22);
sort(z23);
sort(z24);
sort(z25);
sort(z26);
sort(z27);
sort(z28);
sort(z29);
sort(z30);
median_val_ue_z1(counter)=(median(z1))/6-100-10;
median_val_ue_z2(counter)=(median(z2))/6-100-10;
median_val_ue_z3(counter)=(median(z3))/6-100-10;
median_val_ue_z4(counter)=(median(z4))/6-100-10;
median_val_ue_z5(counter)=(median(z5))/6-100-10;
median_val_ue_z6(counter)=(median(z6))/6-100-10;
median_val_ue_z7(counter)=(median(z7))/6-100-10;
median_val_ue_z8(counter)=(median(z8))/6-100-10;
median_val_ue_z9(counter)=(median(z9))/6-100-10;
median_val_ue_z10(counter)=(median(z10))/6-100-10;
median_val_ue_z11(counter)=(median(z11))/6-100-10;
median_val_ue_z12(counter)=(median(z12))/6-100-10;
median_val_ue_z13(counter)=(median(z13))/6-100-10;
median_val_ue_z14(counter)=(median(z14))/6-100-10;
median_val_ue_z15(counter)=(median(z15))/6-100-10;
median_val_ue_z16(counter)=(median(z16))/6-100-10;
median_val_ue_z17(counter)=(median(z17))/6-100-10;
median_val_ue_z18(counter)=(median(z18))/6-100-10;
median_val_ue_z19(counter)=(median(z19))/6-100-10;
median_val_ue_z20(counter)=(median(z20))/6-100-10;
median_val_ue_z21(counter)=(median(z21))/6-100-10;
median_val_ue_z22(counter)=(median(z22))/6-100-10;
median_val_ue_z23(counter)=(median(z23))/6-100-10;
median_val_ue_z24(counter)=(median(z24))/6-100-10;
median_val_ue_z25(counter)=(median(z25))/6-100-10;
median_val_ue_z26(counter)=(median(z26))/6-100-10;
median_val_ue_z27(counter)=(median(z27))/6-100-10;
median_val_ue_z28(counter)=(median(z28))/6-100-10;
median_val_ue_z29(counter)=(median(z29))/6-100-10;
median_val_ue_z30(counter)=(median(z30))/6-100-10;

counter=counter+1;
end

for k=1:26744;
amedian_val_ue_z1=median_val_ue_z1(k);
bmedian_val_ue_z2=median_val_ue_z2(k);
cmmedian_val_ue_z3=median_val_ue_z3(k);
dmedian_val_ue_z4=median_val_ue_z4(k);
emmedian_val_ue_z5=median_val_ue_z5(k);
fmedian_val_ue_z6=median_val_ue_z6(k);
gmedian_val_ue_z7=median_val_ue_z7(k);
hmedian_val_ue_z8=median_val_ue_z8(k);
imedian_val_ue_z9=median_val_ue_z9(k);
jmedian_val_ue_z10=median_val_ue_z10(k);
kmedian_val_ue_z11=median_val_ue_z11(k);
lmedian_val_ue_z12=median_val_ue_z12(k);
mmmedian_val_ue_z13=median_val_ue_z13(k);
nmedian_val_ue_z14=median_val_ue_z14(k);
```


APPENDIX E. MATLAB GENERATED CODE

```
close all;
int32 n;
cycle=1;
%%%%%%%%%%%%%%%%%%%%%%%%%%%%%%%%%%%%%%%%%%%%%%%%%%%%%%%%%%%%%%%%%%%%%%%%
%SA SKA PLOT GENERATOR
%%%%%%%%%%%%%%%%%%%%%%%%%%%%%%%%%%%%%%%%%%%%%%%%%%%%%%%%%%%%%%%%%%%%%%%%
[frq ma_val ni typ avrgval tenpval mi val
sensi ti vi ty]=textread(' rfi _pl ot0. txt', '%f %f %f %f %f %f %f');

for cycle=1: 26668;
    max_val (cycle)=ma_val (cycle);
    ni ntyp(cycle)=ni typ(cycle);
    average(cycle)=avrgval (cycle);
    tenp(cycle)=tenpval (cycle);
    mi nval (cycle)=mi val (cycle);
    frequency(cycle)=frq(cycle);
end;

%%%%%%%%%%%%%%%%%%%%%%%%%%%%%%%%%%%%%%%%%%%%%%%%%%%%%%%%%%%%%%%%%%%%%%%%
%READING FROM FILES
%%%%%%%%%%%%%%%%%%%%%%%%%%%%%%%%%%%%%%%%%%%%%%%%%%%%%%%%%%%%%%%%%%%%%%%%
[scan1_VP]=textread(' amedi an_val ue_z1_V. txt', '%f');
[scan2_VP]=textread(' bmedi an_val ue_z2_V. txt', '%f');
[scan3_VP]=textread(' cmedi an_val ue_z3_V. txt', '%f');
[scan4_VP]=textread(' dmedi an_val ue_z4_V. txt', '%f');
[scan5_VP]=textread(' emedi an_val ue_z5_V. txt', '%f');
[scan6_VP]=textread(' fmedi an_val ue_z6_V. txt', '%f');
[scan7_VP]=textread(' gmedi an_val ue_z7_V. txt', '%f');
[scan8_VP]=textread(' hmedi an_val ue_z8_V. txt', '%f');
[scan9_VP]=textread(' imedi an_val ue_z9_V. txt', '%f');
[scan10_VP]=textread(' jmedi an_val ue_z10_V. txt', '%f');
[scan11_VP]=textread(' kmedi an_val ue_z11_V. txt', '%f');
[scan12_VP]=textread(' lmedi an_val ue_z12_V. txt', '%f');
[scan13_VP]=textread(' mmedi an_val ue_z13_V. txt', '%f');
[scan14_VP]=textread(' nmedi an_val ue_z14_V. txt', '%f');
[scan15_VP]=textread(' omedi an_val ue_z15_V. txt', '%f');
[scan1_HP]=textread(' pmedi an_val ue_z16_H. txt', '%f');
[scan2_HP]=textread(' qmedi an_val ue_z17_H. txt', '%f');
[scan3_HP]=textread(' rmedi an_val ue_z18_H. txt', '%f');
[scan4_HP]=textread(' smedi an_val ue_z19_H. txt', '%f');
[scan5_HP]=textread(' tmedi an_val ue_z20_H. txt', '%f');
[scan6_HP]=textread(' umedi an_val ue_z21_H. txt', '%f');
[scan7_HP]=textread(' wmedi an_val ue_z22_H. txt', '%f');
[scan8_HP]=textread(' xmedi an_val ue_z23_H. txt', '%f');
[scan9_HP]=textread(' ymedi an_val ue_z24_H. txt', '%f');
[scan10_HP]=textread(' zmedi an_val ue_z25_H. txt', '%f');
[scan11_HP]=textread(' aamedi an_val ue_z26_H. txt', '%f');
[scan12_HP]=textread(' bbmedi an_val ue_z27_H. txt', '%f');
[scan13_HP]=textread(' cmedi an_val ue_z28_H. txt', '%f');
[scan14_HP]=textread(' ddmedi an_val ue_z29_H. txt', '%f');
[scan15_HP]=textread(' eemedi an_val ue_z30_H. txt', '%f');

%%%%%%%%%%%%%%%%%%%%%%%%%%%%%%%%%%%%%%%%%%%%%%%%%%%%%%%%%%%%%%%%%%%%%%%%
% DECLARATION BLOCK
%%%%%%%%%%%%%%%%%%%%%%%%%%%%%%%%%%%%%%%%%%%%%%%%%%%%%%%%%%%%%%%%%%%%%%%%
Spectrum_analyzer_uncertainty = 0;

Losses_Sucofl ex_cabl e=11. 37;
Sucofl ex_cabl e_uncertainty = 0. 1;
Losses_Sucofl ex_cabl e_pl us_uncertainty = Losses_Sucofl ex_cabl e +
Sucofl ex_cabl e_uncertainty;
Losses_Sucofl ex_cabl e_mi nus_uncertainty = Losses_Sucofl ex_cabl e -
Sucofl ex_cabl e_uncertainty;

Uncertainty_of_14_dB_amp = 1. 5;
Gai n_14_dB_amp = 14;
Gai n_14_dB_amp_pl us_uncertainty = Gai n_14_dB_amp + Uncertainty_of_14_dB_amp;
Gai n_14_dB_amp_mi nus_uncertainty = Gai n_14_dB_amp - Uncertainty_of_14_dB_amp;

Uncertainty_of_36_dB_amp = 3;
Gai n_36_dB_amp = 40. 3;
Gai n_36_dB_amp_pl us_uncertainty = Gai n_36_dB_amp + Uncertainty_of_36_dB_amp;
Gai n_36_dB_amp_mi nus_uncertainty = Gai n_36_dB_amp - Uncertainty_of_36_dB_amp;

Uncertainty_of_swi tch_s1 = 0. 1;
Losses_s1_swi tch = 0. 2;
Losses_s1_swi tch_pl us_uncertainty = Losses_s1_swi tch + Uncertainty_of_swi tch_s1;
Losses_s1_swi tch_mi nus_uncertainty = Losses_s1_swi tch -
Uncertainty_of_swi tch_s1;

Uncertainty_of_swi tch_s4 = 0. 1;
Losses_s4_swi tch = 0. 2;
Losses_s4_swi tch_pl us_uncertainty = Losses_s4_swi tch + Uncertainty_of_swi tch_s4;
Losses_s4_swi tch_mi nus_uncertainty = Losses_s4_swi tch -
Uncertainty_of_swi tch_s4;

Total_SYS_gai n=56;
```

APPENDIX E. MATLAB GENERATED CODE

```
subscan = 1800000;
data_points=601;
RBW = subscan/data_points;
RBW_MHz=RBW/1000000;
RBW_kHz=3;
c = 300000000;
%%%%%%%%%%%%%%%%%%%%%%%%%%%%%%%%%%%%%%%%%%%%%%%%%%%%%%%%%%%%%%%%%%%%%%%%
int32 i;
int j;
int32 counter;
int32 counter1;
j=1;
counter1=1;
counter=1;

for i =1: 26744;
    n=i;

    if n<2;
        f_MHz=70;
    elseif n>2
        f_MHz=70.000000+((n-1)*RBW_MHz);
    else
        f_MHz=70+RBW_MHz;
    end
    cent_freq(counter)=f_MHz;

    if f_MHz < 80;
        Antenna_uncertainty=0.1;
        Gain_antenna =(f_MHz-70)*0.65;
        Gain_antenna_plus_uncertainty = Gain_antenna + Antenna_uncertainty;
        Gain_antenna_minus_uncertainty= Gain_antenna - Antenna_uncertainty;
    else
        Gain_antenna = 6.5;
    end

    Total_SYS_gain1=56.5;

    spectral_flux_dBm1_VP1= scan1_VP(i) - Gain_antenna-
95.54+(20*log10(f_MHz))-(10*log10(RBW_kHz));
    spectral_flux_dBm1_VP=spectral_flux_dBm1_VP1-Total_SYS_gain1 ;
    power1=spectral_flux_dBm1_VP/10;
    z(j)=real pow(10, power1);
    j=j+1;

    spectral_flux_dBm2_VP1= scan2_VP(i) - Gain_antenna-
95.54+(20*log10(f_MHz))-(10*log10(RBW_kHz));
    spectral_flux_dBm2_VP=spectral_flux_dBm2_VP1-Total_SYS_gain1 ;
    power1=spectral_flux_dBm2_VP/10;
    z(j)=real pow(10, power1);
    j=j+1;

    spectral_flux_dBm3_VP1= scan3_VP(i) - Gain_antenna-
95.54+(20*log10(f_MHz))-(10*log10(RBW_kHz));
    spectral_flux_dBm3_VP=spectral_flux_dBm3_VP1-Total_SYS_gain1 ;
    power1=spectral_flux_dBm3_VP/10;
    z(j)=real pow(10, power1);
    j=j+1;

    spectral_flux_dBm4_VP1= scan4_VP(i) - Gain_antenna-
95.54+(20*log10(f_MHz))-(10*log10(RBW_kHz));
    spectral_flux_dBm4_VP=spectral_flux_dBm4_VP1-Total_SYS_gain1 ;
    power1=spectral_flux_dBm4_VP/10;
    z(j)=real pow(10, power1);
    j=j+1;

    spectral_flux_dBm5_VP1= scan5_VP(i) - Gain_antenna-
95.54+(20*log10(f_MHz))-(10*log10(RBW_kHz));
    spectral_flux_dBm5_VP=spectral_flux_dBm5_VP1-Total_SYS_gain1 ;
    power1=spectral_flux_dBm5_VP/10;
    z(j)=real pow(10, power1);
    j=j+1;

    spectral_flux_dBm6_VP1= scan6_VP(i) - Gain_antenna-
95.54+(20*log10(f_MHz))-(10*log10(RBW_kHz));
    spectral_flux_dBm6_VP=spectral_flux_dBm6_VP1-Total_SYS_gain1 ;
    power1=spectral_flux_dBm6_VP/10;
    z(j)=real pow(10, power1);
    j=j+1;

    spectral_flux_dBm7_VP1= scan7_VP(i) - Gain_antenna-
95.54+(20*log10(f_MHz))-(10*log10(RBW_kHz));
    spectral_flux_dBm7_VP=spectral_flux_dBm7_VP1-Total_SYS_gain1 ;
    power1=spectral_flux_dBm7_VP/10;
    z(j)=real pow(10, power1);
    j=j+1;
```

APPENDIX E. MATLAB GENERATED CODE

```
spectral_flux_dBm8_VP1= scan8_VP(i) - Gain_antenna-
95.54+(20*log10(f_MHz))-(10*log10(RBW_kHz));
spectral_flux_dBm8_VP=spectral_flux_dBm8_VP1-Total_SYS_gain1 ;
power1=spectral_flux_dBm8_VP/10;
z(j)=realpow(10, power1);
j=j+1;

spectral_flux_dBm9_VP1= scan9_VP(i) - Gain_antenna-
95.54+(20*log10(f_MHz))-(10*log10(RBW_kHz));
spectral_flux_dBm9_VP=spectral_flux_dBm9_VP1-Total_SYS_gain1 ;
power1=spectral_flux_dBm9_VP/10;
z(j)=realpow(10, power1);
j=j+1;

spectral_flux_dBm10_VP1= scan10_VP(i) - Gain_antenna-
95.54+(20*log10(f_MHz))-(10*log10(RBW_kHz));
spectral_flux_dBm10_VP=spectral_flux_dBm10_VP1-Total_SYS_gain1 ;
power1=spectral_flux_dBm10_VP/10;
z(j)=realpow(10, power1);
j=j+1;

spectral_flux_dBm11_VP1= scan11_VP(i) - Gain_antenna-
95.54+(20*log10(f_MHz))-(10*log10(RBW_kHz));
spectral_flux_dBm11_VP=spectral_flux_dBm11_VP1-Total_SYS_gain1 ;
power1=spectral_flux_dBm11_VP/10;
z(j)=realpow(10, power1);
j=j+1;

spectral_flux_dBm12_VP1= scan12_VP(i) - Gain_antenna-
95.54+(20*log10(f_MHz))-(10*log10(RBW_kHz));
spectral_flux_dBm12_VP=spectral_flux_dBm12_VP1-Total_SYS_gain1 ;
power1=spectral_flux_dBm12_VP/10;
z(j)=realpow(10, power1);
j=j+1;

spectral_flux_dBm13_VP1= scan13_VP(i) - Gain_antenna-
95.54+(20*log10(f_MHz))-(10*log10(RBW_kHz));
spectral_flux_dBm13_VP=spectral_flux_dBm13_VP1-Total_SYS_gain1 ;
power1=spectral_flux_dBm13_VP/10;
z(j)=realpow(10, power1);
j=j+1;

spectral_flux_dBm14_VP1= scan14_VP(i) - Gain_antenna-
95.54+(20*log10(f_MHz))-(10*log10(RBW_kHz));
spectral_flux_dBm14_VP=spectral_flux_dBm14_VP1-Total_SYS_gain1 ;
power1=spectral_flux_dBm14_VP/10;
z(j)=realpow(10, power1);
j=j+1;

spectral_flux_dBm15_VP1= scan15_VP(i) - Gain_antenna-
95.54+(20*log10(f_MHz))-(10*log10(RBW_kHz));
spectral_flux_dBm15_VP=spectral_flux_dBm15_VP1-Total_SYS_gain1 ;
power1=spectral_flux_dBm15_VP/10;
z(j)=realpow(10, power1);
j=j+1;

spectral_flux_dBm1_HP1= scan1_HP(i) - Gain_antenna-
95.54+(20*log10(f_MHz))-(10*log10(RBW_kHz));
spectral_flux_dBm1_HP=spectral_flux_dBm1_HP1-Total_SYS_gain1;
power1=spectral_flux_dBm1_HP/10;
z(j)=realpow(10, power1);
j=j+1;

spectral_flux_dBm2_HP1= scan2_HP(i) - Gain_antenna-
95.54+(20*log10(f_MHz))-(10*log10(RBW_kHz));
spectral_flux_dBm2_HP=spectral_flux_dBm2_HP1-Total_SYS_gain1;
power1=spectral_flux_dBm2_HP/10;
z(j)=realpow(10, power1);
j=j+1;

spectral_flux_dBm3_HP1= scan3_HP(i) - Gain_antenna-
95.54+(20*log10(f_MHz))-(10*log10(RBW_kHz));
spectral_flux_dBm3_HP=spectral_flux_dBm3_HP1-Total_SYS_gain1;
power1=spectral_flux_dBm3_HP/10;
z(j)=realpow(10, power1);
j=j+1;

spectral_flux_dBm4_HP1= scan4_HP(i) - Gain_antenna-
95.54+(20*log10(f_MHz))-(10*log10(RBW_kHz));
spectral_flux_dBm4_HP=spectral_flux_dBm4_HP1-Total_SYS_gain1 ;
power1=spectral_flux_dBm4_HP/10;
z(j)=realpow(10, power1);
j=j+1;

spectral_flux_dBm5_HP1= scan5_HP(i) - Gain_antenna-
95.54+(20*log10(f_MHz))-(10*log10(RBW_kHz));
spectral_flux_dBm5_HP=spectral_flux_dBm5_HP1-Total_SYS_gain1 ;
power1=spectral_flux_dBm5_HP/10;
z(j)=realpow(10, power1);
```

APPENDIX E. MATLAB GENERATED CODE

```
j=j+1;
spectral_flux_dBm6_HP1= scan6_HP(i) - Gain_antenna-
95.54+(20*log10(f_MHz))-(10*log10(RBW_kHz));
spectral_flux_dBm6_HP=spectral_flux_dBm6_HP1-Total_SYS_gain1 ;
power1=spectral_flux_dBm6_HP/10;
z(j)=realpow(10, power1);
j=j+1;

spectral_flux_dBm7_HP1= scan7_HP(i) - Gain_antenna-
95.54+(20*log10(f_MHz))-(10*log10(RBW_kHz));
spectral_flux_dBm7_HP=spectral_flux_dBm7_HP1-Total_SYS_gain1 ;
power1=spectral_flux_dBm7_HP/10;
z(j)=realpow(10, power1);
j=j+1;

spectral_flux_dBm8_HP1= scan8_HP(i) - Gain_antenna-
95.54+(20*log10(f_MHz))-(10*log10(RBW_kHz));
spectral_flux_dBm8_HP=spectral_flux_dBm8_HP1-Total_SYS_gain1 ;
power1=spectral_flux_dBm8_HP/10;
z(j)=realpow(10, power1);
j=j+1;

spectral_flux_dBm9_HP1= scan9_HP(i) - Gain_antenna-
95.54+(20*log10(f_MHz))-(10*log10(RBW_kHz));
spectral_flux_dBm9_HP=spectral_flux_dBm9_HP1-Total_SYS_gain1 ;
power1=spectral_flux_dBm9_HP/10;
z(j)=realpow(10, power1);
j=j+1;

spectral_flux_dBm10_HP1= scan10_HP(i) - Gain_antenna-
95.54+(20*log10(f_MHz))-(10*log10(RBW_kHz));
spectral_flux_dBm10_HP=spectral_flux_dBm10_HP1-Total_SYS_gain1 ;
power1=spectral_flux_dBm10_HP/10;
z(j)=realpow(10, power1);
j=j+1;

spectral_flux_dBm11_HP1= scan11_HP(i) - Gain_antenna-
95.54+(20*log10(f_MHz))-(10*log10(RBW_kHz));
spectral_flux_dBm11_HP=spectral_flux_dBm11_HP1-Total_SYS_gain1 ;
power1=spectral_flux_dBm11_HP/10;
z(j)=realpow(10, power1);
j=j+1;

spectral_flux_dBm12_HP1= scan12_HP(i) - Gain_antenna-
95.54+(20*log10(f_MHz))-(10*log10(RBW_kHz));
spectral_flux_dBm12_HP=spectral_flux_dBm12_HP1-Total_SYS_gain1 ;
power1=spectral_flux_dBm12_HP/10;
z(j)=realpow(10, power1);
j=j+1;

spectral_flux_dBm13_HP1= scan13_HP(i) - Gain_antenna-
95.54+(20*log10(f_MHz))-(10*log10(RBW_kHz));
spectral_flux_dBm13_HP=spectral_flux_dBm13_HP1-Total_SYS_gain1 ;
power1=spectral_flux_dBm13_HP/10;
z(j)=realpow(10, power1);
j=j+1;

spectral_flux_dBm14_HP1= scan14_HP(i) - Gain_antenna-
95.54+(20*log10(f_MHz))-(10*log10(RBW_kHz));
spectral_flux_dBm14_HP=spectral_flux_dBm14_HP1-Total_SYS_gain1 ;
power1=spectral_flux_dBm14_HP/10;
z(j)=realpow(10, power1);
j=j+1;

spectral_flux_dBm15_HP1= scan15_HP(i) - Gain_antenna-
95.54+(20*log10(f_MHz))-(10*log10(RBW_kHz));
spectral_flux_dBm15_HP=spectral_flux_dBm15_HP1-Total_SYS_gain1 ;
power1=spectral_flux_dBm15_HP/10;
z(j)=realpow(10, power1);
j=j+1;
j=1;
sort(z);
mean_value_spec(i)=10*log10(mean(z));
tenth_percentile_spec(i)=10*log10(prctile(z, 10));
ninety_percentile_spec(i)=10*log10(prctile(z, 90));
ninety_percentile_spec_i_near(i)=(prctile(z, 90));
max_value_spec(i)=10*log10(max(z));
min_value_spec(i)=10*log10(min(z));
median_value_spec(i)=10*log10(median(z));

counter=counter+1;

end

count=1;
```

APPENDIX E. MATLAB GENERATED CODE

```
for count=1:26668;
    min_value_spec1=min_value_spec(count);
    dimwrite('min_value_spec2.txt', min_value_spec1, 'delimiter',
    '\t', 'precision', '9', '-append')

    nitea_p(count)=min_value_spec(count);
end

correlation_coeff = corrcoef(nitea_p, minval)
cent_freq;

%%%%%%%%%%%%%%%%%%%%%%%%%%%%%%%%%%%%%%%%%%%%%%%%%%%%%%%%%%%%%%%%%%%%%%%%
%PLOTTING GRAPHS
%%%%%%%%%%%%%%%%%%%%%%%%%%%%%%%%%%%%%%%%%%%%%%%%%%%%%%%%%%%%%%%%%%%%%%%%
subplot(2, 1, 1);
plot
(cent_freq, min_value_spec); %max_value_spec, cent_freq, nity_percentile_spec, cent
_freq, mean_value_spec, cent_freq, tenth_percentile_spec, cent_freq, min_value_spec
; % , cent_freq, median_value_spec);
ylabel('Spectral Flux Density [dBW/m^2/Hz]');
legend('90 Percentile'); % , 'Max', '90%', '10%', 'Min');
title('Spectral Flux Density vs Frequency');
grid on;

subplot(2, 1, 2);
plot
(frequency, minval); %max_val, frequency, nity_percentile_spec, average, frequency, temp, fr
equency, minval);
xlabel('Frequency [MHz]');
legend('90 Percentile'); % , 'Max', 'Mean', '10%', 'Min');
grid on;

clear cent_freq;
clear all;

correlation_coeff =
    1.0000    0.3020
    0.3020    1.0000
: \MATLAB7\toolbox\matlab\graph2d\grid.m.
```